Light-Driven Energy Production for Cell-Free Metabolic Systems

by

Kyle Andrew Minor

A thesis submitted in partial fulfillment of the requirements for the degree of

Doctor of Philosophy

in

Chemical Engineering

Department of Chemical and Materials Engineering

University of Alberta

Abstract

Industrial biotechnology is used to produce biofuels, pharmaceuticals, chemicals, and other products and for wastewater treatment and soil remediation. Over the last several years, the use of whole-cell biocatalysts (WCB) for sequestering carbon dioxide has gained considerable attention. Although these technologies have been shown to have a significant reduction in CO_2 lifecycle emissions, there are inefficiencies associated with using whole cell biocatalysts. The mechanisms for cellular growth and repair waste energy and nutrients that could otherwise be used for the production of targeted compounds.

Ideally, isolated enzymes responsible for the sequestration of CO_2 in living systems would be advantageous over WCB. Isolated enzymes or cell-free metabolic systems (CFMS) would allow for all carbon and energy to be directed to the formation of the desired product. Before cell-free metabolic systems can become a disruptive technology, providing and adjusting energy at the nanoscale must be addressed. Enzymatic cofactors are the most cost prohibitive component of cell-free metabolic systems and are responsible for providing the energy for enzymes to proceed in otherwise thermodynamically unfavorable reactions. Due to the cost and stability of enzymatic cofactors like nicotinamide (NADH) recycling coenzymes is essential. The focus of this work was to engineer biotic/abiotic organelle capable of reducing NADH using light and water. This device pairs two membrane protein complexes that do not interact naturally: NADH: Ubiquinone oxidoreductase (CMI) and Photosystem II (PSII). Through the controlled directional assembly into 180 nm liposomes, these two proteins function collectively to reduce NAD^+. The significant findings of this work include, the

explicit demonstration of the reversibility of CMI, the inability of Peiricidin A to inhibit NAD^+ reduction by CMI, determined the optimal PSII to CMI ratio and show the rate of NADH production is proportional to quantum flux and has coupling efficiencies near unity. Applying this technology to cell-free metabolic systems will permit control over NADH balance and eliminate constraints on the design of new biosynthetic pathways.

Preface

The research presented in this thesis has been completed to fulfill the requirements of my Ph.D.. This thesis constructed as a paper-based format. Three journal articles have been adapted and are presented as Chapters 2 to 5. I have been the primary person responsible for literature review, laboratory experiments, data analysis, and manuscript preparation. Dr. Carlo Montemagno has been a supervisory co-author. Chapters 2 and 3 have been submitted and chapter 4 is under review. The list of papers is presented below:

1. Minor, K.A., Montemagno, C.D., “A Rapid and Scalable Purification Procedure for Purple Membrane and Bacteriorhodopsin,” *Biotechnology and bioengineering,* **2017,** (Submitted).
2. Minor, K.A., Montemagno, C.D., “Light-Driven Reversibility of Respiratory Complex I for NADH Regeneration,” *Nano Lett,* **2017,** (Submitted)
3. Minor, K.A., Montemagno, C.D, “Light-Driven Biological Recycling of NADH for Fueling Cell-Free Metabolic Systems,” *Nature communications*, **2017**, (Under Review)

Table of Contents

List of Figures

List of Tables

List of Abbreviations, Acronyms, and Symbols

∆pH: pH gradient

∆Ψ: electrical potential

λ_{ex}: excititation wavelength

λ_{em}: emission wavelength

ACMA: 9-amino-6-chloro-2-methoxyacridine

AIEX: anionic exchange chromatography

ATP: adenosine triphosphate

ATPase: adenosine triphosphatase

bR: bacteriorhodopsin

$CaCl_2$: calcium chloride

CCCP: carbonyl cyanide m-chlorophenyl hydrazine

CHAPS: 3-[(3-cholamidopropyl)dimethylammonio]-1-propanesulfonate

CFMS: cell-free metabolic systems

$CHCl_3$: chloroform

chlA: chlorophyll A

CFMS: cell-free metabolic engineering

CMI: complex I

CMC: critical micelle concentration

CoA: coenzyme-A

CV: Column volume

DCBQ: 2,5-dichloro-1,4,-benzoquinone

DCMU: 3-(3,4-dichlorophenyl)-1,1-dimethylurea

DDM: n-dodecyl ß-D-maltoside

DF: diaflitration

DNAase: deoxyribonuclease

DQ: decylubiquinone

DQH_2: decylubiquinol

DTT: dithiothreitol

DV: diavolume

EDTA: ethylene diamine tetra acetic acid

EtOH: ethanol

FDH: formate dehydrogenase

FDR: ferredoxin-NAD(P)$^{+}$ reductase

Fe-S: iron-sulfur

FMN: falvin mononucleotide

GC: glassy carbon

GDH: glucose dehydrogenase

GDHs: glutamate dehydrogenase

H_2: hydrogen

H^{+}: proton

LED: light emitting diode

LVCs: low value chemicals

MES: 2-(n-morpholino)ethanesulfonic acid

$MgCl_2$:magnesium chloride

Mn_4CaO_5: oxygen evolving complex

MSE: mercury/mercurous sulfate electrode

MV^{2+}: methyl viologen

MWCO: molecular weight cutoff

$NaBH_4$: sodium borohydride

NaCl: sodium chloride

NADH: nicotinamide adenine dinucleotide

$Na_2S_2O_4$: sodium dithionite

Na^{+}-NQR: sodium ion-transporting complex I

NDH-1: sodium or proton ion-transporting complex I

Ni: nickel

O_2: oxygen

OG: n-octyl-β-D-glucoside

PCR: photosystem to complex I mole ratio

PM: purple membrane

PMF: proton motive force

PMSF: phenylmethylsulfonyl fluoride

POPE: 1-palmitoyl-2-oleoyl-sn-glycero-3-phosphoethanolamine

POPG: 1-palmitoyl-2-oleoyl-sn-glycero-3-phospho-(1'-rac-glycerol)

PS: photosensitizer

PSII: photosystem II

Pt: platinum

Q: ubiquinone

$Q_{A,B}$: plastoquinone

QH_2: ubiquinonol

Q.S.: quantity sufficient

RB: running buffer

RC: reaction center

RET: reverse electron transport

Rh: rhodium

ROS: reactive oxygen species

RT: room temperature

Ru: ruthenium

SDS-PAGE: sodium dodecyl sulfate–polyacrylamide gel electrophoresis

SEM: standard error of the mean

SMPs: submitochondrial particles

TB: Terrific Broth

TF: turnover frequency

TFF: tangential flow filtration

TiO_4: doped titania

TP: transmembrane protein

TN: turnover number

TTN: total turnover number

TX: Trition X-100

USD: US Dolla

WCB: whole-cell biocatalysts

WV: working volume

1. Introduction

The increasing interest in green chemistry and biofuels in the past decade has made decoupling the cellular machinery responsible for growth and repair from bio-catalytic pathways extraordinarily desirable[1-2]. Through the exploitation of the efficiency and diversity of biochemical machinery of living organisms and engineering, it is possible to build precise and highly specific nanoreactors for high yield chemical synthesis while eliminating waste and byproducts endogenous to living systems. Numerous nanoreactors have been engineered which allow for isolation of catalytic systems while maintaining enzymatic activity [3-7].

The Calvin Cycle, also commonly called the Reductive pentose phosphate pathway[8] is an enzymatic cycle that catalyzes the photosynthetic assimilation of CO_2 and produces pentoses. It is of particular interest of improving on biological CO_2 sequestration technologies by isolation of this complex metabolic cycle in an engineering platform. The primary challenge limiting the usage of isolate enzymes for low-value commodity chemicals is an economical and practically feasible method for cofactor regeneration, which results in the use of WCBs regardless of the numerous disadvantages [9-11].

The goal of this work was to engineer a biologically inspired nanodevice, which couples the activity of PSII and Complex I for the regeneration of NADH. This device provides a green technology, driven by sunlight, and using water as the primary electron donor. The proposed technology could be used for any isolated enzyme process, which requires NADH recycling.

Biocatalysts

The first applications of biocatalysts for the benefit of society were reported in ancient Japan, China, and Mesopotamia. Applications initially, were limited to the production of alcoholic beverages and food but, since the 19th century, the technology has made astonishing advances[12]. With the augmenting social and economic pressures for clean and environmentally friendly production of consumer products many industrial sectors have implemented biocatalysts; production of amino acids, animal feed, textiles, detergents, and pharmaceuticals represent only a few of this sectors[13]. Advancement in biocatalysts has resulted in their usage becoming the preferred method of production of chiral molecules in pharmaceutical and chemical industry[14]. There are significant advantages of biocatalysts over traditional chemical catalysis and organic synthesis [14-18].

Deliberated by most, the most significant advantages of biocatalysts is that they fully reigo-, stero- and chemo-selective. This bestows biocatalysts the potential of producing only the desired product with a high degree of selectivity, particularly advantageous in applications for providing chiral intermediates or end products, where chemical based reactions may lead to undesired side products and/or multiple isomers of a single product. Additionally, because of the high selectivity of biocatalysts, the protection and deprotection of functional groups are unnecessary which can reduce reactions in a synthetic pathway. The exploitation of the advantage mentioned above, especially in the pharmaceutical industry[19] is of considerable interest[10].

Typically, chemical catalysts require high temperatures and pressures and usually acidic or basic condition for the desired reaction to proceed. The energy needs of

chemical catalysts generate high operational costs, elucidate adverse environmental effect and can produce unsafe working conditions. Nature has evolved enzymes to catalyze reactions at low temperatures and pressures using water as the reaction medium. Using biocatalysts can lead to a substantial reduction in energy requirements in comparison to most chemical catalysts as well providing green and safe alternative[15, 17, 19-21].

There are many advantages of biocatalysts over chemical catalysts. The advantages of enzymes include their efficient usage of raw material and their ability to enable reactions, that are otherwise are difficult or impossible through traditional chemical catalysis/synthesis and very high turnover numbers[15].

There are two classes of biocatalysts; whole-cell biocatalysts (WCB) and isolated enzymes. WCBs are living organisms; typically, they have undergone some amount of genetic engineering for desired attributes such as increased capacity for product formation, environmental tolerance, and increased substrate transport across the cell membrane. However, isolated enzymes are proteins, which have been extracted and purified from a host organism. In comparison, each WCB and isolated enzymes have their advantages and disadvantages over one another.

Enzymes

Enzymes are biological catalysts, which facilitate the synthesis of complex organic molecules by stereo-, chemo-, regio-selective bond forming and breaking reactions[21]. They may have metals or other cofactors and partner enzymes for cofactor

regeneration. The number of enzymes identified to date is astounding but, are classified into six classes (Table 1-1), amassed by the chemical transformation they catalyze[22].

Table 1-1 | Classes of Enzymes

Class	Transformation
Oxidoreductase (EC1)	Reduction/Oxidation
Transferases (EC2)	Transfer of functional groups
Hydrolases (EC3)	Hydrolysis
Lyases (EC4)	Addition of multiple bonds
Isomerase (EC5)	Isomerization
Ligase (EC6)	Formation of carbon-heteroatom bonds.

In many ways applying isolated enzymes in an industrial process is much easier then WCBs. From a biomanufacturing perspective, they are considerable advantages for modification, design, and control of biological systems by separating catalysts utilization from catalysts synthesis[9]. Isolated enzymes offer a higher degree of engineering flexibility over WCBs. By removing the enzymes from the cell higher theoretical yields are achieved, a more extensive variety of products are possible, and reaction conditions are more easily manipulated. These advantages are possible because cell viability, complexity, physiology, cellular membranes, and cell walls are no longer issues[18].

The maturity of isolated enzyme technology is much less than that of WCBs. The significant disadvantages in isolated enzymes are costs associated with purification and cofactors and the stability of the isolated enzymes[9]. The issue of enzyme stability is circumvented by immobilizing or entrapment techniques[13, 15, 21-27]. The primary challenge limiting the usage of isolate enzymes for low-value commodity chemicals is

an economical and practically feasible method for cofactor regeneration, which results in the use of WCBs regardless of the many disadvantages[9-11].

Whole Cell Bio-catalysts

Albeit WCBs have proven to be a potent tool to produce chemicals, biofuels, and pharmaceuticals, there are inefficiencies and difficulties associated with them[9, 28-29]. The inherent limitations imposed by the cell are the most significant challenge. Once an organism has been engineered to increase the activity of a synthetic pathway, it is currently impossible to balance the intracellular fluxes while satisfying the maintenance and growth required by the organism. This results in a lost carbon and energy resources intended for product generation to cellular functions. The intracellular production of the desired product is limited to nontoxic levels and byproducts are typically prevalent in such systems[9, 14, 22].

Another challenge in using WCBs is the transport of the substrate across the cellular membrane and cell wall; commonly the rate-limiting step of the production process. Typically, to circumvent substrate uptake limitations is to introduce detergents or solvents to increase the permeability of the cell membrane. This practice can often cause cell lysis, interfere with downstream processes and decrease cell viability[18].

There are some advantages of using whole cells for biochemical transformations. The two most significant being **1)** the enzyme remains in its natural environment and stabilized and **2)** easier regeneration of co-factors *in situ* avoiding the addition of expensive co-factors, consumed in stoichiometric amounts during conversion[18]. Although usage of WC redox reactions is far greater then isolated enzyme systems if

primarily owed to endogenous cofactor regeneration machinery of metabolically active cells[9, 12, 30].

Cofactors/NADH

Many desirable enzymatic reactions for manufacturing purposes require cofactors. Enzymatic cofactors such as Adenosine Triphosphate (ATP), Nicotinamide adenine dinucleotide (NADH) and Acetyl Coenzyme-A (Acetyl CoA) provide the necessary energy or reduction/oxidation potential for the enzymatic reactions to proceed averse to high energetic barriers. Most of the industries that have adopted cofactor-dependent enzymatic reactions are limited to those which produce high-value commodity chemicals, owing to the high cost of enzyme cofactors and associated technological difficulties in cofactor regeneration[9].

In 2011, there were more than 500 commercial products produced using enzymes[22]. Approximately 50% of the reactions used to produce commercial products rely on redox reactions catalyzed by Oxidoreductases (EC1)[31]. A majority of these enzymes require cofactors, which are the actual active sites for electron transfer. In these reactions, it is the cofactor that is reduced or oxidized leaving the enzyme unmodified to continue catalyzing the reaction[10].

The most frequently required cofactors for oxidoreductase activity are NAD^+/NADH and $NADP^+$/NADPH redox couples [9]. These NAD containing molecules, function as universal energy carriers performing reversible two-electron, single proton transfers in a variety of reactions[32]. Since cofactors undergo chemical modification during the catalytic reaction, they are required at stoichiometric quantities. The cost of NADH is

approximate $200USD/gram[33] and is not economical to continually append stoichiometric amounts during the reaction. Thus, reduction of oxidized NAD^+ is of particular interest because of the known oxidoreductases, 80% of them require NADH[33].

NADH Regeneration

Many methods are available for the regeneration of the reduced form of NADH and are categorized into four types; enzymatic, electrochemical, chemical, photochemical, and biological methods[10-11, 33-36]. Any industrially feasible regeneration method must be practical, efficient, have a high TTN (total turnover number), and should enable the enzymatic process to be economical[10-11, 33, 35-36]. The criterion for commercial application, the TTN should be greater than 1,000[30]. The continuous regeneration of coenzymes has additional benefits to the reaction process. By continuously, eliminating the oxidized cofactor the reaction equilibrium will be is shifted to product formation and eliminates the need for separation of cofactor from the synthetic reaction.

Electrochemical Reduction

The use of electrochemistry for the reduction of NAD^+ has gained considerable attention over the past two decades. The attractiveness of electrochemical methods is owed to several reasons: electrical power is the cheapest redox equivalent[37], easy isolation of products, no cosubstrate is required, and the redox potential is easily controlled[30, 34, 38-39]. There are two types of electrochemical methods for the reduction of NAD^+, direct and indirect.

Direct Electrochemical Reduction

Direct electrochemical reduction the cathode provides electrons directly, and the aqueous reaction media supplies the protons [10, 34]. The reduction of NAD^+ on an electrode proceeds through a two-single electron transfers[39-40]. The first electron-transfer is a reversible reaction while generates the NAD-radical. Upon formation of the NAD-radical, the second reduction and protonation lead to the enzymatically active 1,4-NADH. The primary challenge of this reaction mechanism is the NAD-radical may dimerize forming NAD_2 or be reduced to enzymatically inactive 1,6-NADH [39]. The kinetics of the dimerization reaction is faster than the desired second electron-transfer and protonation and resulting from poor selectively continuous recycling results in significant amounts of 1,6-NADH [41]. Omanovic and et al. have demonstrated that 100% reduction of NADH to the enzymatically active 1,4-NADH is possible on glassy carbon (GC) surface at high overpotentials (-2.3 volts (V) vs. MSE (mercury/mercurous sulfate electrode)). Though, the TTN was not reported by this work to give any indication of its industrial viability. Other disadvantages of the direct method are, the requirement of high overpotential, electrode fouling and rate of NAD^+ reduction is slow [33].

Modifications of the electrode surface with nanostructures have been reported to minimize the undesirable characteristics of the direct electrochemical method. Electrochemically depositing platinum (Pt) or nickel (Ni) nanoparticles on GC electrodes have been reported to have substantially ameliorated performance over bare GC electrodes [38]. The resulting modified electrode had higher selectively and required lower overpotentials, producing 100% 1,4-NADH at -1.6V and -1.5V for Pt and Ni respectively [39]. The nanoparticle deposits function in two ways to improve the performance; as

spacers to prevent the collisions between neighboring NAD-radicals and the subsequent formation of NAD_2 and as efficient hydrogen evolution catalyst accelerating protonation of the free radical [39].

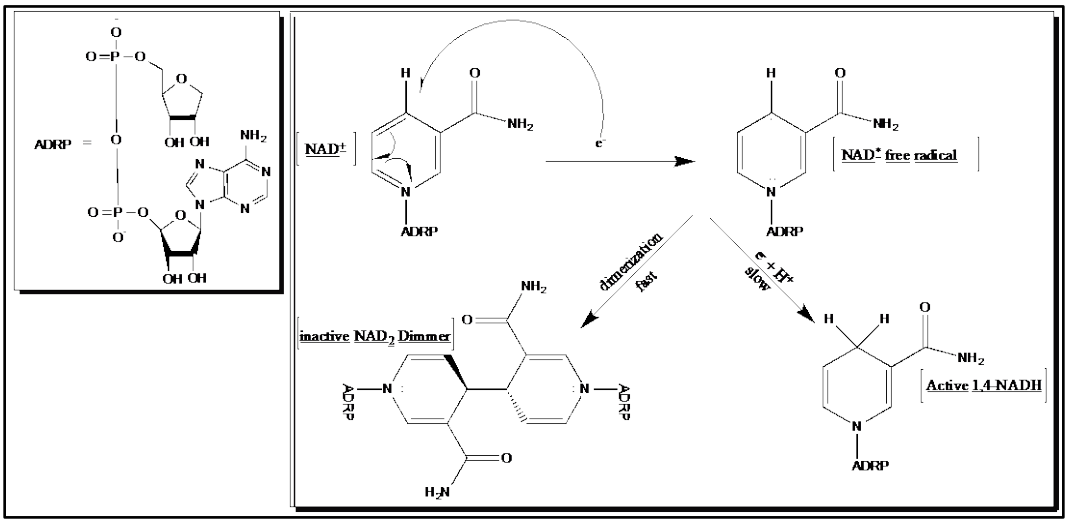

Figure 1.1 | The mechanism of electrochemical reduction of NAD+ to the enzymatically active and inactive forms of NADH[38].

Indirect Electrochemical Reduction

To circumvent the drawbacks indirect electrochemical approach, the use of redox mediators have developed which act as electron transfer catalysts between the electrode and NAD^+ [33, 36, 42]. Either an organic or organometallic molecule is respiratory as the mediator. To be a successful mediator it must, at a minimum, present three characteristics [43]: First, the catalytic mechanism must act through a single two-electron transfer to entirely suppress the formation of the free radical intermediate. The two requirements are; the electrochemical potential must be more anionic than the first reduction potential of NAD^+, and it must exclusively produce 1,4-NADH.

Indirect electrochemical methods for NADH regeneration began to be published in the early 1980's. The first generation of mediators typically depended on the use of rhodium (Rh) and ruthenium (Ru)-based catalysts[36]. The catalytic performance of the Rh-based catalyst, $([Rh(bpy)_3])^{3+}$ was largely increased by using the Cp* ligand. The activated form of this organometallic mediator $([Cp^*Rh(bpy)_3]H)^+$ acts as a hydride transfer reagent with >99% regio-specificity in the placement of the hydride on the pyridinium ring of NAD^+ [35]. To reactive $([Cp^*Rh(bpy)_3](H_2O))^{2+}$ to catalytically active form it undergoes two single electron-transfer steps at the cathode and coordinates a proton into its ligand sphere for the aqueous media[30, 42]. To date, this Rh complex and its derivatives are the most dominate mediators used in the indirect electrochemical reduction of NAD^+. Advancements of mediators struggle from solubility issues in aqueous solution[30].

The combination of enzymatic NADH-dependent processes with transition metal-based mediators suffers from significant performance issues. The primary issue is mutual deactivation of the mediator and the enzyme [36]. Many of the publications on these system report low TTNs. Studies conducted focused on this issued proved that accessible nucleophilic amino acid residues, lysine, and cysteine on the enzyme interact with the metal center of the organometallic catalyst causing deactivation[44]. Along with the compatibly issues mention, the reduction of the complex suffers from dilatory electron-transfer kinetics resulting in a comparatively poor TF (turnover frequency) [30].

Enzymatic Regeneration

This method of regeneration has advantages over the over three methods. First and most importantly, it typically has higher TTNs and faster TFs. The other advantages are: it is more accessible to couple the biological procedure since it occurs in mild reaction conditions, it does not require a mediator and is highly selective. There are numerous enzymatic methods, which have been adopted by industry and others that are currently in development. Enzymatic cofactor requires a second enzyme or second substrate and can be segregated into two different categories: substrate-coupled and enzyme-coupled. The substrate-coupled system uses one enzyme to catalyze the synthesis of the desired product and the regeneration of the cofactor with a second sacrificial substrate. The enzyme-coupled approach uses a second enzyme to catalyze the regeneration of NADH separate from the NADH-dependent enzyme producing the desired product [45].The challenges associated with enzymatic regeneration is determining a suitable enzyme to couple to the co-substrate, engineering an efficient separation strategy and ultimately designing a rational reaction route[10-11, 33, 36].

Substrate-coupled

The substrate-couple method is theoretically the most straightforward approach for reducing NAD^+ making it the preferred enzymatic method. This method is the use of a single enzyme for both production of the desired product and the regeneration of the cofactor through the simultaneous oxidation of an inexpensive co-substrate. The significant disadvantage of this method is resulting from the thermodynamic limitations of the reaction. To drive the reaction equilibrium to product formation requires large quantities of the second substrate or the continuous removal of the co-substrate

product[45]. The excess of the co-substrate may lead to enzymatic deactivation; thus, the enzyme must be engineered to tolerate high concentrations of co-substrate. This method is only economically practical if an inexpensive co-substrate is available.

Enzyme-coupled

The enzyme-coupled method uses a second EC1 type enzyme with a high affinity for the co-substrate. For this approach, to be successful, the primary enzyme must not accept the co-substrate or byproduct formation will arise. This method has been the dominant of the two enzyme-based methods. The second enzyme approach is possible *in vitro* with isolated enzymes or *in vivo* with a genetically modified organism[10].

The most frequently used enzymes for *in situ* NAD^+ regeneration are glucose dehydrogenase (GDH), glutamate dehydrogenases (GDHs), NAD(P) oxidases, and formate dehydrogenase (FDH), the last being the most popular[30]. Many of these enzyme's final product is CO_2. These enzymes are not viable options for a green CO_2 sequestration platform, as they would result in a net zero consumption of CO_2.

NAD(P) oxidases have just recently started to gain attention. One example in which this method is used for NAD^+ reduction is by employing the soluble hydrogenase from *Ralstonia eutropha*. This enzyme uses molecular hydrogen (H_2) as the electron donor to regenerate NADH. Although this presents a convenient method for producing NADH, the drawbacks are the instability of the multi-subunit enzyme[46] and the poor solubility of H_2 (0.1-0.2 mM). To overcome the solubility of H_2, the reactions must happen in a pressurized H_2 environment, which is energy intensive[35].

Chemical Regeneration

Only a few methods of chemical regeneration of NADH are presented in literature, owed to their unwanted side product formation, expensive reagents and incompatible reaction conditions[45]. Inorganic salts such as sodium borohydride ($NaBH_4$) and sodium dithionite ($Na_2S_2O_4$) act as redox agents in chemical regeneration procedures. The inorganic salts are appended in stoichiometric amounts to the product and not recycled. The accumulation of the salts results in enzymatic deactivation at higher concentrations, and therefore the oxidized salts must be continuously removed. Resulting from the large consumption of the salts there are high-cost contributions to the product and environmental issues.

Organometallic complexes can be used to activate H_2 for the reduction of NAD^+. This method is a captivating approach because of the low cost of H_2[37] as a reducing agent. However, the organometallic complexes used in this approach are the same as used in indirect electrochemical techniques[30, 42, 45] resulting in the same mutual deactivation, low TTNs and TNs discussed earlier.

Photochemical Regeneration

A relatively new and novel method, photochemical regeneration has captured considerable interest by the academic community because of the abundance of clean solar energy. Analogous to chemical regeneration, the photochemical approach using a photosensitizer (PS), a primary electron acceptor, and a sacrificial electron donor. PS's are dye-based molecules excited by visible light. Upon excitation the PS, it receives an electron for the sacrificial electron donor (e.g., EDTA). The excited-state PS* transfers

an electron to the primary electron acceptor such as methyl viologen (MV^{2+}) which mediates the reduction of NAD^+ by an enzymatic catalyst (e.g., FDR)[33, 45].

The challenges for photo-energy conversion systems for the regeneration of NADH are finding a stable photosensitizer using visible-light and an efficient electron mediator. Until these barriers are overcome, photochemical methods will suffer from low TTNs with chemical and indirect electrochemical methods[33, 45]. Currently, the most widely used electron mediator and PS are Rh complex M and doped titania (TiO_2), respectively[33].

Artificial Organelles

An organelle is a metabolically functional structure, surrounded by a barrier of such as a lipid monolayer, lipid-protein monolayer, or a unit membrane[47]. Examples of these cellular structures are the mitochondria, chloroplasts, and golgi[48]. Each of these organelles compartmentalizes a particular metabolic system, allowing cells to have precise control of all biochemical reactions. There has been a considerable effort in mimicking these metabolic structures for several applications including, energy transduction[6], regeneration of ATP[4, 7], voltage-gated valves[49-51] and even therapeutic applications[52].

Transmembrane Proteins

Transmembrane proteins (TP) are a class of proteins, with multiple hydrophobic domains spanning across the biological lipid bilayer membrane. This class of proteins serves a variety of functions to mediate a cell's response to changes in its environment[53]. Most of TPs function as transporters, receptors, or enzymes. Many TPs

simultaneously have multiple functions catalyzing reaction(s) and transporting solutes[53-54].

Transporters are classified into four subgroups: Channels, Solute carriers, Active Transporters, and Other transporters. They selectively move substrates across by using energy from chemical gradients and electrochemical gradients. They can respond to osmotic pressure, changes in pH, light, and many other stimuli[54]. Transport TPs can be rationalized by considering them biochemical machines, functioning as selective unit operations. Analogs to traditional chemical unit operations they perform the same functions as separators, pumps, catalysts, and energy transducers[55].

NADH: Ubiquinone Oxidoreductase

NADH: Ubiquinone oxidoreductase (Complex I) is the first enzyme of the respiratory chain in both bacteria and mitochondria. There are three types of Complex I which are currently known: H^+ or Na^+ ion-translocating Complex I (NDH-1 in bacterial), Na^+ ion-translocating Complex I (Na^+-NQR), and the non-electrogenic Complex I (NDH-2) found in both prokaryotes and eukaryotes[56].

One of the largest membrane proteins known, the crystal structure of the entire Complex I from *Thermus thermophilus* was just recently solved[57]. The prokaryotic NDH-1 is comprised of 16 subunits containing seven Fe_4S_4 and two Fe_2S_2 iron-sulfur clusters and one bound flavin mononucleotide (FMN) with an aggregate molecular weight of 536 kDa[57]. The enzyme is divided into two major domains; the membrane-bound and aqueous domains. The aqueous domain stands tangent to the membrane-bound embedded portion giving it an L-shaped structure[58]. NDH-1 is comprised of three

specialized modules: (1) The hydrophilic NADH oxidizing/reducing module (N-module); (2) the hydrophobic module responsible for proton transport (P-Module); and (2) A Q-binding domain connecting the other two modules (Q-module).

The primary role of Complex I is the catalytic transfer of two electrons through oxidation of NADH produced in catabolic pathways into the respiratory chain[58]. It is vectorial proton pump driven, moving protons from the positively charged to the negatively charged side of the membrane during forward electron transport. The translocation of protons is coupled to electron transfer, upon binding NADH, electrons are transferred to the bound FMN and passed through seven iron-sulfur (Fe-S) clusters to reduce ubiquinone (Q)[59]. The reduced form of Q, QH_2 acts as a reducing agent for subsequent enzymes in the respiratory system. Coupled to this electron transfer reaction, is the transport of into the periplasm, assisting in the generation of the proton motive force (PMF) used for drive ATP synthase[60]. It has been reported that Complex I is a reversible machine which can utilize the PMF for the reduction of NAD^+ to NADH[61-63]. It has been reported that PMF dependent electron transport can occur reducing NADH through QH_2. In this process, Q is reduced through the oxidation of succinate by membrane-bound succinate dehydrogenase[64-65].

$$\mathrm{NADH} + \mathrm{H^+} + \mathrm{Q} + 4\mathrm{H_N^+} \leftrightarrow \mathrm{NAD^+} + \mathrm{H^+} + \mathrm{QH_2} + 4\mathrm{H_P^+} \quad (1.1)$$

Photosystem II

Photosystem II (PSII) from oxygenic phototrophs is a multi-subunit pigment-protein, transmembrane protein[66]. It is embedded in the thylakoid membrane of cyanobacteria, higher plants, and algae[67]. Functioning as a light-driven Water:Quinone oxidoreductase,

its primary function is charge generation. PSII is the first protein complex in the photosynthesis chain. PSII harvests solar energy producing a charge separation catalyzing the splitting of water, extracting electrons, producing O_2 and protons contributing to the PMF for ATP synthesis[68].

The primary photochemical reaction takes place within the reaction center (RC), the core of PSII. The RC is comprised of two protein subunits D1 and D2. Bound to the RC are CP43 and CP47 proteins, which are responsible for the adsorption of light energy[69]. The excitation energy absorbed by these pigment-containing proteins is transferred to the RC[70]. These subunits contain all the cofactors involved in photochemical charge separation, Q-reduction and the oxidation of water[70]. To drive these reactions, 680nm photons are adsorbed by P680, the primary oxidant of PSII. There are four chlorophyll *a* (chlA) molecules and two pheophytin *a* ($Pheo_{D1}$/ $Pheo_{D2}$) molecules, which form P680. Excitation of P680 promotes several electron transfer reactions[71].

Upon excitation of a Chla, P680 is converted to a strong reducing agent $P680^*$. Very rapidly, a Pheo molecule is reduced by $P680^*$ forming a radical pair state $P680^{*-}Phe^{*-}$. Within in a few picoseconds, $Pheo^{*-}$ reduces a plastoquinone (Q_A) molecule tightly bound to the D2 domain producing $P680^{*+}PheoQ_A^-$. With a redox potential >1V, $P680^{*+}$ oxidizes a tyrosine residue (Y_Z) located in the D1 domain within nanoseconds, forming $Y_Z^{*+}P680PheoQ_A^-$. The $Y_Z^{*+}P680PheoQ_A^-$ complex is responsible for the reduction of a second plastoquinone (Q_B) within the D1 protein forming $Y_Z^{*+}P680PheoQ_AQ_B^-$. The oxidized tyrosine extracts an electron, and a proton from one of four manganese atoms in the oxygen-evolving complex (Mn_4CaO_5) ligated to the D1 and CP43 subunits[72]. This entire process is repeated to reduced Q_B^- to Q_B^{-2}, which is released into Q-pool

contained within lipid bilayer following protonation to QH_2. Two more photochemical turnovers provide the manganese cluster with four oxidizing equivalents necessary to split the two bound water molecules[69]. The overall reaction of water oxidation by PSII is given in (2.1)[73].

$$2H_2O + 2Q + 4H^+_N \rightarrow O_2 + 2QH_2 + 4H^+_P \qquad (2.1)$$

Hypothesis

The work conducted in this thesis is to demonstrate that an artificial organelle containing PSII and CMI can convert light energy into chemical energy in the form of reduced NADH. As delineated earlier PSII is excited by sunlight leading to the oxidation of water, generation of a PMF and of QH_2, which is used as a reducing agent by other enzymes in the photosynthetic pathway. It is hypothesized that the PMF and QH_2 generated by PSII will promote "reverse electron transport" in Complex I. If Complex I is inserted into the membrane in the opposite direction it is found endogenously, the PMF would supply the energy necessary to drive the unfavorable reduction of NAD^+ from QH_2. The newly form NADH would then be available for enzymes on the outside of the vesicle.

Multiple steps are leading to the demonstration of NAD^+ photoreduction by PSII-CMI proteoliposomes. Following the isolation of the required enzymes for this work. First, it was necessary to show CMI from *E. coli* can operate in R.E.T.. After, determination of a working procedure for the co-reconstitution of PSII and CMI experiments were conducted to demonstrate the dependence of NAD^+ photoreduction rate and quantum

flux, the coupling efficiency between PSII and CMI, and the dependence on ΔpH on the rate of NADH production.

References

1. Ardao, I.; Hwang, E. T.; Zeng, A. P., In vitro multienzymatic reaction systems for biosynthesis. *Advances in biochemical engineering/biotechnology* **2013,** *137*, 153-84.

2. van Oers, M. C. M.; Rutjes, F.; van Hest, J. C. M., Cascade reactions in nanoreactors. *Current Opinion in Biotechnology* **2014,** *28*, 10-16.

3. Ho, D.; Chu, B.; Lee, H.; Brooks, E. K.; Kuo, K.; Montemagno, C. D., Fabrication of biomolecule-copolymer hybrid nanovesicles as energy conversion systems. *Nanotechnology* **2005,** *16* (12), 3120-3132.

4. Choi, H. J.; Montemagno, C. D., Artificial organelle: ATP synthesis from cellular mimetic polymersomes. *Nano Lett* **2005,** *5* (12), 2538-2542.

5. Choi, H. J.; Lee, H.; Montemagno, C. D., Toward hybrid proteo-polymeric vesicles generating a photoinduced proton gradient for biofuel cells. *Nanotechnology* **2005,** *16* (9), 1589-1597.

6. Chu, B. M.; Ho, D.; Lee, H.; Kuo, K.; Montemagno, C., Coupled-protein functionality for energy conversion in biomimetic systems. *2005 IEEE International Conference on Robotics and Biomimetics* **2006**, 356-359.

7. Choi, H. J.; Montemagno, C. D., Light-driven hybrid bioreactor based on protein-incorporated polymer vesicles. *Ieee T Nanotechnol* **2007,** *6* (2), 171-176.

8. Heldt, H.-W.; Heldt, F., 6 - The Calvin cycle catalyzes photosynthetic CO2 assimilation. **2005**.

9. Dudley, Q. M.; Karim, A. S.; Jewett, M. C., Cell-free metabolic engineering: Biomanufacturing beyond the cell. *Biotechnol J* **2014**.

10. Uppada, V.; Bhaduri, S.; Noronha, S. B., Cofactor regeneration - an important aspect of biocatalysis. *Curr Sci India* **2014,** *106* (7), 946-957.

11. Liu, W.; Wang, P., Cofactor regeneration for sustainable enzymatic biosynthesis. *Biotechnol Adv* **2007,** *25* (4), 369-84.

12. Bornscheuer, U. T.; Buchholz, K., Highlights in Biocatalysis – Historical Landmarks and Current Trends. *Eng Life Sci* **2005,** *5* (4), 309-323.

13. Tufvesson, P.; Fu, W.; Jensen, J. S.; Woodley, J. M., Process considerations for the scale-up and implementation of biocatalysis. *Food and Bioproducts Processing* **2010,** *88* (1), 3-11.

14. Nestl, B. M.; Nebel, B. A.; Hauer, B., Recent progress in industrial biocatalysis. *Current Opinion in Chemical Biology* **2011,** *15* (2), 187-193.

15. Wells, A., 9.11 Industrial Applications of Biocatalysis: An Overview. In *Comprehensive Chirality*, Carreira, E. M.; Yamamoto, H., Eds. Elsevier: Amsterdam, 2012; pp 253-287.

16. Sanchez, S.; Demain, A. L., Enzymes and Bioconversions of Industrial, Pharmaceutical, and Biotechnological Significance. *Org Process Res Dev* **2011,** *15* (1), 224-230.

17. Solano, D. M.; Hoyos, P.; Hernaiz, M. J.; Alcantara, A. R.; Sanchez-Montero, J. M., Industrial biotransformations in the synthesis of building blocks leading to enantiopure drugs. *Bioresource Technol* **2012,** *115*, 196-207.

18. de Carvalho, C. C. C. R., Enzymatic and whole cell catalysis: Finding new strategies for old processes. *Biotechnol Adv* **2011,** *29* (1), 75-83.

19. Wandrey, C.; Liese, A.; Kihumbu, D., Industrial biocatalysis: Past, present, and future. *Org Process Res Dev* **2000,** *4* (4), 286-290.

20. Sheldon, R. A.; van Rantwijk, F., Biocatalysis for sustainable organic synthesis. *Australian journal of chemistry* **2004,** *57* (4), 281-289.

21. Nestl, B. M.; Hammer, S. C.; Nebel, B. A.; Hauer, B., New Generation of Biocatalysts for Organic Synthesis. *Angew Chem Int Edit* **2014,** *53* (12), 3070-3095.

22. Illanes, A.; Cauerhff, A.; Wilson, L.; Castro, G. R., Recent trends in biocatalysis engineering. *Bioresource Technol* **2012,** *115* (0), 48-57.

23. Sahare, P.; Ayala, M.; Vazquez-Duhalt, R.; Agrawal, V., Immobilization of peroxidase enzyme onto the porous silicon structure for enhancing its activity and stability. *Nanoscale research letters* **2014,** *9* (1), 409.

24. Jang, E.; Ryu, B. H.; Kim, T. D., Identification, characterization, and immobilization of an organic solvent-stable alkaline hydrolase (PA27) from Pseudomonas aeruginosa MH38. *Molecules* **2014,** *19* (9), 14396-405.

25. Talbert, J. N.; Wang, L. S.; Duncan, B.; Jeong, Y.; Andler, S. M.; Rotello, V. M.; Goddard, J. M., Immobilization and Stabilization of Lipase (CaLB) through Hierarchical Interfacial Assembly. *Biomacromolecules* **2014**.

26. Vashist, S. K.; Lam, E.; Hrapovic, S.; Male, K. B.; Luong, J. H., Immobilization of Antibodies and Enzymes on 3-Aminopropyltriethoxysilane-Functionalized Bioanalytical Platforms for Biosensors and Diagnostics. *Chem Rev* **2014**.

27. Lee, J. H.; Nam, D. H.; Lee, S. H.; Park, J. H.; Park, S. J.; Lee, S. H.; Park, C. B.; Jeong, K. J., New Platform for Cytochrome P450 Reaction Combining in Situ Immobilization on Biopolymer. *Bioconjugate chemistry* **2014**.

28. Straathof, A. J. J., Transformation of Biomass into Commodity Chemicals Using Enzymes or Cells. *Chem Rev* **2013,** *114* (3), 1871-1908.

29. Kaur, G.; Srivastava, A. K.; Chand, S., Advances in biotechnological production of 1,3-propanediol. *Biochemical Engineering Journal* **2012,** *64*, 106-118.

30. Hollmann, F.; Arends, I. W. C. E.; Buehler, K., Biocatalytic Redox Reactions for Organic Synthesis: Nonconventional Regeneration Methods. *Chemcatchem* **2010,** *2* (7), 762-782.

31. Meyer, H. P.; Eichhorn, E.; Hanlon, S.; Lutz, S.; Schurmann, M.; Wohlgemuth, R.; Coppolecchia, R., The use of enzymes in organic synthesis and the life sciences: perspectives from the Swiss Industrial Biocatalysis Consortium (SIBC). *Catal Sci Technol* **2013,** *3* (1), 29-40.

32. Kuchel, P. W., Biochemistry. In *Schaum's outline series* [Online] 3rd ed.; McGraw-Hill: New York, 2012; pp. 1 online resource (xiii, 492 p.). http://accessengineeringlibrary.com/browse/schaums-outline-of-biochemistry-third-edition.

33. Wu, H.; Tian, C.; Song, X.; Liu, C.; Yang, D.; Jiang, Z., Methods for the regeneration of nicotinamide coenzymes. *Green Chem* **2013,** *15* (7), 1773-1789.

34. Chenault, H. K.; Whitesides, G. M., Regeneration of Nicotinamide Cofactors for Use in Organic-Synthesis. *Applied biochemistry and biotechnology* **1987,** *14* (2), 147-197.

35. Hollmann, F.; Schmid, A., Electrochemical regeneration of oxidoreductases for cell-free biocatalytic redox reactions. *Biocatal Biotransfor* **2004,** *22* (2), 63-88.

36. Quinto, T.; Kohler, V.; Ward, T. R., Recent Trends in Biomimetic NADH Regeneration. *Top Catal* **2014,** *57* (5), 321-331.

37. Wandrey, C., Biochemical reaction engineering for redox reactions. *Chem Rec* **2004,** *4* (4), 254-265.

38. Ali, I.; Soomro, B.; Omanovic, S., Electrochemical regeneration of NADH on a glassy carbon electrode surface: The influence of electrolysis potential. *Electrochem Commun* **2011,** *13* (6), 562-565.

39. Ali, I.; Gill, A.; Omanovic, S., Direct electrochemical regeneration of the enzymatic cofactor 1,4-NADH employing nano-patterned glassy carbon/Pt and glassy carbon/Ni electrodes. *Chem Eng J* **2012,** *188*, 173-180.

40. Azem, A.; Man, F.; Omanovic, S., Direct regeneration of NADH on a ruthenium modified glassy carbon electrode. *J Mol Catal a-Chem* **2004,** *219* (2), 283-299.

41. Man, F.; Omanovic, S., A kinetic study of NAD(+) reduction on a ruthenium modified glassy carbon electrode. *J Electroanal Chem* **2004,** *568* (1-2), 301-313.

42. Vuorilehto, K.; Lutz, S.; Wandrey, C., Indirect electrochemical reduction of nicotinamide coenzymes. *Bioelectrochemistry* **2004,** *65* (1), 1-7.

43. Steckhan, E., Electroenzymatic Synthesis. *Electrochemistry V* **1994,** *170*, 83-111.

44. Lutz, J.; Hollmann, F.; Ho, T. V.; Schnyder, A.; Fish, R. H.; Schmid, A., Bioorganometallic chemistry: biocatalytic oxidation reactions with biomimetic NAD(+)/NADH co-factors and [Cp*Rh(bpy)H](+) for selective organic synthesis. *J Organomet Chem* **2004,** *689* (25), 4783-4790.

45. Truppo, M. D., 7.4 Cofactor Recycling for Enzyme Catalyzed Processes. In *Comprehensive Chirality*, Carreira, E. M.; Yamamoto, H., Eds. Elsevier: Amsterdam, 2012; pp 46-70.

46. Walsh, K. A. J.; Daniel, R. M.; Morgan, H. W., A Soluble Nadh Dehydrogenase (Nadh-Ferricyanide Oxidoreductase) from Thermus-Aquaticus Strain T351. *Biochemical Journal* **1983,** *209* (2), 427-433.

47. Shively, J. M.; Cannon, G. C.; Heinhorst, S.; Fuerst, J. A.; Bryant, D. A.; Gantt, E.; Maupin-Furlow, J. A.; Schüler, D.; Pfeifer, F.; Docampo, R.; Dahl, C.; Preiss, J.; Steinbüchel, A.; Federici, B. A., Intracellular Structures of Prokaryotes: Inclusions, Compartments and Assemblages. In *Encyclopedia of Microbiology (Third Edition)*, Schaechter, M., Ed. Academic Press: Oxford, 2009; pp 404-424.

48. Marguet, M.; Bonduelle, C.; Lecommandoux, S., Multicompartmentalized polymeric systems: towards biomimetic cellular structure and function. *Chemical Society reviews* **2013,** *42* (2), 512-529.

49. Ho, D.; Chu, B.; Schmidt, J. J.; Brooks, E. K.; Montemagno, C. D., Hybrid protein-polymer biomimetic membranes. *Ieee T Nanotechnol* **2004,** *3* (2), 256-263.

50. Ho, D.; Schmidt, J. J.; Montemagno, C. D., Protein/polymer hybrid biomimetic valves. *Bioinspired Nanoscale Hybrid Systems* **2003,** *735*, 45-48.

51. Ho, D.; Chu, B.; Schmidt, J. J.; Brooks, E. K.; Montemagno, C. D., Hybrid protein/polymer biomimetic membranes. *2003 Third Ieee Conference on Nanotechnology, Vols One and Two, Proceedings* **2003**, 379-382.

52. Tanner, P.; Egli, S.; Balasubramanian, V.; Onaca, O.; Palivan, C. G.; Meier, W., Can polymeric vesicles that confine enzymatic reactions act as simplified organelles? *FEBS letters* **2011,** *585* (11), 1699-1706.

53. Almen, M. S.; Nordstrom, K. J. V.; Fredriksson, R.; Schioth, H. B., Mapping the human membrane proteome: a majority of the human membrane proteins can be classified according to function and evolutionary origin. *Bmc Biol* **2009,** *7*.

54. Nelson, D. L.; Lehninger, A. L.; Cox, M. M., *Lehninger principles of biochemistry*. 5th ed.; W.H. Freeman: New York, 2008; p 1158, [105] p.

55. Choi, H. J.; Montemagno, C. D., Recent Progress in Advanced Nanobiological Materials for Energy and Environmental Applications. *Materials* **2013,** *6* (12), 5821-5856.

56. Steffen, W.; Steuber, J., Cation transport by the respiratory NADH: quinone oxidoreductase (complex I): facts and hypotheses. *Biochemical Society transactions* **2013,** *41*, 1280-1287.

57. Baradaran, R.; Berrisford, J. M.; Minhas, G. S.; Sazanov, L. A., Crystal structure of the entire respiratory complex I. *Nature* **2013,** *494* (7438), 443-448.

58. Brandt, U., Energy Converting NADH: Quinone Oxidoreductase (Complex I). *Annual review of biochemistry* **2006,** *75* (1), 69-92.

59. Efremov, R. G.; Baradaran, R.; Sazanov, L. A., The architecture of respiratory complex I. *Nature* **2010,** *465* (7297), 441-U61.

60. Ohnishi, T.; Nakamaru-Ogiso, E.; Ohnishi, S. T., A new hypothesis on the simultaneous direct and indirect proton pump mechanisms in NADH-quinone oxidoreductase (complex I). *FEBS letters* **2010,** *584* (19), 4131-4137.

61. Nore, B. F., ΔpH driven energy-linked NAD+ reduction in Rhodospirillum rubrum chromatophores. *Archives of biochemistry and biophysics* **1989,** *274* (1), 285-289.

62. Kriegel, S.; Uchida, T.; Osawa, M.; Friedrich, T.; Hellwig, P., Biomimetic Environment to Study E. coli Complex I through Surface-Enhanced IR Absorption Spectroscopy. *Biochemistry-Us* **2014**.

63. Ohnishi, T.; Ohnishi, S. T.; Shinzawa-Ito, K.; Yoshikawa, S., Functional role of Coenzyme Q in the energy coupling of NADH-CoQ oxidoreductase (Complex I): Stabilization of the semiquinone state with the application of inside-positive membrane potential to proteoliposomes. *BioFactors* **2008,** *32* (1-4), 13-22.

64. Selivanov, V. A.; Votyakova, T. V.; Pivtoraiko, V. N.; Zeak, J.; Sukhomlin, T.; Trucco, M.; Roca, J.; Cascante, M., Reactive Oxygen Species Production by Forward and Reverse Electron Fluxes in the Mitochondrial Respiratory Chain. *Plos Comput Biol* **2011,** *7* (3).

65. Kotlyar, A. B.; Borovok, N., NADH oxidation and NAD+ reduction catalysed by tightly coupled inside-out vesicles from Paracoccus denitrificans. *European journal of biochemistry / FEBS* **2002,** *269* (16), 4020-4.

66. Wang, Z. G.; Xu, T. H.; Liu, C.; Yang, C. H., Fast Isolation of Highly Active Photosystem II Core Complexes from Spinach. *J Integr Plant Biol* **2010,** *52* (9), 793-800.

67. Ramesh, V. M.; Fish, A.; Michaeli, D.; Keren, N.; Ohad, I.; Vorchovsky, L.; Nechushtai, R., Isolation and characterization of an oxygen evolving photosystem 2 core complex from the thermophilic cyanobacterium Mastigocladus laminosus. *Photosynthetica* **2002,** *40* (3), 355-361.

68. Kato, M.; Zhang, J. Z.; Paul, N.; Reisner, E., Protein film photoelectrochemistry of the water oxidation enzyme photosystem II. *Chemical Society reviews* **2014,** *43* (18), 6485-6497.

69. Barber, J., Photosystem II: a multisubunit membrane protein that oxidises water. *Current opinion in structural biology* **2002,** *12* (4), 523-530.

70. Saito, K.; Rutherford, A. W.; Ishikita, H., Mechanism of proton-coupled quinone reduction in Photosystem II. *P Natl Acad Sci USA* **2013,** *110* (3), 954-959.

71. Mavelli, F.; Trotta, M.; Ciriaco, F.; Agostiano, A.; Giotta, L.; Italiano, F.; Milano, F., The binding of quinone to the photosynthetic reaction centers: kinetics and thermodynamics of reactions occurring at the Q(B)-site in zwitterionic and anionic liposomes. *Eur Biophys J Biophy* **2014,** *43* (6-7), 301-315.

72. Glockner, C.; Kern, J.; Broser, M.; Zouni, A.; Yachandra, V.; Yano, J., Structural Changes of the Oxygen-evolving Complex in Photosystem II during the Catalytic Cycle. *Journal of Biological Chemistry* **2013,** *288* (31), 22607-22620.

73. Brudvig, G. W., Water oxidation chemistry of photosystem II. *Philosophical Transactions of the Royal Society B: Biological Sciences* **2008,** *363* (1494), 1211-1219.

2. A Rapid and Scalable Purification Procedure for Purple Membrane and Bacteriorhodopsin.

Abstract

Bacteriorhodopsin (bR), found in the purple membrane (PM) of Halobacterium, is a transmembrane 26 kDa photoreceptor protein that functions as a light-activated proton pump. Patches of the PM consist of approximately 75% bR and 25% lipid by mass. Within the PM, bR is organized as trimers arranged in a 2D hexagonal crystalline lattice, forming sheets on the micron scale[1-3].

With the advancement in nanotechnology, bR has become a leading candidate for application in devices, including three-dimensional optical memories, real-time holographic media, photovoltaic cells[4] and artificial retinas[5]. Purification methods are currently unsuitable for commercial scale production of PM and bR, limited by size-exclusion chromatography[6], ultracentrifugation[7-8], density gradient separations[9], and use of specialized equpitment[10]. A considerable amount of effort has been conduction of the recombinant expression of bR in *E. coli*, using affinity tags to simplify isolation of the protein[11-12]. As with most recombinant expression of exogenous membrane proteins issues of low yields and improper folding are problematic[13]. However, with optimized growth conditions, *H. salinarum* is capable of producing > 230 mg bR L^{-1} of culture medium[14] far exceeding the yields of recombinant systems[12].

In this research, we sought to develop a robust, scalable procedure for the isolation of PM and the solubilized bR. Taking advantage of the large size of PM patches and the

use of tangential flow filtration (TFF), we present a simple, rapid and robust procedure for the isolation of large quantiles of PM, bR with purities exceeding 99% and recovery of > 90%.

Results and Discussion

Determination TFF Parameters

We based our selection of the appropriate MWCO for the filter module by the resulting purity, total retention of PM and processing time. We found that modules with an MWCO < 500 kDa resulted in poor purity (

Figure 2.2A), and long processing times as expected from their lower permeate rates. When an MWCO of 750 kDa was used the purity of PM increased by 10.13 ± 1.88% over the 500 kDa module. Additionally, 196 ± 11% reduction in processing time was also achieved. Further increasing the cut-off of the module into the microfiltration (0.1 & 0.2 μM) the retention of PM was inconsistent, and the data is not included in this report.

Our analysis of the content in the permeate fractions by SDS-PAGE showed that the 750 kDa module retains nearly all the PM/bR with only 0.57 ± 0.68% of the total protein found in the permeate being PM/bR (Figure 2.1). The highest relative percent of PM/bR content is found in fractions during the 1st concentration and DF step (Figure 2.3C).

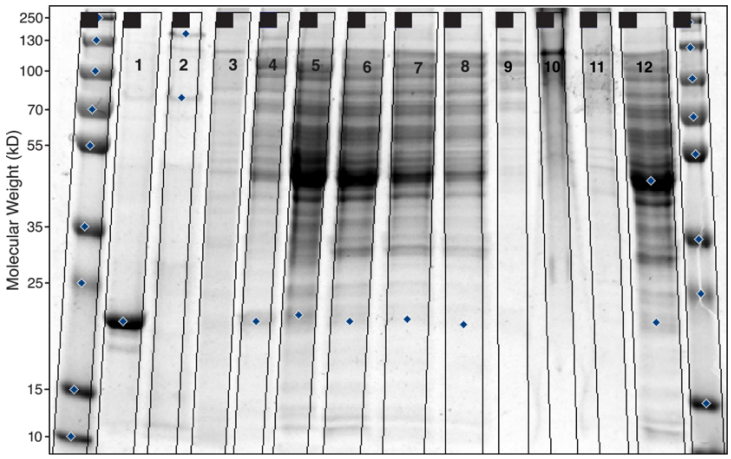

Figure 2.1 | SDS-PAGE of permeate fractions: permeate fractions, 1-5 are shown in lanes labeled 5-9. Lane labeled 12 is 10 µL of the 60x concentration of the remaining permeate fractions.

As shown in Figure 2.2B the protein content found in the permeate decreases exponentially with only ~30% of the initial protein content found after the third DV in first DF step at which point CHAPS was included into the DF buffer.

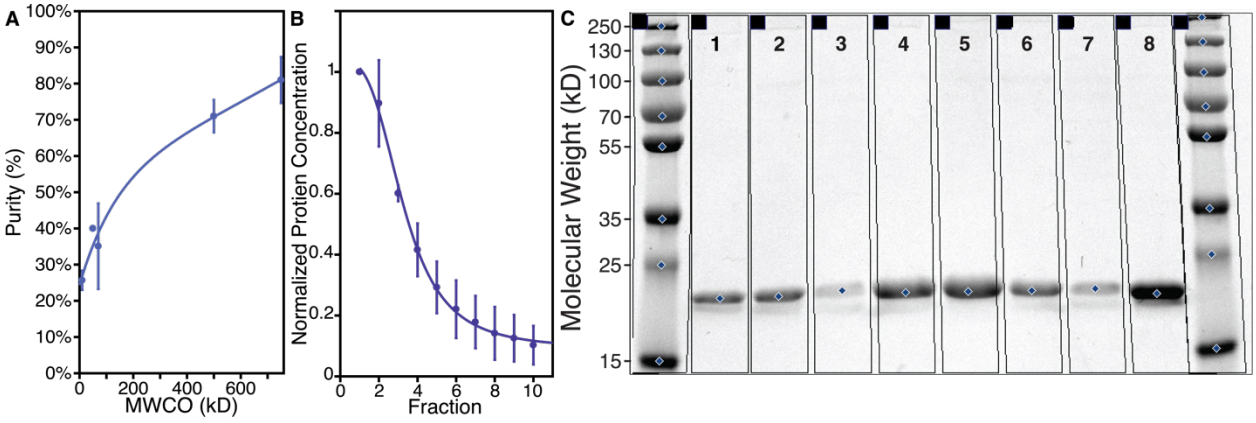

Figure 2.2 | A, Purity of PM of post TFF for various MWCO filters, n = 3 for all except for 70 kDa (n = 1). B, Normalized permeate protein concentration, each fraction represents 1 WV (n = 3). The error bars in A & B represent the standard deviation. C, SDS-PAGE of 8 independent preparations, labeled 1-8, of PM following the cell debris removal step. The

first and last lane contain molecular weight markers with their weights (kDa) labeled on the left of the gel.

We selected CHAPS to be used for the delipidation step for several reasons. The first reason, CHAPS is incapable of solubilizing PM into multimeric/monomeric bR and only capable of removing excess lipid from PM[15]. To avoid unwanted concentration of the detergent during the TFF process, a detergent which does not form high molecular weight micelles and ideally has a high critical micelle concentration (CMC), both properties of CHAPS[16] is required.

The protein content found in the fractions during the delipidation process was low and does not significantly decrease over the duration of the delipidation step. However, almost immediately after 1 DV permeates the permeate color becomes a crimson-red color, due to the presence of red carotenoid pigments lipids[9, 17]. It is important to note, during the delipidation step vigorous mixing within the reservoir is required. If mixing is not adequate phase separation will occur between the buffer and the PM fragments. The lack of mixing can result in over-pressurization of the filter module and premature concentration of the PM.

In our initial experiments, we performed the low-speed centrifugation step for the removal of cellular debris before the TFF process. We opted to move the cellular debris removal step following the TFF process because large PM fragments that pelleted with the debris is difficult to resuspend without reintroducing debris to the bulk phase. Furthermore, the cellular debris persistently remained post the TFF procedure. Using this processing scheme (Figure 2.3C), there are no impurities seen by SDS-PAGE analysis of 8 independent preparations with purities of 98.58 ± 1.53% (

Figure 2.2C).

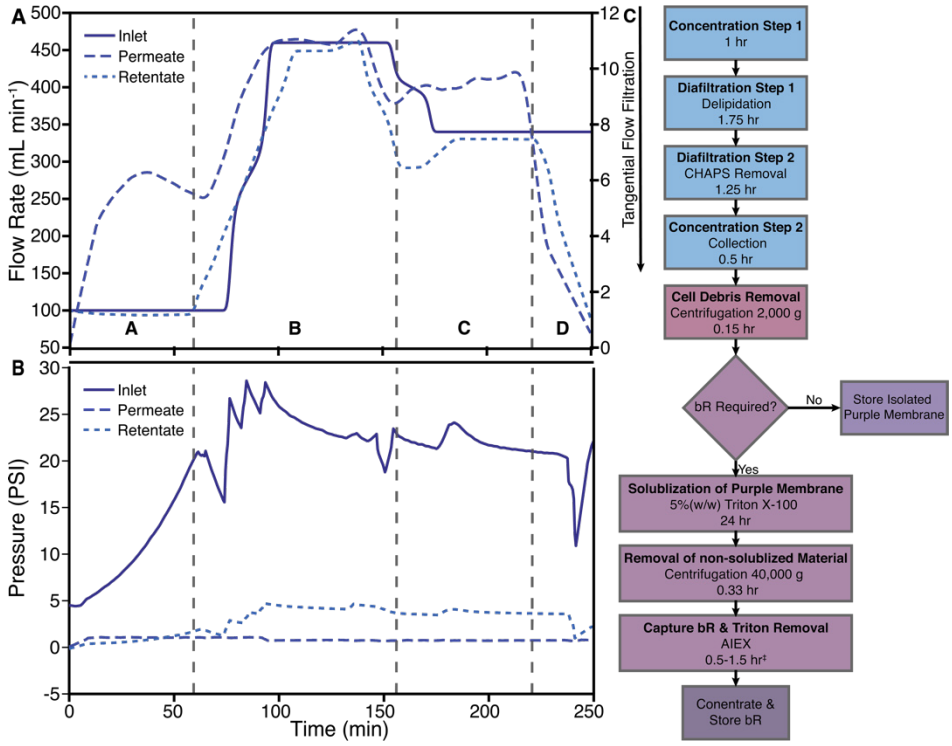

Figure 2.3 | A, Traces of Flow Rates for a 235 cm^2 membrane with an MWCO of 750 kDa, the permeate flow rate (mL min^{-1}) is located on the right y-axis B, Traces of pressures for a 235 cm^2 membrane with an MWCO of 750 kDa. Areas labeled A, B, C, and D are traces for concentration step 1, diafiltration step 1, diafiltration step 2 and concentration step 2, respectively. C, process flow diagram for the isolation of PM and solubilized bR.

<u>bR capture and removal/exchange of Triton X-100 by AIEX</u>

PM is notoriously challenging to solubilize into bR and Triton X-100 (TX) has been shown to be the most successful[15]**.** The consequences of using TX are due to its low CMC and the high MW of the micelles it forms[18]. These properties of TX make the removal of the high concentrations of TX required for solubilization or the exchange of TX to a different detergent non-practical by dialysis or TFF because of the volume of buffer and time required[19].

By taking advantage of the low isoelectric point of bR[20] and the use of a strong anionic exchange resin, makes it possible for the rapid removal/exchange of TX and concentration of bR. The high purity of the material resulting from the TFF procedure permits the use of a steep linear gradient (1-2 CVs) or a step gradient (

Figure 2.4). However, if a monodispersed population of monomeric of trimeric bR is required, a 10 CV linear gradient from 0-600 mM NaCl can be used, with higher order multimers eluting later as expected (Figure 2.5)

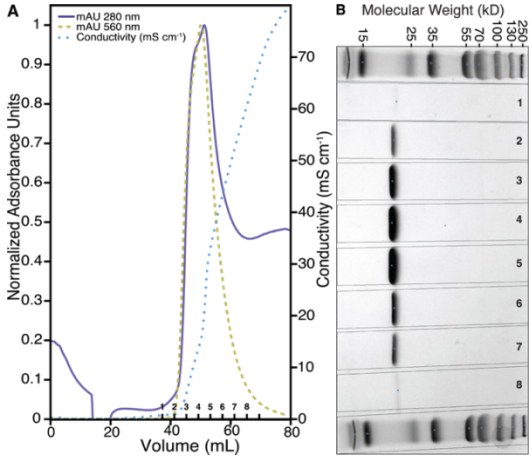

Figure 2.4 | A, Chromatogram of AIEX chromatographic capture of solubilized bR and removal of excess Triton X-100. Located on the left y-axis the normalized absorbance units for 280 nm (solid line) and 560 nm (dashed line). The right y-axis is the conductivity (do *dotted line*). The solid black and labeled lines on the inside of the x-axis for the corresponding (1-8) fraction volumes. B, SDS-PAGE of fractions 1-8 as indicated by the solid black labeled lines on figure A. The top and bottom lanes are molecular weight markers with their weights (kDa) labeled on the top of the gel.

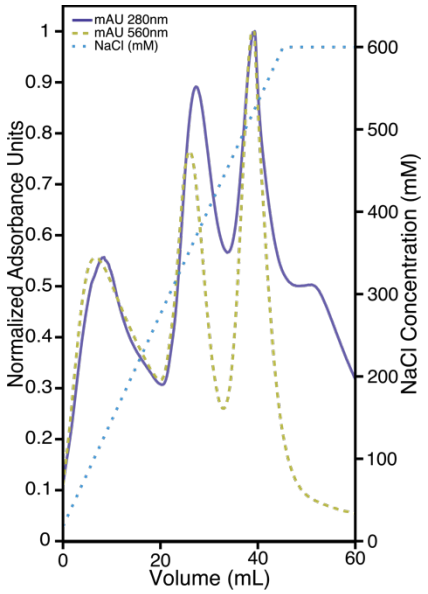

Figure 2.5 | Elution profile of solubilized bR using a 10 CV linear gradient. The first peak is weakly bound sample washed away from the change in flow direction. The second and third peaks are monomeric and trimeric bR, respectively.

Following the concentration of the pooled fractions from the AIEX the homogeneity of the sample was determined by size exclusion chromatography (Figure 2.6A). The chromatogram has four distinct peaks, three of which of different forms of bR. The first peak (**a**) makes up < 3% of the total peak area, elutes at the void volume of the column indicating, non-solubilized PM. The following two peaks (**b & c**) are trimeric and monomeric bR, respectively. The elution volumes of peaks b and c are in good agreement with MW of their DDM bound counterparts and strengthen by SDS-PAGE analysis (Figure 2.6B). The final peak, having no detectable absorbance at 560 nm or protein following 25x concentration we hypothesis is TX-DDM mixed micelles[21] formed by a small amount of TX that remains tightly bound to bR following detergent exchange in the previous step.

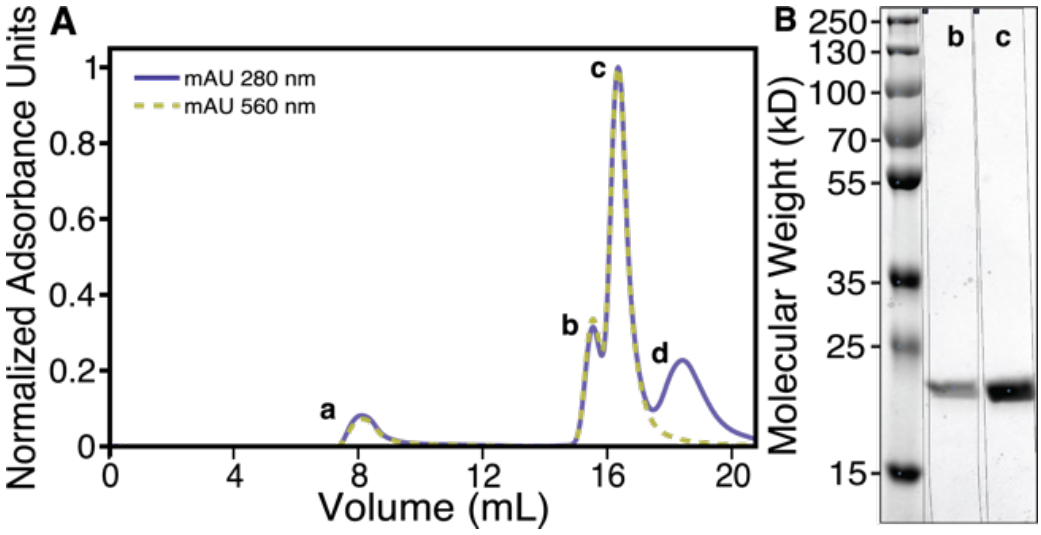

Figure 2.6 | Chromatogram of size exclusion of solubilized bR following AIEX. A, The normalized absorbance units for 280 nm (solid line) and 560 nm (dashed line) are located on the left y-axis. B, SDS-PAGE of peaks labeled b & c in figure A. The left lane is the is the molecular weight markers with their weights (kDa) labeled on the left of the gel.

The solubilized bR retained 82.5 ± 0.5% of its activity for 24 months as measured by the total ACMA quenching over a 30 min illumination cycle remained when at 4°C (Figure 2.7A) with no proteolytic fragments or change in apparent molecular weight (Figure 2.7B).

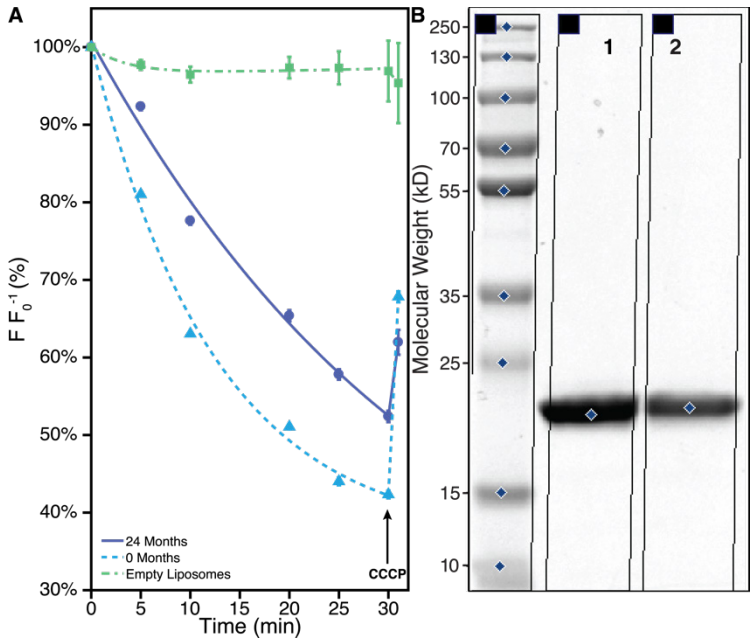

Figure 2.7 | A, ∆pH generation by reconstituted solubilized bR at 0 months of storage (dashed line) and 24 months of storage (solid line) and the empty liposomes control sample (dash-dotted line). At 30 min 5 µM CCCP indicated by the CCCP labeled arrow was added to the samples to abolish the ∆pH. B, SDS-PAGE of solubilized bR at 0 months (lane labeled 1) and 24 months of storage (lane labeled 2). The left lane is the molecular weight markers with their weights (kDa) labeled on the left of the gel.

Materials and Methods

All chromatographic steps were performed using an ÄKTA Avant 150 (GE Healthcare Life Sciences, Inc.) at room temperature (RT) while monitoring the absorbance at 280 nm and 550 nm. All centrifugation steps use a Beckman Coulter Type 70-Ti Rotor unless indicated otherwise. Protein concentration was determined using Millipore Direct Detect® infrared spectrometer (EMD Millipore, Inc.). We performed all enzymatic activity assays at 28°C. Fluorescence measurements were done using a Flexstation 3 (Molecular Devices, Inc.). To measure proton gradient

generation, we employed the pH-sensitive fluorophore 9-amino-6-chloro-2-methoxyacridine (ACMA) and measured the quenching of the signal (λ_{ex} = 410nm, λ_{em} = 480nm).

Growth of Cells and Cell Lysis

H. salinarum S9 cultures were grown as previously described[22] with the addition of light. Cells were harvested by centrifugation at 10,000 rcf x 20 min using a JLA-9.1000 rotor in early stationary phase as monitor by absorbance at 600 nm. Cells that we did not immediately use for protein purification are stored at -20°C. Cells were disrupted by osmotic shock by suspending the cell pellets at 10 mL g wet cell^{-1} in 4.2 mM $MgSO_4$ supplemented with 100 μg mL^{-1} DNase I and continuously stirred at room temperature overnight. Cellular debris was removed from the cell lysis by centrifugation at 2,000 rcf x 10 min. The purple membrane containing supernatant was decanted and used for further processing.

Isolation and Delipidation of Purple Membrane

The clarified cell lysis, 5 mg cell mass per cm^2 membrane surface area, was subjected to TFF using a KR2 TFF system (Spectrum, Inc.) with size 16 peristaltic tubing (Cole-parmer Instrument Company, LLC.). We tested multiple process variables and membrane molecular weight cut-off (MWCO) for best product purity, retention and overall processing time. The backpressure valve was set to maintain the permeate pressure to 1 psig. The first step of the TFF scheme (Figure 2.3C) was the 5x concentration of clarified cell lysis at inlet flow-rate of 100 mL min^{-1} followed by the diafiltration (DF) of the concentrate against 10 diavolumes (DVs) of 10mM Tris, 2 mM 3-[(3-cholamidopropyl)dimethylammonio]-1-propanesulfonate (CHAPS), 50mM NaCl, pH

7.0. After each subsequent DV, we gradually increase the inlet flow rate until the maximum flow rate is reached while maintaining the inlet pressure below 30 psig. The third step is DF with 3 DVs of 10mM Tris, 50mM NaCl, pH 8.0 to remove the CHAPS while reducing the flow rate to avoid over pressurizing the filter after which the sample can be further concentrated but not necessary. The isolated PM is collected and centrifuged at 2,000 g for 10 min to remove any remaining organelles and was aliquoted, flash frozen and stored at -80°C.

Isolation of bR and excess detergent removal/exchange.

For the solubilization of the PM, we diluted the PM at 1 mg mL^{-1} in 50mM Tris, pH 7.5 with 5% (w/w) TX and incubated overnight with gentle stirring in the dark. Following solubilization, we remove the non-solubilized material by centrifugation (40,000 g x 20 min).

We used Anionic exchange chromatography (AIEX) to remove excess TX or exchange it for n-dodecyl ß-D-maltoside (DDM). The solubilized protein captured using Capto Q resin (GE Healthcare Life Sciences, Inc.) pre-equilibrated with running buffer (RB, 50mM Tris buffer, pH 7.5 containing 0.01%(w/w) TX). The sample is loaded at a linear flow rate of 700 cm h^{-1}. If desired, TX can be exchanged for 0.03%(w/w) DDM. After sample loading, a wash step continued until the A_{280} signal stabilized. The stable A_{280} signal indicates the removal of excess TX or the complete exchange of TX with DDM. We eluted the bR in up-flow operation with a linear flow rate of 250 cm h^{-1}, using 20% of RB with 1M NaCl. Using a reduced linear flow rate and up-flow operation results in a higher concentration of bR in the elution fractions.

The pooled fractions were desalted by 3x DF into RB and concentrated to ~ 4 mg mL^{-1} with Amicon Ultra-15 spin tubes (3kDa MWCO) centrifuged at 4,000 g for 30 min. The protein was aliquoted, flash frozen using liquid nitrogen and stored at -80°C.

Unilamellar Liposome preparation

POPE and POPG lipids at a 3:1 (w/w) (Avanti Lipids Polar, Inc.) were dissolved in Chloroform ($CHCl_3$) at 20 mg mL^{-1} in a glass scintillation vial. A thin film formed by removal of the $CHCl_3$ under vacuum using a rotary evaporator set to 0 psig. The thin film is rehydrated to 15.34 mg mL^{-1} using 5 mM MES, pH 6.5 50 mM KCl, 5 mM $MgCl_2$ 2 mM $CaCl_2$ buffer and placed in a sonication bath for 5 min followed by two freeze-thaw cycles before being extruded through a 0.4 μm polycarbonate membrane 21 times.

Enzyme Reconstitution

The unilamellar liposomes suspension is diluted to a final lipid concentration of 4 mg mL^{-1} and CHAPS concentration of 5 mM by the combination of appropriate amounts of the corresponding buffer, 200 mM CHAPS in the corresponding buffer and concentrated protein. The liposomes-detergent mixture was incubated for 10 min before the addition of protein. The appropriate amount of bR (4.0 mg mL^{-1}) was added to the CHAPS-solubilized preformed liposomes and incubated for 30 min at RT under gentle mixing in the dark. For control experiments, which did not contain an bR, the difference in volume was adjusted with buffer.

After the incubation period, the detergent was removed from the lipid-detergent-protein mixture by three successive additions of Bio-Beads SM-2 (80 mg mL^{-1}) every 60 min followed by a final addition of 240 mg mL^{-1} and 60 min incubation.

Activity Assay

To measure the light activated proton-pumping activity of bR, proteoliposomes (25µL) was added to the assay mixture to obtain a final concentration of 0.2 µM valinomycin, 2.5 µM 9-amino-6-chloro-2-methoxyacridine (ACMA) in the corresponding buffer. The final assay volume was 200 µL. We incubated the sample for 5 min before initiating by the addition by green light (1800 µmol photons s^{-1} m^{-2}). For decoupling assays 5 µM Carbonyl cyanide m-chlorophenyl hydrazine (CCCP) was added at the indicated time point.

References

1. Neugebauer, D.-C.; Zingsheim, H.-P.; Oesterhelt, D., [21] Biogenesis of purple membrane in halobacteria. In *Methods in Enzymology*, Academic Press: 1983; Vol. Volume 97, pp 218-226.

2. Krebs, M. P.; Isenbarger, T. A., Structural determinants of purple membrane assembly. *Biochimica et biophysica acta* **2000,** *1460* (1), 15-26.

3. Stoeckenius, W.; Lozier, R. H.; Bogomolni, R. A., Bacteriorhodopsin and the purple membrane of halobacteria. *Biochimica et Biophysica Acta (BBA) - Reviews on Bioenergetics* **1979,** *505* (3), 215-278.

4. Mahyad, B.; Janfaza, S.; Hosseini, E. S., Bio-nano hybrid materials based on bacteriorhodopsin: Potential applications and future strategies. *Advances in colloid and interface science* **2015,** *225*, 194-202.

5. Wagner, N. L.; Greco, J. A.; Ranaghan, M. J.; Birge, R. R., Directed evolution of bacteriorhodopsin for applications in bioelectronics. *Journal of the Royal Society Interface* **2013,** *10* (84).

6. Huang, K. S.; Bayley, H.; Khorana, H. G., Delipidation of bacteriorhodopsin and reconstitution with exogenous phospholipid. *Proceedings of the National Academy of Sciences of the United States of America* **1980,** *77* (1), 323-7.

7. Yu, S. M.; McQuade, D. T.; Quinn, M. A.; Hackenberger, C. P.; Krebs, M. P.; Polans, A. S.; Gellman, S. H., An improved tripod amphiphile for membrane protein solubilization. *Protein science : a publication of the Protein Society* **2000,** *9* (12), 2518-27.

8. Shiu, P.-J.; Ju, Y.-H.; Chen, H.-M.; Lee, C.-K., Facile isolation of purple membrane from Halobacterium salinarum via aqueous-two-phase system. *Protein expression and purification* **2013,** *89* (2), 219-224.

9. Becher, B. M.; Cassim, S. Y., Improved Isolation Procedures for the Purple Membrane of Halobacterium Halobium. *Preparative biochemistry* **1975,** *5* (2), 161-178.

10. Shiu, P.-J.; Chen, H.-M.; Lee, C.-K., One-step purification of delipidated Bacteriorhodopsin by aqueous-three-phase system from purple membrane of Halobacterium. *Food and Bioproducts Processing* **2014,** *92* (2), 113-119.

11. Genji, T.; Nozawa, A.; Tozawa, Y., Efficient production and purification of functional bacteriorhodopsin with a wheat-germ cell-free system and a combination of Fos-choline and CHAPS detergents. *Biochemical and biophysical research communications* **2010,** *400* (4), 638-42.

12. Nekrasova, O. V.; Wulfson, A. N.; Tikhonov, R. V.; Yakimov, S. A.; Simonova, T. N.; Tagvey, A. I.; Dolgikh, D. A.; Ostrovsky, M. A.; Kirpichnikov, M. P., A new hybrid protein for production of recombinant bacteriorhodopsin in Escherichia coli. *Journal of biotechnology* **2010,** *147* (3), 145-150.

13. Link, A. J.; Georgiou, G., Advances and challenges in membrane protein expression. *AIChE Journal* **2007,** *53* (4), 752-756.

14. Ghasemi, M. F.; Shodjai-Arani, A.; Moazami, N., Optimization of bacteriorhodopsin production by Halobacterium salinarium PTCC 1685. *Process Biochemistry* **2008,** *43* (10), 1077-1082.

15. Seigneuret, M.; Neumann, J. M.; Rigaud, J. L., Detergent delipidation and solubilization strategies for high-resolution NMR of the membrane protein bacteriorhodopsin. *Journal of Biological Chemistry* **1991,** *266* (16), 10066-10069.

16. Linke, D., Chapter 34 Detergents: An Overview. In *Methods in Enzymology*, Burgess, R. R.; Deutscher, M. P., Eds. Academic Press: 2009; Vol. 463, pp 603-617.

17. Sehgal, S. N.; Kates, M.; Gibbons, N. E., LIPIDS OF HALOBACTERIUM CUTIRUBRUM. *Canadian Journal of Biochemistry and Physiology* **1962,** *40* (1), 69-81.

18. Paradies, H. H., Shape and size of a nonionic surfactant micelle. Triton X-100 in aqueous solution. *The Journal of Physical Chemistry* **1980,** *84* (6), 599-607.

19. Rigaud, J. L.; Levy, D., Reconstitution of membrane proteins into liposomes. *Liposomes, Pt B* **2003,** *372*, 65-86.

20. Miercke, L. J.; Ross, P. E.; Stroud, R. M.; Dratz, E. A., Purification of bacteriorhodopsin and characterization of mature and partially processed forms. *Journal of Biological Chemistry* **1989,** *264* (13), 7531-7535.

21. Tschapek, B.; Smits, S. H. J.; Schmitt, L., Analyzing the Physico-Chemical Parameters of Detergents and Detergent Mixtures. *Advances in Chemical Engineering and Science* **2015,** *Vol.05No.03*, 10.

22. Lee, H.; Ho, D.; Kuo, K.; Montemagno, C. D., Vectorial insertion of bacteriorhodopsin for directed orientation assays in various polymeric biomembranes. *Polymer* **2006,** *47* (9), 2935-2941.

3. Light-Driven Reversibility of Respiratory Complex I for NADH Regeneration.

Introduction

Over recent years cell-free metabolic systems have gained considerable attention. Cell-free metabolic systems have many advantages over traditional chemistry. By capitalizing on the ability of biological molecules to catalyze reactions with unprecedented specificity at physiological temperatures and pH a plethora of green alternative synthetic pathways become available to replace traditional chemistry. Before cell-free metabolic systems can become a disruptive technology, providing and adjusting energy at the nanoscale must be addressed. Enzymatic cofactors are the most cost prohibitive component of cell-free metabolic systems and are responsible for providing the energy for enzymes to proceed in otherwise thermodynamically unfavorable reactions. Due to the cost and stability of enzymatic cofactors like nicotinamide adenine dinucleotide (NADH) recycling coenzymes is essential. Here we introduce a proof of principle engineered biotic/abiotic organelle capable of reducing NADH. This device pairs two membrane protein complexes that do not interact naturally: NADH: Ubiquinone oxidoreductase (CMI) and bacteriorhodopsin (bR). Through the controlled directional insertion into 180 nm liposomes, these two proteins function collectively to reduce NAD^+. In this study, we demonstrate the use of CMI for NAD^+ reduction showing that bR can provide the proton motive force necessary for CMI to transfer electrons from quinonol to NAD^+. Additionally, we show the introduction of the CMI inhibitor piericidin A, enhances NAD^+ reduction rates.

Cell-free metabolic engineering (CFME) has been gaining considerable attention for a variety of technologies over recent years[1]. Decoupling the cellular machinery responsible for cellular maintenance and growth from the biochemical pathway of interest yields many advantages. After eliminating the biological constraints and by directing all biochemical resources to an individual aim, results in high production yields, permits broad reaction conditions, simpler metabolic pathway engineering and control. Cell-free metabolic system (CFMS) platforms for producing low-value chemicals (LVCs), fine chemicals and biologics[2] have become increasingly elaborate. For example, demonstrations of systems using 8[3], 16[4], and 28 enzymes[5], which shows cell-free metabolic systems have the potential of developing into a disruptive technology to microbial fermentation.

For CFMS to be self-sustaining and have high productivity, replenishing energy to the system as enzymatic cofactors like ATP and NAD(P)H is imperative. Maintaining energy requirements is a considerable challenge for CFMS due to the absence of the complicated regulatory networks that produce and balance enzymatic cofactors. When designing in vitro metabolic pathways, ATP and NAD(P)H balance is a crucial consideration as imbalances will lead to incomplete conversions. Furthermore, the cost of simple addition of cofactors is cost prohibitive and can be deleterious, leading to enzymatic inhibition. In some cases, it has been possible to form redox neutral pathways[6-8], or include purge mechanisms to remove excess cofactor[9-10]. Nevertheless, these approaches place inflexible constraints on designs, need additional enzymes increasing complexity, or exclusively applicable to one biosynthetic scheme.

Ideally, a device must regulate cofactor balance without impacting carbon flux, only require inexpensive and abundant inputs and be compatible with any CFMS. An example of such a device is an artificial organelle which ATPase and bacteriorhodopsin (bR) are co-reconstituted into a membrane for ATP regeneration[11-12]. bR functions by harvesting light and translocating protons (H^+) creating a pH gradient (ΔpH) across the membrane. The ΔpH provides the potential to drive ATPase to form ATP[3]. The rate of ATP formation corresponds to the magnitude of the ΔpH which is proportional to the intensity of light[13]. This ATPase/bR artificial organelle makes it possible to regenerate ATP from light for artificial photosynthesis[3]. Until now, no device with similar attributes was available for NADH recycling and balance. Ordinarily, the NADH regeneration is done using single- or two-enzyme substrate coupled systems[14-16]. NADH regeneration through these techniques has various shortcomings. The addition of exogenous substrate serving as an electron donor creates byproducts, shifting the reaction equilibrium and inhibiting enzymatic cascades. These are considerable drawbacks for any CFMS making them incapable of self-sustainability and any additive cost is prohibitive in producing LVCs.

In this study, we engineered an artificial organelle capable of photoreduction of NAD^+ by integrating bR and CMI into liposomes in specific directions (

Figure 3.1). The power source for this device is light which activates the proton translocation by bR. As a result, the accumulation of H^+ within the lumen creates a proton motive force (PMF). The PMF is requisite to diminish the thermodynamic gap of the standard redox potentials between NADH/NAD^+ and QH_2/Q. Reducing the thermodynamic barrier enables CMI to perform reverse electron transfer (RET) from

QH_2 to NAD^{+}[17-18]. Combing the associated actives of these two enzymes demonstrates the foundation of a platform for NADH recycling for cell-free metabolic systems.

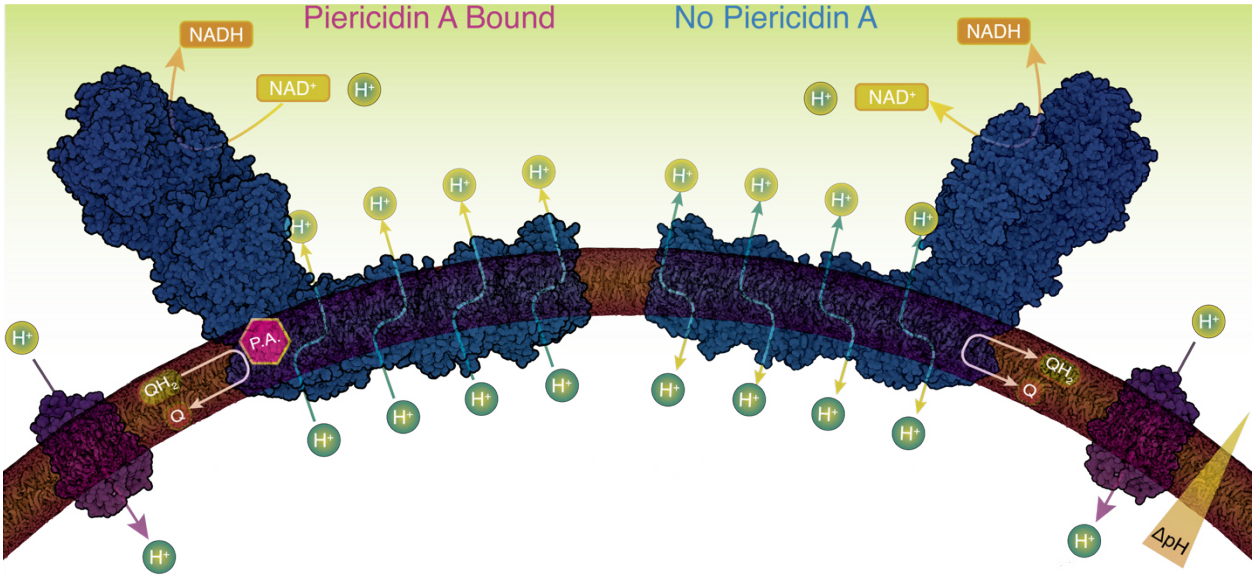

Figure 3.1 | Illustration of Complex I and Bacteriorhodopsin reconstituted into liposomes. The purple enzyme icon represent bR and the large blue icon represents CMI. The illustration on the right, No Piercidin A, depicts CMI working in the forward and reverse direction while the figure on the left depicts the Piercidin A (P.A.) bound CMI working in exclusively in reverse direction (NAD^{+} reduction). The pink arrows represent the flow of Q and QH_2 in and out of CMI to membrane pool. The green H^{+} translocated by bR generate a PMF within the lumen liposome depicted by the arrow labeled ΔpH. The oxidation of QH_2 by CMI is coupled to H^{+}-translocation and the reduction of NAD^{+} to NADH. This illustration was created using the crystal structures of CMI from *T. thermophilus*[19] and *H. salinarum* for bR[20].

Results and Discussion

The experiments we initially conducted were to conclude that the (+)CMI(+)bR proteoliposomes could reduce NAD^{+} and find suitable assay conditions.

Other publications suggest RET by CMI has a higher dependence on the ΔpH then the ΔΨ electrical component of the PMF for RET[21]. To generate a higher ΔpH, we included valinomycin in the assay. Valinomycin is a potassium ionophore and in turn, eliminates the electrical component of the PMF allowing bR to generate higher pH gradients[22]. However, it has reported that high concentrations of valinomycin can have an inhibitory effect on bR[23]. We tested two concentrations of valinomycin 0.1 μM and 0.2 μM. There is a significant and moderately strong correlation ($r > 0.44$) and between valinomycin concentrations and NAD^+ reductase rate only when P.A. is present (Figure 2). In proton pumping assays, 0.2 μM valinomycin quenched the ACMA more than 0.1 μM. The results of our experiments are in agreement other reports that RET by CMI has a higher dependence on ΔpH then ΔΨ and we proceeded to use 0.2 μM valinomycin in additional experiments.

Reactive oxygen species (ROS) generation by mammalian CMI during RET is well documented[24]. Published information is limited for RET by *E. coli* CMI but, given the conservative nature of CMI between species, it is logical that bacterial CMI would also produce ROS during RET. To mitigate the possible detrimental effects that ROS would have on the device we opted to investigate if including dithiothreitol (DTT) would have a positive effect of NAD^+ reduction. We found when 1.0 mM DTT was present that there is a significant (*p*-value < .01) and adverse effect on the reduction of NAD^+ whereas 0.2 and 0.4 mM had no significant effect. These results are unexpected, and the cause for these findings are outside the scope of this work but may be caused by the electron transfer reactions between the FMN containing active site of CMI with DTT[25].

One of the most significant findings in this work was the effect of piericidin A (P.A.) on the reduction of NAD^+. P.A. is a well-known and potent inhibitor of the oxidation of NADH by CMI[26]. When we included 50 µM P.A., NADH oxidation was inhibited > 95% (see SI for further information) however, the NAD^+ reductase rates were significantly increased with a strong positive correlation coefficient (r > 0.92). This finding was most prominent in the in experiments that contained 0.0 and 1.0 mM DTT (Figure 3.2A, D, E & H), resulting in rates nearly 3 and 4 times that of samples which contain no P.A.. Kotlyar and et. el. reported similar findings for the inhibitor rotenone in CMI from *Paracoccus denitrificans*[27]. The two-quinone binding sites may explain the inability for P.A. to inhibit RET[28-29].

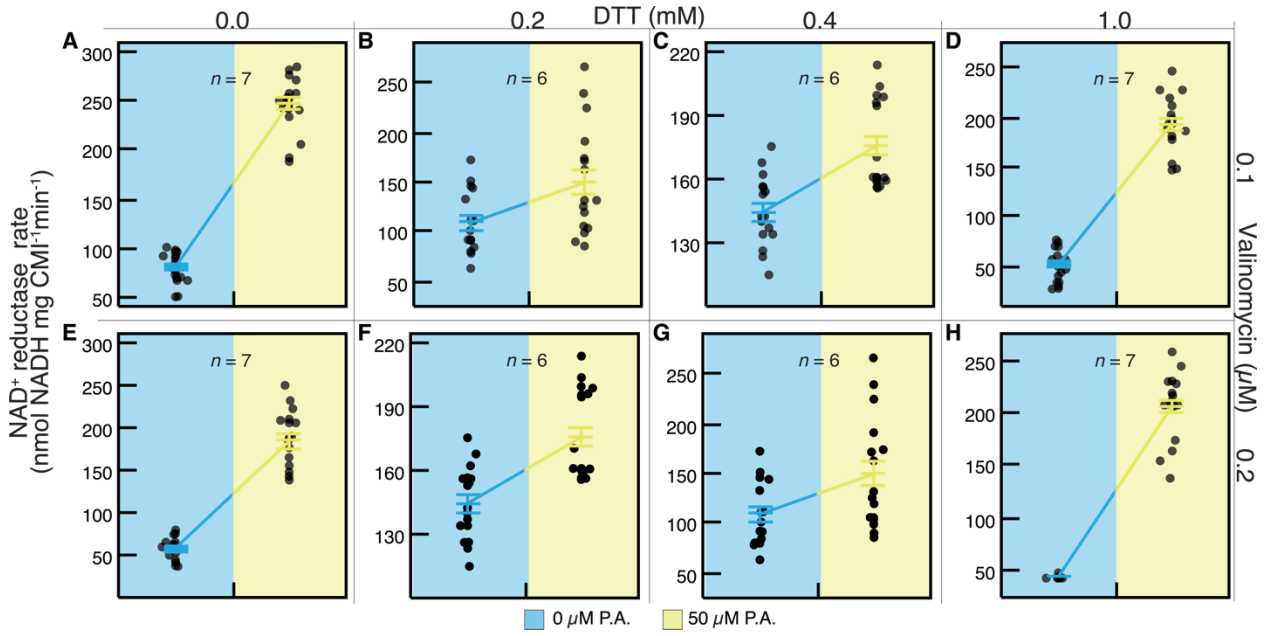

Figure 3.2 | NAD^+ reductase rate CMI BR proteoliposomes varying DTT and valinomycin concentrations one-way ANOVA of 0 µM P.A. vs. 50 µM P.A. DTT concentration increase from left to right (0.0, 0.2, 0.4, 1.0 mM) and valinomycin concentration increases top to bottom (0.1 and 0.2 µM). Points within the blue region of each panel have 0 µM P.A. and

points in the yellow region have 50 μM P.A.. The error bars represent the standard error of the mean of n biological replicates indicated in each figure panel.

To confirm that NADH is produced we performed control experiments at multiple points along the mechanism of the device. We tested proteoliposomes that did not contain bR for confirmation that bR was providing a ∆pH to activate RET by CMI (Figure 3.3A-D). When incorporating bR into the proteoliposomes with CMI, there was a significant difference with strong positive correlation coefficients for all conditions tested indicating that bR is responsible for creating a ∆pH. We then compared samples incubated under light and dark conditions (Figure 3.3E-F). We found that when the samples incubated in the dark produced little or no NADH and light was responsible for the NADH production through the activation of bR ($r > 0.96$). Additionally, the experiments showed no significant difference between the (-)bR samples and the (-)Light samples and similar slopes in the response found in (±)bR. Moreover, to determine if the ∆pH generated by bR was necessary for NADH production we included 5 μM CCCP, a protonophore (Figure 3.3G-H). With CCCP present a ∆pH is unable to establish and results in negative and significant response (*p*-value < .001 & < .0001, $r < -0.95$ for 0.0 and 1.0 mM DTT respectively).

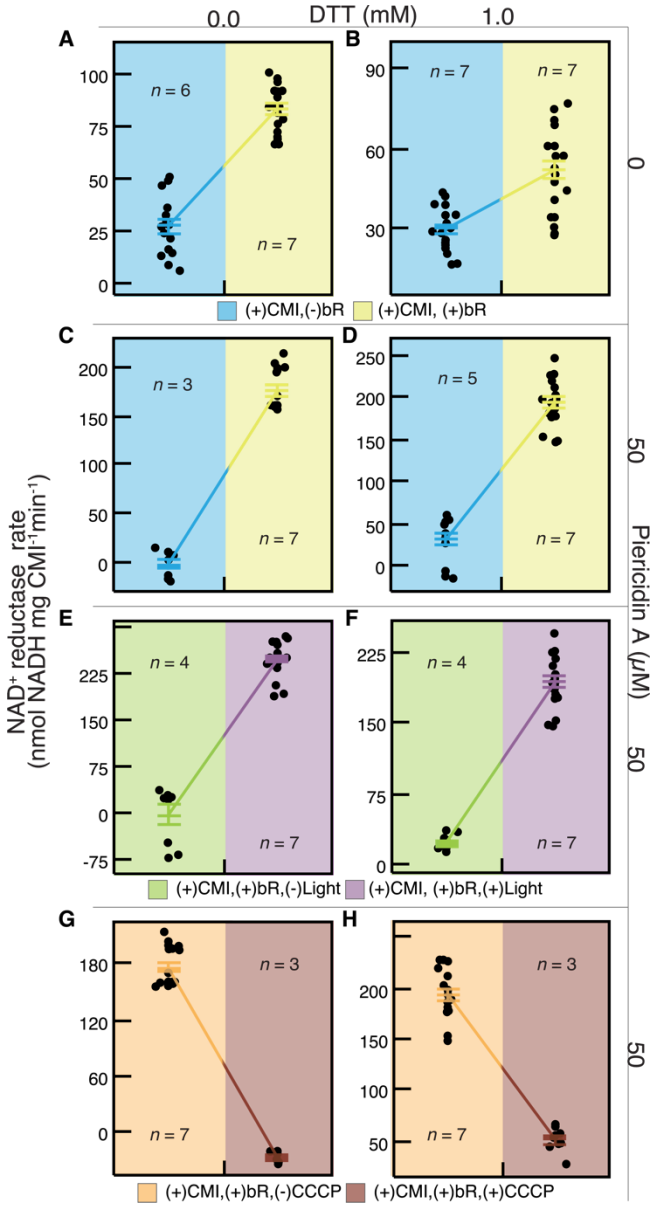

Figure 3.3 | NAD+ reductase rate proteoliposomes under different control conditions Two Sample T-Test. DTT concentration increase from left to right (0.0 mM,1.0 mM). A & B, (+)CMI(±)bR(-)P.A., C & D, (+)CMI(±)bR(+)P.A., E & F, (+)CMI(+)bR(+)P.A.(±)Light G & H, (+)CMI(+)bR(+)P.A.(+)Light(±)CCCP. The error bars represent the standard error of the mean of n biological replicates indicated in each figure panel.

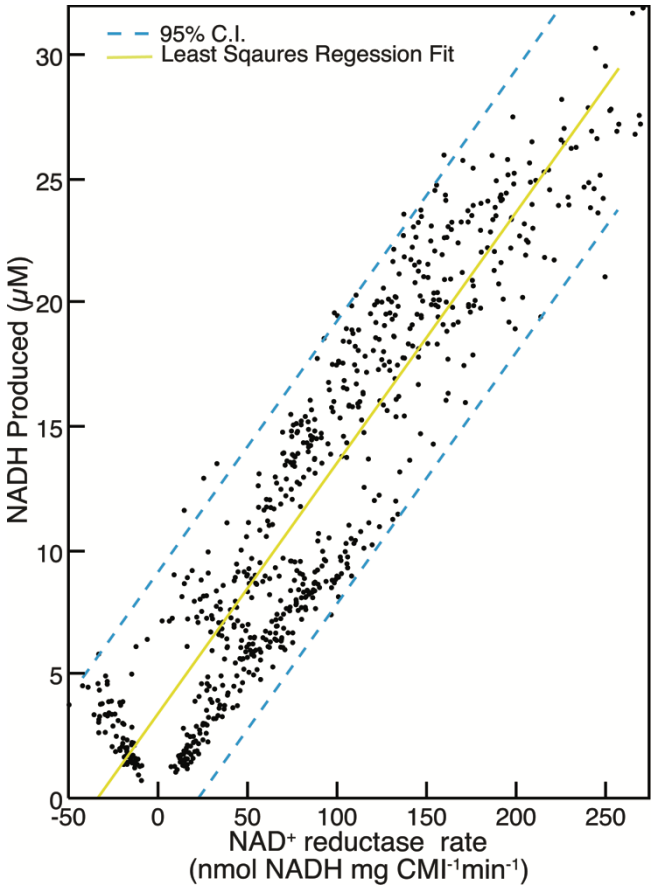

Figure 3.4 | The relationship between NAD^+ reductase rate (nmol NADH mg CMI^{-1} min^{-1}) and NADH produced (μM). The formula for the linear less-squares fit is shown in the figure legend (p-value >.0001, R^2>0.85). The fit was generated using all observations (N = 732) from all conditions tested.

To determine if the rate of NAD^+ reductase had a relationship to the total NADH produced (μM) we performed a linear least squares regression on 734 observations (*N* = 762) of (+)CMI(+)bR proteoliposomes, under all conditions we tested (Figure 3.4). The estimated gradient 0.1 ± 0.002 (mg CMI min^{-1} nmol $NADH^{-1}$), predicts an increase in NAD^+ reductase rate of 10 (NADH mg CMI^{-1} min^{-1}) with increase in the NADH produced by 1 μM. The effect is small and statistically significant, and the coefficient of correlation (r > 0.92) indicates a strong positive linear relationship. Although several data points are

negative slopes with a net production in NADH, the rates are the absolute maximum steady state values while the NADH produced represents a localized maximum.

We employed the pH-sensitive fluorophore 9-amino-6-chloro-2-methoxyacridine (ACMA) to conduct proton pumping assays. We measured the rates of ACMA quenching for CMI bR independently. Because of the non-linear relationship between ACMA quenching and ΔpH[30-31], we calculated the rate of ACMA quenching and de-quenching using the linear region of the ACMA signal, between 40-70% of the baseline. Light-induced activation of bR causes the ACMA signal to decrease at a rate of -1.51 ± 0.62 ACMA% min^{-1} (Figure 3.5). During photoreduction of samples with no P.A. present (Figure 3.6), the signal increased by 1.63 ± 0.15 and 1.34 ± 0.37 ACMA% min^{-1} for 0.0 and 1.0 mM DTT, respectively. When 50 μM P.A. was present the rate the signal increased nearly doubled to 3.96 ± 0.64 and 3.15 ± 0.94 ACMA% min^{-1} for 0.0 and 1.0 mM DTT, respectively. These results are in good agreement with measured rates of NAD^+ reduction for two reasons. Since ACMA reports the signal for the entire population of proteoliposomes and P.A. only inhibits the oxidation of NADH by CMI, proteoliposomes may be oxidizing NADH and simultaneously reduced by another population. Furthermore, when P.A. is present the rate of NADH produced reduces by 95% after 35 minutes while with no P.A. the rate reduced by 72% (Figure 3.6A-B). As shown in Figure 3.6 E & F there is effectively no ΔpH remaining for CMI to reduce NAD+ after 35 min when P.A. is present in comparison when P.A. is not present a ΔpH is present for the all but the last 5 min of the 60-min assay.

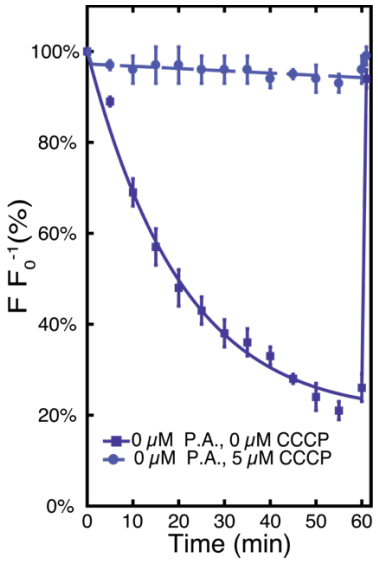

Figure 3.5 | Proton pumping by bR. Typical results from (-)CMI(+)bR proteoliposomes Samples were incubated for 5 to allow the ACMA signal to stabilize before starting the experiments. After 60 min 5 μM CCCP was added to abolish the proton gradient. The results are the representation of three technical repeats of 5 biological replicates.

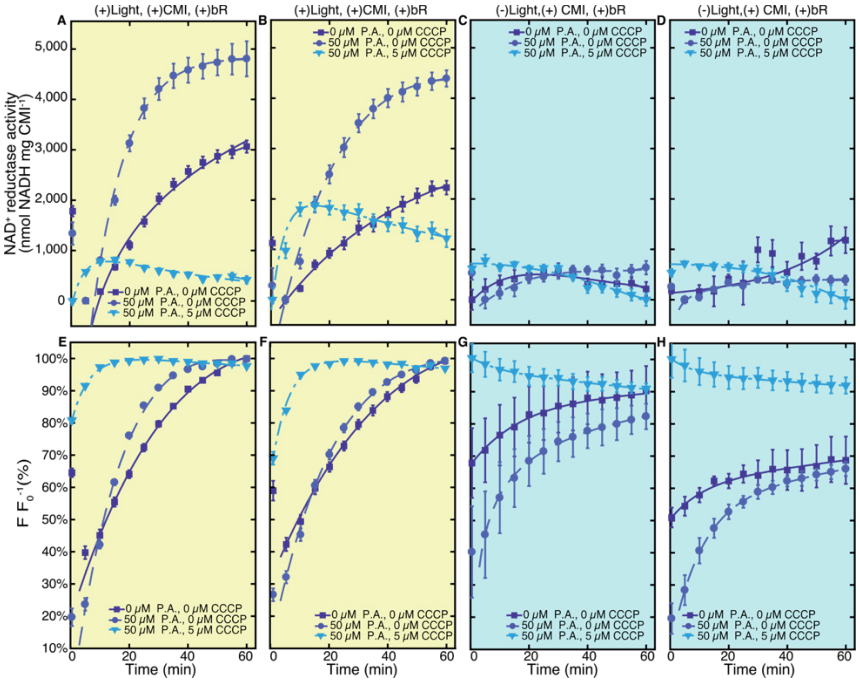

Figure 3.6. | NAD$^+$ Reductase Activity and ACMA Quenching for (+)CMI, (+)bR proteoliposomes. Figures with yellow background are incubated in light and blue

backgrounds are samples incubated in the dark. Figures A,C,E & G have 0.0 mM DTT and figures B, D, F & H have 1.0 mM DTT. Each trace represents the 7 biological replicates with 21 observations (n = 7, N = 21).

Another interesting finding from the proton pumping assays occurring during the initial 5 mins of illumination. When P.A. is not present there is an initial decrease of ACMA quenching before dequenching and starting NADH production. This phenomena is not evident when P.A. is present or in dark incubated samples Figure 3.6(G-H). The ACMA data is difficult to interrupt and precisely decouple the actions of each of the two enzymes but, we can attribute this initial decrease in ACMA signal to a charging of the system by bR. This observation indicates that RET through CMI may require a specific magnitude of ΔpH before switching on and continuing.

Herein, for the first time, we engineered and demonstrated an artificial organelle that enables reduction of NAD^+. The significances of findings reported here are that the reversible machine CMI can utilize a ΔpH to transfer electrons from QH_2 to NAD^+ while the addition of P.A. enhances NAD^+ reduction by inhibiting the oxidation of NADH by CMI. This, in turn, allows NADH to be readily available for synthetic biochemical reaction pathways. This work is the foundation for further development of a device for power generation and balance in vitro metabolic system. Additionally, this technology reduces the constraints on designing metabolic pathways found in other methods for maintaining redox balance, enabling development of more diverse and complex CFMS. Coupling this system, with ATP-producing artificial organelles, will create a biological energy power pack that will allow the use of CFMS for applications not previously possible.

Materials and Methods

We performed all chromatographic steps using a GE ÄKTA pure 25 or ÄKTA Avant 125 (GE Healthcare Life Sciences, Inc.) at 4°C. All ultracentrifugation steps use a Beckman Coulter Type 45-Ti Rotor unless indicated otherwise. Protein concentration was determined using Millipore Direct Detect® infrared spectrometer (EMD Millipore, Inc.). All chemicals used in this study were purchased from Sigma-Aldrich unless otherwise stated.

Statistics

We performed all statistical analysis using JMP V.13.0 (SAS Institute, Inc.) with levels of significance ($\alpha = 0.05$). For linear regression analysis to determine the steady-state rates of NAD^+ Reductase (nmol NADH mg CMI^{-1} min^{-1}) and nonlinear regression analysis we used Matlab R2017a (The Mathworks, Inc.). All error bars represent the standard error mean. All p-values were <.0001 unless indicated otherwise.

Unilamellar Liposome preparation

Total E. *coli* lipid extract (Avanti Lipids Polar, Inc.) were dissolved in Chloroform ($CHCl_3$) at 20 mg mL^{-1} in a glass scintillation vial. A thin film formed by removal of the $CHCl_3$ under vacuum using a rotary evaporator set to 0 psig. The thin film is rehydrated to 15.34 mg mL^{-1} using 5 mM MES, pH 6.5 50 mM KCl, 5 mM $MgCl_2$ 2 mM $CaCl_2$ buffer and placed in a sonication bath for 5 min followed by two freeze-thaw cycles before being extruded through a 0.4 μm polycarbonate membrane 21 times. Typically, the mean diameter as measured by dynamic light scattering of preparations were 180 nm.

Enzyme Reconstitution

The unilamellar liposomes suspension is diluted to a final lipid concentration of 4 mg mL^{-1} and CHAPS concentration of 5 mM by the combination of appropriate amounts of the corresponding buffer, 200 mM CHAPS in the corresponding buffer and concentrated protein. We incubated the liposomes-detergent mixture for 10 min before the addition of protein. The appropriate amount of CMI (4.7 mg mL^{-1}, 50 mM MES, pH 6.0, 50 mM NaCl 1.95 mM DDM) and bR (4.0mg mL^{-1}, 50 mM MES, pH 6.0 0.78 mM DDM) were added to the CHAPS-solubilized preformed liposomes and incubated for 30 min at 4°C under gentle mixing in the dark. We used a bR:CMI ratio of 20. For control experiments, which did not contain an enzyme, we adjusted the difference in volume with buffer.

After the incubation period, we removed the detergent from the lipid-detergent-protein mixture by three successive additions of Bio-Beads SM-2 (80 mg mL^{-1}) every 60 minutes followed by a final addition of 240 mg mL^{-1} and 60 min incubation.

NAD^+ photoreduction and Proton Pumping assays

Photoreduction of NAD^+ by proteoliposomes was performed in 5 mM MES, pH 6.5 50 mM KCl, 5 mM MgCl2. We added 25 µL of proteoliposomes to the assay mixture containing 50 µM decylubiquinone, 0.2 µM valinomycin, 5 µM ACMA and for inhibition and uncoupling assays and 50 µM Piericidin A and 5 µM CCCP are included. The samples were incubated for 5 min before the addition of 200 µM NADH. We allowed the oxidation of NADH by CMI to come to pseudo equilibrium before beginning photoreduction. The final assay volume was 200 µL. A custom L.E.D. array with Luxeon Rebel diodes (Lumileds Holdings B.V.) with a wavelength centered at 530 nm for the

light source. The intensity of the light was kept at 1100 µmol photons m^{-2} s^{-1} for all experiments.

All enzymatic activity assays were conducted at 28°C. Fluorescence measurements were done using a Flexstation 3 (Molecular Devices, Inc.). We measured NADH concentration using (λ-$_{ex}$=340 nm, λ-$_{em}$ =455 nm). Proton gradient generation was measured through the quenching/dequenching of ACMA (λ-$_{ex}$ =410 nm, λ-$_{em}$ =480 nm) using the same samples.

Purification of NADH: Ubiquinone oxidoreductase (Complex I)

We purified Complex I (CMI) from an E. *coli* overexpression strain ANN0221 that was kindly provided by Dr. Friedrich (University of Freiburg, Germany)[32-33]. The chromatographic procedure was modified from previously published methods[32-33] by omitting the anion exchange step and adding a size exclusion step[33]. Following solubilization of the membranes and removal of non-solubilized materials by ultra-centrifugation (200,000 rcf x 20 min), the extract was diluted to 10 mg ml^{-1}. The diluted extract was adjusted to a final imidazole concentration of 50 mM and 200 mM NaCl.

The extract is applied to an equilibrated (50mM MES pH 6.0, 200mM NaCl, 50mM Imidazole, 0.1%(w/v) n-dodecyl β-D-maltoside (DDM)) Tricorn 10 mm x 100 mm (GE Healthcare Life Sciences, Inc.) column packed with High-Performance Ni^{2+} resin (GE Healthcare Life Sciences, Inc.) (Figure 3.7A**)**. Sample loading was done at a flow velocity of 153 cm h^{-1}, continuing with buffer until the Abs_{280} reaches 200 mAU. Contaminating proteins are removed using a wash step with 150 mM imidazole that

continues until the Abs_{280} reaches 200 mAU. A step gradient with 375 mM imidazole at 76.5 cm h^{-1} in up-flow operation elutes CMI.

The fractions containing CMI were concentrated using a 100 kD MWCO Amicon® Ultra centrifugal filter (EMD Millipore, Inc.) to 2-3 mL. The concentrated protein sample was polished and desalted into 50 mM MES, pH 6.0, 50 mM NaCl 0.1%(w/v) DDM by applying to a HiLoad 16/600 Superdex 200 (GE Healthcare Life Sciences, Inc.) size exclusion column at 22 cm h^{-1}(Figure 3.7B). Fractions containing CMI were concentrated to 4-5 mg mL^{-1} using Amicon® Ultra centrifugal filters, aliquoted, snap frozen and stored at -80˚C.

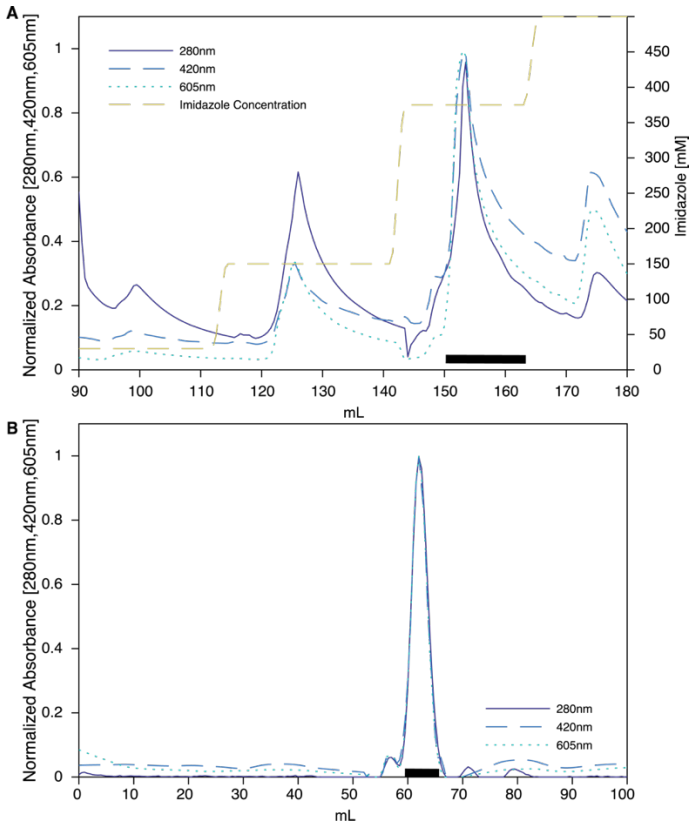

Figure 3.7 | Purification of Complex I. Absorbance at each wavelength are normalized. A, Chromatogram from nickel affinity purification of Complex I. B, Chromatogram of

material from Fig. A applied to a HiLoad 16/600 Superdex 200 column. The black bars indicate the fractions which are pooled for subsequent steps.

Purification of Bacteriorhodopsin

Bacteriorhodopsin was purified using methods discussed in Chapter 2 using tangential flow filtration, followed by solubilization with 5% (w/w) Trion X-100 at 1 mg ml^{-1} for 24 hours. Solubilized bR was captured and detergent was exchanged using anion exchange chromatography.

References

1. Efrati, A.; Lu, C.-H.; Michaeli, D.; Nechushtai, R.; Alsaoub, S.; Schuhmann, W.; Willner, I., Assembly of photo-bioelectrochemical cells using photosystem I-functionalized electrodes. *Nature Energy* **2016,** *1*, 15021.

2. Carlson, E. D.; Gan, R.; Hodgman, C. E.; Jewett, M. C., Cell-free protein synthesis: Applications come of age. *Biotechnol Adv* **2012,** *30* (5), 1185-1194.

3. Wendell, D.; Todd, J.; Montemagno, C., Artificial Photosynthesis in Ranaspumin-2 Based Foam. *Nano Lett* **2010,** *10* (9), 3231-3236.

4. Keller, M. W.; Schut, G. J.; Lipscomb, G. L.; Menon, A. L.; Iwuchukwu, I. J.; Leuko, T. T.; Thorgersen, M. P.; Nixon, W. J.; Hawkins, A. S.; Kelly, R. M.; Adams, M. W. W., Exploiting microbial hyperthermophilicity to produce an industrial chemical, using hydrogen and carbon dioxide. *Proceedings of the National Academy of Sciences* **2013,** *110* (15), 5840-5845.

5. Schultheisz, H. L.; Szymczyna, B. R.; Scott, L. G.; Williamson, J. R., Pathway Engineered Enzymatic de Novo Purine Nucleotide Synthesis. *Acs Chem Biol* **2008,** *3* (8), 499-511.

6. Mutti, F. G.; Knaus, T.; Scrutton, N. S.; Breuer, M.; Turner, N. J., Conversion of alcohols to enantiopure amines through dual-enzyme hydrogen-borrowing cascades. *Science* **2015,** *349* (6255), 1525-1529.

7. Guterl, J. K.; Garbe, D.; Carsten, J.; Steffler, F.; Sommer, B.; Reisse, S.; Philipp, A.; Haack, M.; Ruhmann, B.; Koltermann, A.; Kettling, U.; Bruck, T.; Sieber, V., Cell-Free Metabolic Engineering: Production of Chemicals by Minimized Reaction Cascades. *ChemSusChem* **2012,** *5* (11), 2165-2172.

8. Krutsakorn, B.; Honda, K.; Ye, X.; Imagawa, T.; Bei, X.; Okano, K.; Ohtake, H., In vitro production of n-butanol from glucose. *Metabolic engineering* **2013,** *20*, 84-91.

9. Opgenorth, P. H.; Korman, T. P.; Bowie, J. U., A synthetic biochemistry module for production of bio-based chemicals from glucose. *Nature chemical biology* **2016,** *12* (6), 393-U29.

10. Opgenorth, P. H.; Korman, T. P.; Bowie, J. U., A synthetic biochemistry molecular purge valve module that maintains redox balance. *Nature communications* **2014,** *5*, 4113.

11. Lee, H.; Ho, D.; Kuo, K.; Montemagno, C. D., Vectorial insertion of bacteriorhodopsin for directed orientation assays in various polymeric biomembranes. *Polymer* **2006,** *47* (9), 2935-2941.

12. Luo, T. J. M.; Soong, R.; Lan, E.; Dunn, B.; Montemagno, C., Photo-induced proton gradients and ATP biosynthesis produced by vesicles encapsulated in a silica matrix. *Nature materials* **2005,** *4* (3), 220-224.

13. Pitard, B.; Richard, P.; Dunach, M.; Rigaud, J. L., ATP synthesis by the F0F1 ATP synthase from thermophilic Bacillus PS3 reconstituted into liposomes with bacteriorhodopsin .2. Relationships between proton motive force and ATP synthesis. *European Journal of Biochemistry* **1996,** *235* (3), 779-788.

14. Zhang, Y.-H. P., Production of biofuels and biochemicals by in vitro synthetic biosystems: Opportunities and challenges. *Biotechnol Adv* **2015,** *33* (7), 1467-1483.

15. Uppada, V.; Satpute, K.; Noronha, S. B., 10 - Redesigning Cofactor Availability: An Essential Requirement for Metabolic Engineering. In *Current Developments in Biotechnology and Bioengineering*, Elsevier: 2017; pp 223-242.

16. Bezborodov, A. M.; Zagustina, N. A., Enzymatic biocatalysis in chemical synthesis of pharmaceuticals (Review). *Applied Biochemistry and Microbiology* **2016,** *52* (3), 237-249.

17. Brandt, U., Energy Converting NADH: Quinone Oxidoreductase (Complex I). *Annual review of biochemistry* **2006,** *75* (1), 69-92.

18. Armstrong, F. A.; Hirst, J., Reversibility and efficiency in electrocatalytic energy conversion and lessons from enzymes. *Proceedings of the National Academy of Sciences* **2011,** *108* (34), 14049-14054.

19. Baradaran, R.; Berrisford, J. M.; Minhas, G. S.; Sazanov, L. A., Crystal structure of the entire respiratory complex I. *Nature* **2013,** *494* (7438), 443-448.

20. Faham, S.; Yang, D.; Bare, E.; Yohannan, S.; Whitelegge, J. P.; Bowie, J. U., Side-chain Contributions to Membrane Protein Structure and Stability. *Journal of molecular biology* **2004,** *335* (1), 297-305.

21. Pryde, K. R.; Hirst, J., Superoxide Is Produced by the Reduced Flavin in Mitochondrial Complex I A Single, Unifed Mechanism that Applies During Both Forward and Reverse Electron Transfer. *Journal of Biological Chemistry* **2011,** *286* (20), 18056-18065.

22. Seigneuret, M.; Rigaud, J. L., Analysis of Passive and Light-Driven Ion Movements in Large Bacteriorhodopsin Liposomes Reconstituted by Reverse-Phase Evaporation .2. Influence of Passive Permeability and Back-Pressure Effects Upon Light-Induced Proton Uptake. *Biochemistry-Us* **1986,** *25* (21), 6723-6730.

23. Hazard, A.; Montemagno, C., Improved purification for thermophilic F1F0 ATP synthase using n-dodecyl beta-D-maltoside. *Archives of biochemistry and biophysics* **2002,** *407* (1), 117-124.

24. Vinogradov, A. D.; Grivennikova, V. G., Oxidation of NADH and ROS production by respiratory complex I. *Biochimica et Biophysica Acta (BBA) - Bioenergetics* **2016,** *1857* (7), 863-871.

25. Zu, Y.; Shannon, R. J.; Hirst, J., Reversible, Electrochemical Interconversion of NADH and NAD+ by the Catalytic (Iλ) Subcomplex of Mitochondrial NADH:Ubiquinone Oxidoreductase (Complex I). *J Am Chem Soc* **2003,** *125* (20), 6020-6021.

26. Friedrich, T.; Ohnishi, T.; Forche, E.; Kunze, B.; Jansen, R.; Trowitzsch, W.; Hofle, G.; Reichenbach, H.; Weiss, H., 2 Binding-Sites for Naturally-Occurring Inhibitors in Mitochondrial and Bacterial Nadh-Ubiquinone Oxidoreductase (Complex-I). *Biochemical Society transactions* **1994,** *22* (1), 226-230.

27. Kotlyar, A. B.; Borovok, N., NADH oxidation and NAD+ reduction catalysed by tightly coupled inside-out vesicles from Paracoccus denitrificans. *European journal of biochemistry / FEBS* **2002,** *269* (16), 4020-4.

28. Ohnishi, S. T.; Salerno, J. C.; Ohnishi, T., Possible roles of two quinone molecules in direct and indirect proton pumps of bovine heart NADH-quinone oxidoreductase (complex I). *Biochimica et Biophysica Acta (BBA) - Bioenergetics* **2010,** *1797* (12), 1891-1893.

29. Belevich, N.; Belevich, G.; Chen, Z.; Sinha, S. C.; Verkhovskaya, M., Activation of respiratory Complex I from Escherichia coli studied by fluorescent probes. *Heliyon* **2017,** *3* (1), e00224.

30. Casadio, R., Measurements of Transmembrane Ph Differences of Low Extents in Bacterial Chromatophores - a Study with the Fluorescent-Probe 9-Amino, 6-Chloro, 2-Methoxyacridine. *European Biophysics Journal* **1991,** *19* (4), 189-201.

31. D'Alessandro, M.; Turina, P.; Melandri, B. A., Quantitative evaluation of the intrinsic uncoupling modulated by ADP and Pi in the reconstituted ATP synthase of Escherichia coli. *Biochimica et Biophysica Acta (BBA) - Bioenergetics* **2011,** *1807* (1), 130-143.

32. Spehr, V.; Schlitt, A.; Scheide, D.; Guenebaut, V.; Friedrich, T., Overexpression of the Escherichia coli nuo-operon and isolation of the overproduced NADH:ubiquinone oxidoreductase (complex I). *Biochemistry-Us* **1999,** *38* (49), 16261-7.

33. Pohl, T.; Uhlmann, M.; Kaufenstein, M.; Friedrich, T., Lambda Red-mediated mutagenesis and efficient large scale affinity purification of the Escherichia coli NADH:ubiquinone oxidoreductase (complex I). *Biochemistry-Us* **2007,** *46* (37), 10694-702.

4. Light-Driven Biological Recycling of NADH for Fueling Cell-Free Metabolic Systems.

Abstract

Cell-free metabolic engineering (CFME) has tremendous value in energy generation, biosensors, protein synthesis and for expanding the diversity of biosynthesized compounds. To prepare cell-free systems as an economical commercial application requires the circumvention of a major technical issue. Providing and adjusting the energy needs at the nanoscale as enzymatic cofactors are the most significant and cost prohibitive limitations of CFME. Due to the cost and stability of enzymatic cofactors like nicotinamide (NADH) recycling coenzymes is essential. Here we introduce an engineered biotic/abiotic organelle capable of recycling NADH, merely requiring light and water. This device pairs two membrane protein complexes that do not interact naturally: Photosystem II (PSII) and NADH:Ubiquinone oxidoreductase (CMI). Through the controlled directional insertion into 180 nm liposomes, these two proteins function collectively to reduce NAD^+. In this study, we determined the optimal PSII to CMI ratio and show the rate of NADH production is proportional to quantum flux and has coupling efficiencies near unity. Applying this technology to cell-free metabolic systems (CFMS) will permit control over NADH balance and eliminate constraints on the design of new biosynthetic pathways.

Introduction

CFME has been gaining considerable attention for a variety of technologies over recent years[1]. Decoupling the cellular machinery responsible for cellular maintenance

and growth from the biochemical pathway of interest yields many advantages. After eliminating the biological constraints and by directing all biochemical resources to an individual aim, results in high production yields, permits broad reaction conditions, simpler metabolic pathway engineering, and control. CFMS platforms for producing low-value chemicals (LVCs), fine chemicals and biologics[2] have become increasingly elaborate. For example, demonstrations of systems using 8[3], 16[4], and 28 enzymes[5], which shows cell-free metabolic systems have the potential of developing into a disruptive technology to microbial fermentation.

For CFMS to be self-sustaining and have high productivity, replenishing energy to the system as enzymatic cofactors like ATP and NAD(P)H is imperative. Maintaining energy requirements is a considerable challenge for CFMS due to the absence of the complicated regulatory networks that produce and balance enzymatic cofactors. When designing in vitro metabolic pathways, ATP and NAD(P)H balance is a crucial consideration as imbalances will lead to incomplete conversions. Furthermore, the cost of simple addition of cofactors is cost prohibitive and can be deleterious, leading to enzymatic inhibition. In some cases it has been possible to form redox neutral pathways[6-8], or include purge mechanisms to remove excess cofactor[9-10]. Nevertheless, these approaches place inflexible constraints on designs, need additional enzymes increasing complexity, or exclusively applicable to one biosynthetic scheme.

Ideally, a device must regulate cofactor balance without impacting carbon flux, only require inexpensive and abundant inputs and be compatible with any CFMS. An example of such a device is an artificial organelle which ATPase and Bacteriorhodopsin (bR) are co-reconstituted into a membrane for ATP regeneration[11-12]. bR functions by

harvesting light and translocating protons (H^+) creating a pH gradient (ΔpH) across the membrane. The ΔpH provides the potential to drive ATPase to form ATP[3]. The rate of ATP formation corresponds to the magnitude of the ΔpH which is proportional to the intensity of light[13]. This ATPase/bR artificial organelle makes it possible to regenerate ATP from light for artificial photosynthesis[3]. Until now, no device with similar attributes was available for NADH recycling and balance. Ordinarily, the NADH regeneration is done using single- or two-enzyme substrate coupled systems[14-16]. NADH regeneration through these techniques has various shortcomings. The addition of exogenous substrate serving as an electron donor creates byproducts, shifting the reaction equilibrium and inhibiting enzymatic cascades. These are considerable drawbacks for any CFMS making them incapable of self-sustainability and any additive cost is prohibitive in producing LVCs.

In this study, we engineered an artificial organelle capable of photoreduction of NAD^+ by integrating PSII and CMI into liposomes in specific orientations (Figure 4.1). The power source for this device is light. Light enables PSII to oxidize water generating oxygen (O_2) and H^+. Then PSII transfers electrons from water to ubiquinone (Q) to produce ubiquinol (QH2)[17-18]. As a result, the accumulation of H^+ within the lumen creates a proton motive force (PMF). The PMF is requisite to diminish the thermodynamic gap of the standard redox potentials between NADH/NAD^+ and QH_2/Q. Reducing the thermodynamic barrier enables CMI to perform reverse electron transfer (RET) from QH_2 to NAD^+[19-20]. Connecting the associated metabolisms of these two enzymes produces NADH using water as the substrate, generating oxygen as the sole by-product.

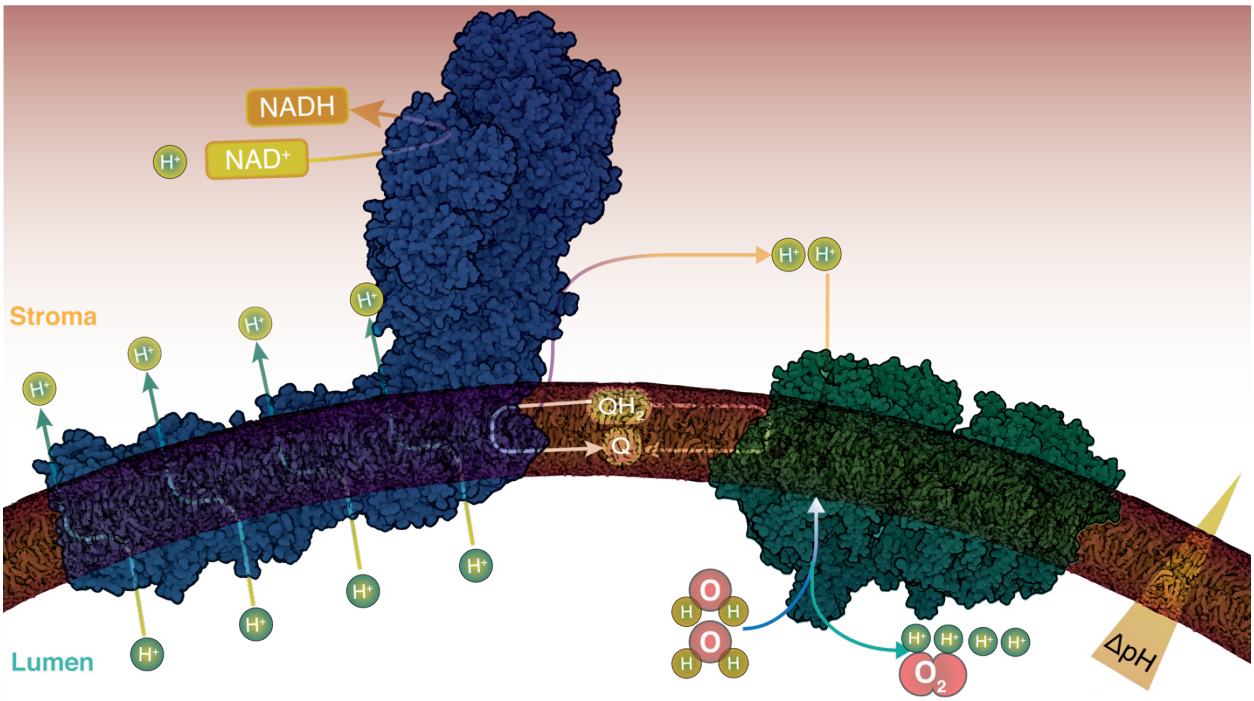

Figure 4.1 | Illustration of Photosystem II and Complex I reconstituted into liposomes. The enzyme icons and their respective reaction equations are located in the top left. The purple arrows represent the flow of Q and QH_2 between CMI to PSII. The green H^+ generated from the oxidation of water by PSII generate a PMF within the lumen liposome depicted by the arrow labeled ΔpH. The oxidation of QH_2 by CMI is coupled to H^+-translocation and the reduction of NAD^+ to NADH. This illustration was created using the crystal structures of CMI from *T. thermophilus*[21] and *T. valcuanus*[22] for PSII.

Results and Discussion

Protein Reconstitution

The isolated enzymes were reconstituted into liposomes made from E. coli total lipid extract following the methods delineated by Riguard[23]. Determination of the conditions for the co-reconstitution in the of the enzymes in the desired orientation into a single liposome required detergent screening experiments. First, we reconstituted the enzymes separately (Table 4-3 & Table 4-4). Using the extent of both PMF generation and each enzyme's associated activity as the metrics for these experiments, we concluded the zwitterionic surfactant CHAPS at 5 mM was best suited for co-reconstitution. Next, to ascertain the formulation that provided the highest rates of NAD^+ photoreduction, we altered the PSII to CMI mole ratio (PCR) while adhering to a lipid to PSII weight ratio of 30:1 (w/w).

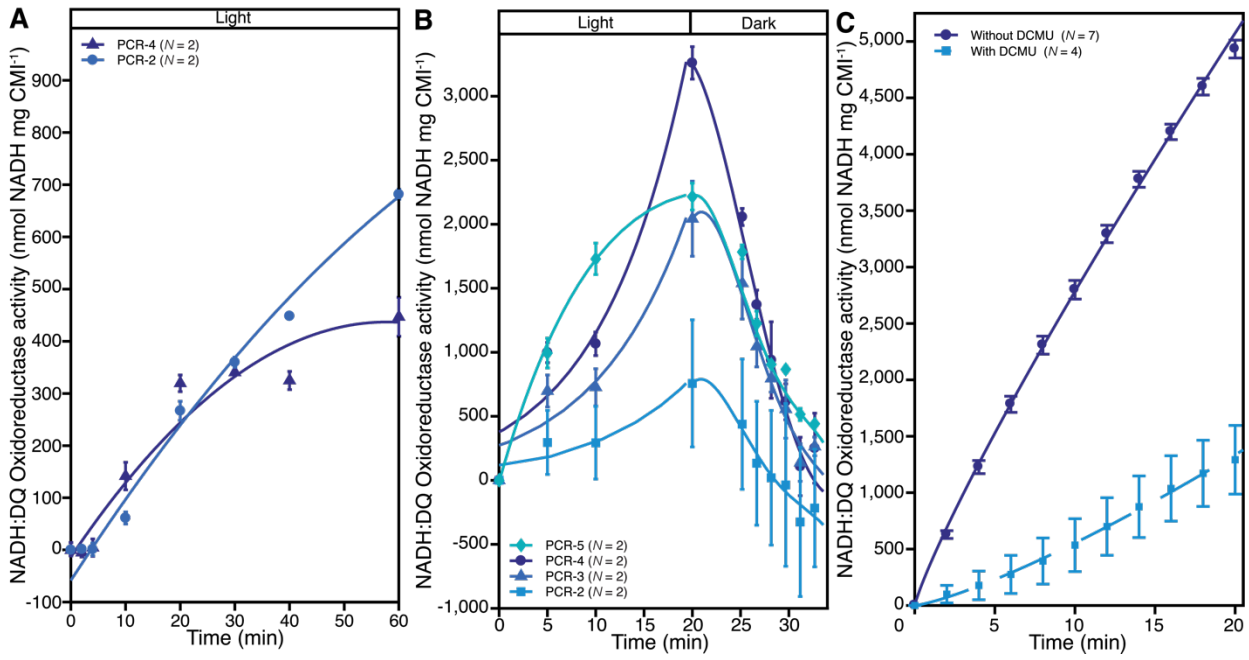

Figure 4.2 | Photoreduction of NAD^+ by PSII:CMI proteoliposomes. NADH:DQ oxidoreductase (nmol NADH mg CMI^{-1}) activity versus time (min). A, Proteoliposomes with a PCR of 2 and 4 using 1mM NAD^+ as substrate. B, Proteoliposomes with PCRs of 2-5 using 200 μM NADH as substrate after the oxidation of NADH by CMI. The light or dark condition is indicated along the top x-axis. C, Seven independently prepared proteoliposomes with PCR-4 under light without DCMU with DCMU. The error bars represent the standard error of the mean (SEM) of N biological replicates with three technical replicates. Curves were fit to exponential functions following Michaelis-Menten kinetics

<u>NAD^+ Photoreduction</u>

In our first series of photoreduction experiments the substrate used was 1 mM NAD^+ (Figure 4.2A). Linear regression of the results revealed that the rate of NAD^+ photoreduction of PCR-4 to be 20.2 ± 5.2 nmol min^{-1} mg CMI^{-1}, twice that of PCR-2, 9.6 ± 4.4 nmol min^{-1} mg CMI^{-1}. Previous investigations of succinate-supported NAD^+

oxidoreduction with sub-mitochondrial particles (SMPs) published the addition of NADH activates CMI, accelerating rates of RET[24-25]. Thus, prompting our examination of using NADH as a substrate. When using NADH, we added 200 μM to the proteoliposomes while continuing to monitor its oxidation by CMI (Figure 4.7). Only after reaching equilibrium and a 10-minute incubation phase, using light, we started photoreduction. These trials (Figure 4.2B) produced NADH at rates of 203.5 ± 54.9 and 60.5 ± 18.3 nmol min^{-1} mg CMI^{-1}, for proteoliposomes with PCR-4 and 2, correspondingly. Encouraged by rates an order of magnitude higher than our 1 mM NAD^+ experiments, we tested PCRs 3 and 5. Markedly, the rate of NAD^+ photoreduction increased linearly with PCR between 2 and 4 (71.5 nmol min^{-1} mg CMI^{-1} PCR^{-1}) than declining between 4 and 5 (Figure 4.8). Following the removal of the samples from the light the NADH concentration depleted, maintaining that NADH is forming (Figure 4.2B). We concluded PCR-4 is optimal for NAD^+ photoreduction with the hypothesis that the balance of QH_2 and PMF generation by PSII and their utilization by CMI was the principle for higher performance. In following experiments, we only use PCR-4 with 200 μM NADH as substrate.

We made and tested seven independent preparations using the same procedure for the validation of the consistency of our assembly methods (Figure 4.2C). The rate of NAD^+ photoreduction is 302.5 ± 9.9 nmol min^{-1} mg CMI^{-1} over the first 5-minutes of illumination after adjusting the results by subtracting the rate of proteoliposomes left in the dark (Figure 4.9). Therefore, the conclusion is our methods are robust as they provide proteoliposomes with consistent NADH production rates.

To reinforce that PSII is providing electrons to CMI through decylubiquinol (DQH_2), we executed experiments using 3-(3,4-dicholorophenyl)-1,1-dimethylurea (DCMU), an inhibitor of PSII[26-27] which does not affect CMI[28-30] (Figure 4.2C). Before starting photoreduction, the proteoliposomes are incubated with 100 μM DCMU for 5-minutes. Consequently, the DCMU treated samples had an NAD^+ photoreduction rate of 42.5 ± 6.3 nmol min^{-1} mg CMI^{-1} or 14.0 ± 1.6% of samples without DCMU. The diminished rate substantiates PSII is providing electrons to NAD^+ by CMI.

Influence of PMF on NADH production

Employing the pH sensitive fluorophore 9-amino-6-chloro-2-methoxyacridine (ACMA) fluorescence under light and dark conditions, we can determine the influence of the PMF on NAD^+ photoreduction. After exposing the samples to light, ACMA fluorescence and NADH continue increasing (Figure 4.3A-D). The simultaneous increase advocates that CMI is pumping H^+ out of the proteoliposomes as it is reducing NAD^+. The rate of NAD^+ photoreduction remains linear (241.5 ± 4.6 nmol min^{-1} mg CMI^{-1}) nearly the entire 20-minute illumination period (Figure 4.3A) while de-quenching of the ACMA signal is exponentially increasing to 33.9 ± 0.7% (Figure 4.3C). Once removed from light both signals decline as expected from H^+ influx associated with NADH oxidation by CMI.

Introducing DCMU to the samples causes the rate of NADH production to diminish but, remains linear (64.8 ± 1.5 nmol min^{-1} mg CMI^{-1}). Unlike the samples without DCMU the change in ACMA signal does not show biphasic behavior. After 10 minutes the signal plateaus reaching a maximum of 23.9 ± 0.7% at 13 minutes. Additionally, the signal begins to decline before withdrawing the samples from light (Figure 3.3D). The

addition of DCMU reduces the NADH production rate by 73.2 ± 0.2%, despite there only being 29.7 ± 2.2 % reduction in ΔACMA. The non-linear relationship of ACMA quenching to ΔpH[31-32] explains why the decline in ΔACMA is not equivalent to that seen NADH production. The reduction in the rate of NADH production corresponds to our direct measurements of inhibition of PSII by DCMU (68.1 ± 6.1%) (Figure 3.3E). Overall, the results indicate that PMF generating activity of PSII has a relationship with NADH production.

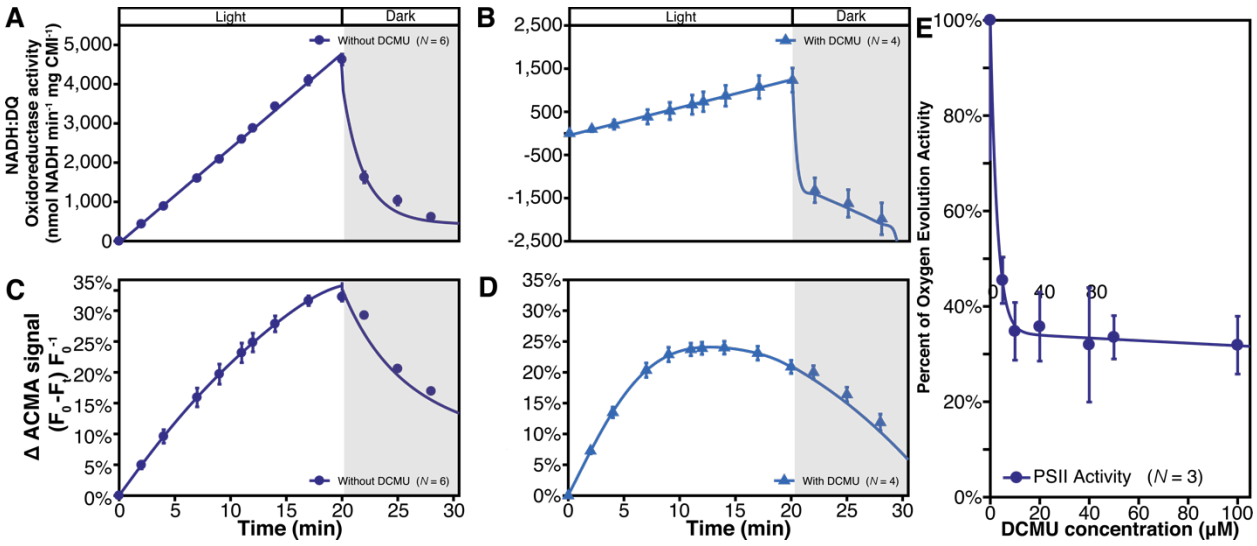

Figure 4.3 | Relationship between NAD^+ Photoreduction activity and ACMA signal of PCR-4 proteoliposomes. NADH:DQ oxidoreductase (nmol NADH mg CMI^{-1}) activity of proteoliposomes with PCR-4 A, Without DCMU and B, with DCMU. Percent change in ACMA fluorescence of proteoliposomes C, Without DCMU and D, With DCMU. The light or dark condition is indicated along the top x-axis. E, Oxygen evolution activity vs. DCMU concentration for PCR-4 proteoliposomes. The error bars represent the SEM of N biological replicates with three technical replicates for fig. A-D and N biological replicates with one technical replicate for fig. E.

Light-Dark Cycles

Previous experiments show when exposing the proteoliposomes to light for longer than 20 minutes, NADH production rates start to decrease. To determine if this is due to disruption of the system's integrity, we performed light-dark cycle experiments (Figure 4.4A**,** Figure 4.10). At each light phase, the linear regions of the rates remain consistent: 241.7 ± 4.6, 299.8 ± 54.8, and 306.9 ± 18.1 nmol min^{-1} mg CMI^{-1}. However, the decline in NADH production is most prominent during the second light phase; the rate restores following the dark period. These results advocate the construct remain functional, and

NADH must have an inhibitory effect on RET by CMI. To strengthen this interpretation, we conducted NADH titration experiments. We found an inflection point of the NADH production rate at 200 μM (Figure 4.4B). Moreover, the total NADH production reduces by a factor of 5 (Table 4-2). Published information is limited for RET for E. *coli* CMI, however, several publications exist on the ATP-driven, succinate-supported RET in SMPs. They all report NADH having an inhibitory effect on the reduction of NAD^+ by CMI[33-36]. Despite the mode of inhibition being outside this work, given the conservative nature of CMI between species, it is logical that NADH would have an inhibitory effect on RET in this system.

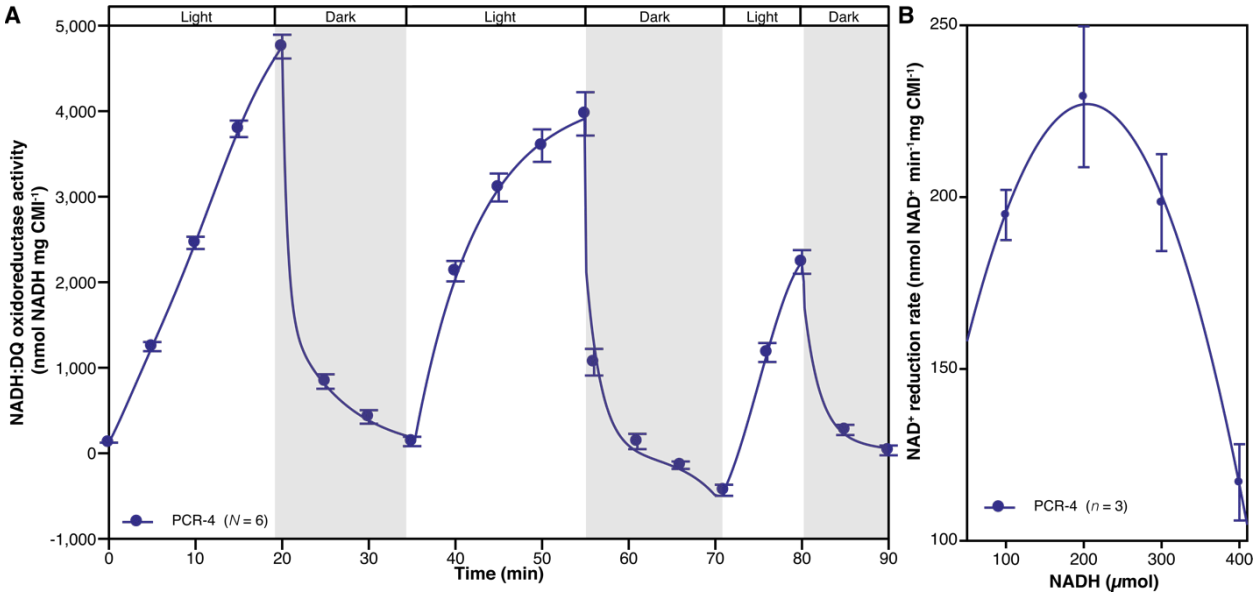

Figure 4.4 | Photoreduction of NAD^+ by PCR-4 proteoliposomes through multiple light-dark cycles. A, NADH:DQ oxidoreductase activity of PCR-4 proteoliposomes (nmol NADH mg CMI^{-1}) versus time (min). The light or dark condition is indicated along the top x-axis. B, NAD^+ reduction rate (nmol NADH min^{-1} mg CMI^{-1}) versus initial concentration of NADH (μmol) added. The error bars represent the SEM of N biological replicates each with three

technical replicates for fig. A and the standard deviation for n technical replicate for a single biological replicate for fig. B.

Control and efficiency of NADH production

As mentioned previously, for CFMS to operate efficiently, matching the rate of cofactor recycling with consumption to avoid inhibitory effects is essential. We fabricated an L.E.D. array with similar optical characteristics of the diodes used in our Clark-type electrode system (Table 4-5) enabling control over the quantum flux. In these trials, we average the NAD^+ photoreduction rate over 10-minutes at various quantum flux values. The results displayed in Figure 4.5A verify quantum flux can modulate NADH production rates and is exponentially proportional. However, the average rates are not illustrative of the maximum rates of NAD^+ reduction the proteoliposomes are capable of for reasons outlined earlier. Applying linear regression to the first four minutes of NADH production under 3,000 µmol photons s^{-1} m^{-2} because the data indicates that reaction is far enough from equilibrium that it remains constant. The result is a rate of 622.8 ± 37.0 nmol min^{-1} mg CMI^{-1} (Figure 4.5B). This rate is more than two times than the average of the rate over ten minutes.

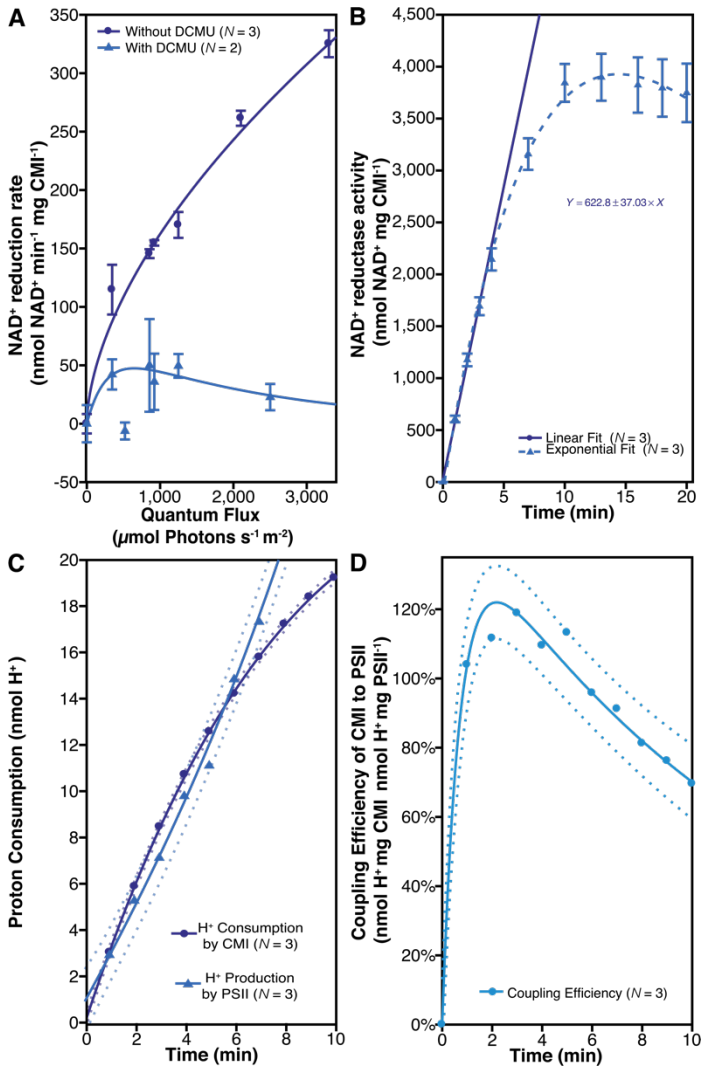

Figure 4.5 | Activity versus quantum flux and Coupling efficiency of PSII and Complex I. A, NAD^+ reduction rate vs. quantum flux of PCR-4 proteoliposomes with and without inhibition by DCMU. B, NAD^+ reduction rate of PCR-4 proteoliposomes with at 3,000 μmol photons s^{-1} m^{-2} with linear equation fit for the first 3 minutes and exponential fit over 20 minutes of illumination. C, Rates of H^+ consumption by CMI and production by PSII at 3,000 μmol photons s^{-1} m^{-2}. D, The coupling efficiency based on the stoichiometric H^+ and consumption and production by CMI and PSII, respectively at 3,000 μmol photons s^{-1} m^{-2}. Dotted lines in fig. C and fig. D are the 95% confidence bounds of the exponential best-fit

equation. The error bars represent the SEM of N biological replicates with three technical replicates

Furthermore, this L.E.D. array enables an accurate comparison of NAD^+ photoreduction to O_2 evolution under the same optical characteristics and quantum flux between the respective instruments. We measured the rate of O_2 evolution and NAD^+ photoreduction of multiple preparations under the equivalent conditions to evaluate the coupling efficiency between PSII and CMI. Basing the calculation on the H^+ stoichiometry of each enzyme's associated metabolism (Figure 4.1**,** Figure 4.5C). Using the ratio of H^+ consumed by CMI to the H^+ produced by PSII, integrating the fitted equation and averaging over 10 minutes, the outcome was a coupling efficiency of 95.0 ± 10.6%(Figure 4.5D). This finding shows that the proteoliposomes utilize protons near unity.

It is worth mentioning reconstitution of PSII results in a 92.2 ± 1.7% decrease in its activity verse when using optimal assay conditions of isolated enzyme. The decreased PSII activity suggests it is restricting the rate of NAD^+ reduction by CMI. Although we did not evaluate this in our study, we postulate the decline in activity of PSII, once reconstituted, is due to differences in lipid composition between E. *coli* total lipid extract[37], and its native thylakoid membrane environment[38-39].

Conclusion

Herein, for the first time, we engineered and demonstrated an artificial organelle that enables reduction of NAD^+. We show that following our procedure, these proteoliposomes have consistent performance, the light intensity can modulate NADH production rates, and the coupling efficiency of PSII and CMI is near unity. This device

can replace the cellular machinery needed for power generation and balance in vitro metabolic system. Additionally, this technology reduces the constraints on designing metabolic pathways found in other methods for maintaining redox balance, enabling development of more diverse and complex CFMS. Coupling this system, with ATP-producing artificial organelles, will create a biological energy power pack that will allow the use of CFMS for applications not previously possible.

Materials and Methods

All chromatographic steps were performed using a GE ÄKTA pure 25 or ÄKTA Avant 125 (GE Healthcare Life Sciences, Inc.) at 4°C. All ultracentrifugation steps use a Beckman Coulter Type 45-Ti Rotor unless indicated otherwise. Protein concentration was determined using Millipore Direct Detect® infrared spectrometer (EMD Millipore, Inc.). All enzymatic activity assays were conducted at 28°C. Fluorescence measurements were done using a Flexstation 3 (Molecular Devices, Inc.). NADH was measured using (λ_{ex} = 340 nm, λ_{em} = 455 nm). Proton gradient generation was determined by quenching of ACMA (λ_{ex} = 410nm, λ_{em} = 480nm).

Reagents

All chemicals used in this study were purchased from Sigma-Aldrich unless otherwise stated.

Purification of NADH:Ubiquinone oxidoreductase (Complex I)

We purified Complex I (CMI) from an E. *coli* overexpression strain ANN0221 that was kindly provided by Dr. Friedrich (University of Freiburg, Germany)[40-41]. The chromatographic procedure was modified from previously published methods[414141414140-

[41] by omitting the anion exchange step and adding a size exclusion step[41]. Following solubilization of the membranes and removal of non-solubilized materials by ultra-centrifugation (200,000 rcf x 20 min), the extract was diluted to 10 mg mL^{-1}. The diluted extract was adjusted to a final imidazole concentration of 50 mM and 200 mM NaCl.

The extract is applied to a equilibrated (50mM MES pH 6.0, 200mM NaCl, 50mM Imidazole, 0.1%(w/v) n-dodecyl β-D-maltoside (DDM) Tricorn 10 mm x 100 mm (GE Healthcare Life Sciences, Inc.) column packed with High-Performance Ni^{2+} resin (GE Healthcare Life Sciences, Inc.) (Figure 4.11a). Sample loading was done at a flow velocity of 153 cm h^{-1}, continuing with buffer until the Abs_{280} reaches 200 mAU. Contaminating proteins are removed using a wash step with 150 mM imidazole that continues until the Abs_{280} reaches 200 mAU. A step gradient with 375 mM imidazole at 76.5 cm h^{-1} in up-flow operation elutes CMI.

The fractions containing CMI were concentrated using a 100 kD MWCO Amicon® Ultra centrifugal filter (EMD Millipore, Inc.) to 2-3 mL. The concentrated protein sample was polished and desalted into 50 mM MES, pH 6.0, 50 mM NaCl 0.1%(w/v) DDM by applying to a HiLoad 16/600 Superdex 200 (GE Healthcare Life Sciences, Inc.) size exclusion column at 22 cm h^{-1}(Figure 4.11b). Fractions containing CMI were concentrated to 4-5 mg mL^{-1} using Amicon® Ultra centrifugal filters, aliquoted, snap frozen and stored at -80 °C.

Purification of Photosystem II

PSII with a histidine tag located on the CD47 subunit was isolated from cyanobacterium *Synechocystis* 6803[42] graciously provided by Dr. Bicker (Louisiana

State University, USA). Isolated Thylakoid membranes were resuspended to 1 mg ChlA mL^{-1} in 50 mM MES, pH 6.0 10 mM $MgCl_2$, 5 mM $CaCl_2$, 25% (v/v) glycerol. The membranes were solubilized by drop-wise addition of 20% (w/v) DDM to a final concentration of 0.8% (w/v) and incubated at 4°C for 20 min. Non-solubilized material is removed by centrifugation using a multiple speed increase: 100 rcf x 1 min, 2,900 rcf x 1 min, 4,900 rcf x 1 min, 8,000 rcf x 1 min, 15,100 rcf x 1 min and 22,100 rcf x 10 min.

The extract is applied to a pre-equilibrated (50mM MES pH 6.0, 50mM NaCl, 10 mM $MgCl_2$, 5 mM $CaCl_2$, 25% (v/v) glycerol, 0.03%(w/v) DDM) XK 20/10 column (GE Healthcare Life Sciences, Inc.) packed with High-Performance Ni^{2+} resin (GE Healthcare Life Sciences, Inc.) at a linear flow rate of 38 cm h^{-1}(Figure 4.13a). Following sample loading, contaminating proteins were removed with binding buffer at 38 cm h^{-1} until Abs_{280} fell below 90 mAU. PSII was eluted using 87.5 mM Imidazole in up-flow operation at 22.6 38 cm $h^{-1,}$ and 2 mL fractions were collected.

Fractions containing PSII were pooled and concentrated using a 100 kD MWCO Amicon® Ultra centrifugal filter (EMD Millipore, Inc.). Removal of Imidazole was completed by diluting the concentrated sample 10-fold with binding buffer and concentrated; this was repeated three times. The final purified sample was tested for homogeneity using a Superose 6 Increase 10/300 (GE Healthcare Life Sciences, Inc.) size exclusion column using a flow velocity of 38 cm h^{-1}(Figure 4.13b). Samples were concentrated to 4-5 mg mL^{-1} using Amicon® Ultra centrifugal filters, aliquoted, snap frozen and stored at -80 °C. chlA concentration was determined using 80% (v/v) acetone extraction[43].

Unilamellar Liposome preparation

Total E. *coli* lipid extract (Avanti Lipids Polar, Inc.) were dissolved in chloroform ($CHCl_3$) at 20 mg mL^{-1} in a glass scintillation vial. A thin film formed by removal of the $CHCl_3$ under vacuum using a rotary evaporator set to 0 psig. The thin film is rehydrated to 15.34 mg mL^{-1} using 5 mM MES, pH 6.5 50 mM KCl, 5 mM $MgCl_2$ 2 mM $CaCl_2$ buffer and placed in a sonication bath for 5 min followed by two freeze-thaw cycles before being extruded through a 0.4 μm polycarbonate membrane 21 times. Typically, the mean diameter as measured by dynamic light scattering of preparations were 180 nm.

Enzyme Reconstitution

The unilamellar liposomes suspension is diluted to a final lipid concentration of 4 mg mL^{-1} and CHAPS concentration of 5 mM by the combination of appropriate amounts of the corresponding buffer, 200 mM CHAPS in the corresponding buffer and concentrated protein. The liposomes-detergent mixture was incubated for 10 min before the addition of protein. The appropriate amount of CMI (4.7 mg mL^{-1}, 50 mM MES, pH 6.0, 50 mM NaCl 1.95 mM DDM) and PSII (5.5 mg mL^{-1}, 50 mM MES, pH 6.0 10 mM $MgCl_2$, 5 mM $CaCl_2$, 25% (v/v) glycerol, 0.78mM DDM) were added to the CHAPS-solubilized preformed liposomes and incubated for 30 min at 4 °C under gentle mixing in the dark. For control experiments, which did not contain an enzyme, the difference in volume was adjusted with buffer.

After the incubation period, the detergent was removed from the lipid-detergent-protein mixture by three successive additions of Bio-Beads SM-2 (80 mg mL^{-1}) every 60 minutes followed by a final addition of 240 mg mL^{-1} and 60 min incubation.

Complex I activity measurements

Proteoliposomes (25 µL) were added to the assay mixture containing 50 µM DQ, 0.2 µM valinomycin, 2.5 µM ACMA in the corresponding buffer. The sample was incubated for 5 min before initiating by the addition 200 µM NADH. For decoupling and inhibition assays 5 µM CCCP and 50 µM piericidin A, respectively, were added to the assay mixture (Figure 4.6). When conducting inhibition assays, proteoliposomes were incubated for 5 min with piericidin A before the addition of DQ.

Photosystem II activity measurements

The oxygen evolution assays for isolated PSII were performed using 50 mM MES, pH 6.5, 10 mM NaCl, 5 mM $MgCl_2$, 20 mM $CaCl_2$ using a Clarke-type electrode (Hansatech Instruments, Ltd.). 2 mM ferricyanide and either 300µM 2,5-Dicholor-1,4-benzoquinone (DCBQ) or 50 µM DQ were added as electron acceptor with 5-10 µg of ChlA of the sample to a final volume of 2 mL. The reaction was initiated by red light (3000 µmol s^{-1} m^{-2}) (Figure 4.14).

The activity of reconstituted PSII samples was tested using 5 mM MES, pH 6.5 50 mM KCl, 5 mM $MgCl_2$ 2 mM $CaCl_2$ with 50 µM DQ and 2 mM ferricyanide. The reaction volume was 400 µL and proteoliposomes containing ~1 µg of chlA was added. Proton gradient generation was measured by quenching of ACMA using the same procedure as done with CMI proteoliposomes. PSII was activated used white light >1,800 µmol photons m^{-2} s^{-1} provided by a 100 W Mercury lamp and the light was passed through a 2 L water filter.

NAD^+ photoreduction assays of PSII:CMI proteoliposomes

Photoreduction of NAD^+ by CMI:PSII proteoliposomes was performed in 5 mM MES, pH 6.5 50 mM KCl, 5 mM $MgCl_2$ 2 mM $CaCl_2$, 25 µL of proteoliposomes were added to the assay mixture containing 50 µM DQ, 0.2µM valinomycin, 2.5 µM ACMA and for inhibition assays and 100 µM DCMU was included. The samples were incubated for 5 minutes before the addition of NADH. The final assay volume was 200µL. In experiments except in the "*Control and Efficiency of NADH production*" white light >1,800 µmol photons m^{-2} s^{-1} was provided by a 100 W Mercury lamp and the light was passed through a 2 L water filter. In the "*Control and Efficiency of NADH production*" our L.E.D. array with Luxeon Rebel diodes with a wavelength centered at 627nm were used for the light source.

Oxygen evolution assays of PSII:CMI proteoliposomes

The oxygen evolution activity of PSII:CMI proteoliposomes were tested using 5 mM MES, pH 6.5 50 mM KCl, 5 mM $MgCl_2$ 2 mM $CaCl_2$ with 50 µM DQ and 200µM NADH. The reaction volume was 400 µL and proteoliposomes containing 1.32 µg of PSII. After the addition of NADH the samples were incubated in the dark for 25 minutes. PSII was activated using red light 3,000 µmol photons m^{-2} s^{-1}.

Supplementary Material

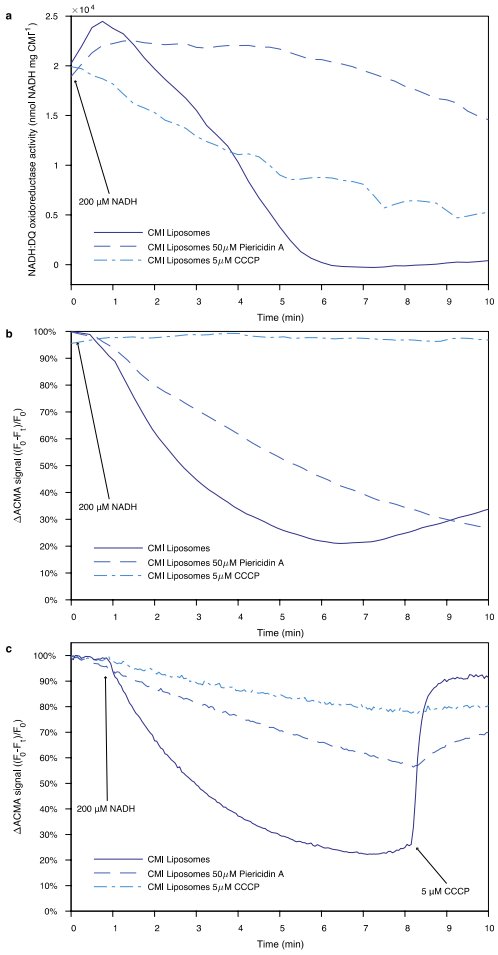

Figure 4.6 | NADH:DQ oxidoreductase activity of Complex I proteoliposomes. After 5 minutes of incubation at 28°C, 200µM NADH was added (indicated by the arrow) to samples that included Piericidin A, and CCCP. a, The NADH:DQ Oxidoreductase activity versus Time b, ΔACMA vs. Time. c, The same as fig. b but at 8 min 5µM CCCP was added to all samples to confirm the change in ΔACMA was caused by abolishing a proton gradient. Each trace is the mean of three technical repeats of a single biological replicate.

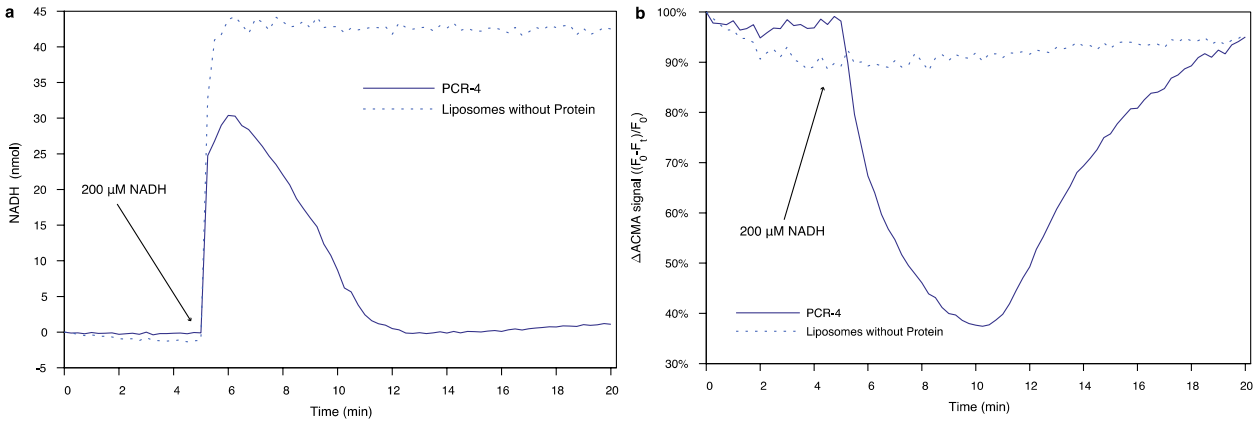

Figure 4.7 | Pre-initiation of NAD^+ photoreduction. Typical results from experiments which used 200 μM NADH as substrate before initiating photoreduction. Samples were incubated for 5 minutes prior to addition of 200 μM NADH indicated by the labeled arrows and incubated for an additional 10-15 minutes to allow the ACMA signal to stabilize before starting photoreduction experiments. a, NADH and b, ACMA signal for PCR-4 and Liposomes without Protein. The results are the representation of three technical repeats of single biological replicate.

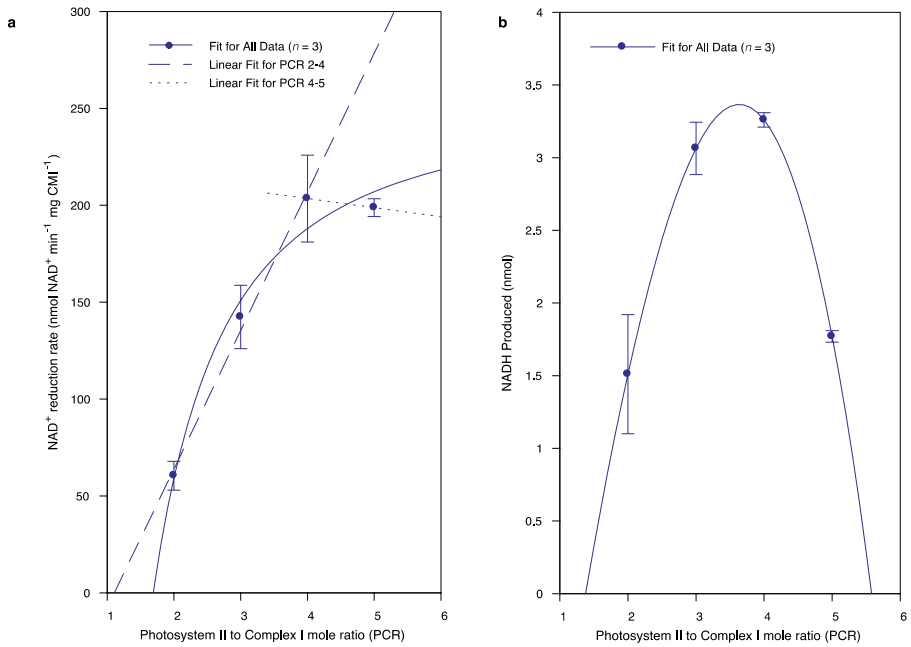

Figure 4.8 | The relationship between PCR and NADH production rate and total NADH produced. a, the rate of NAD^+ reduction versus Photosystem II to Complex I mole ratio (PCR). b, NADH produced (nmol) versus the Photosystem II to Complex I mole ratio (PCR). The error bars represent the standard deviation of n technical repeats of single biological replicate.

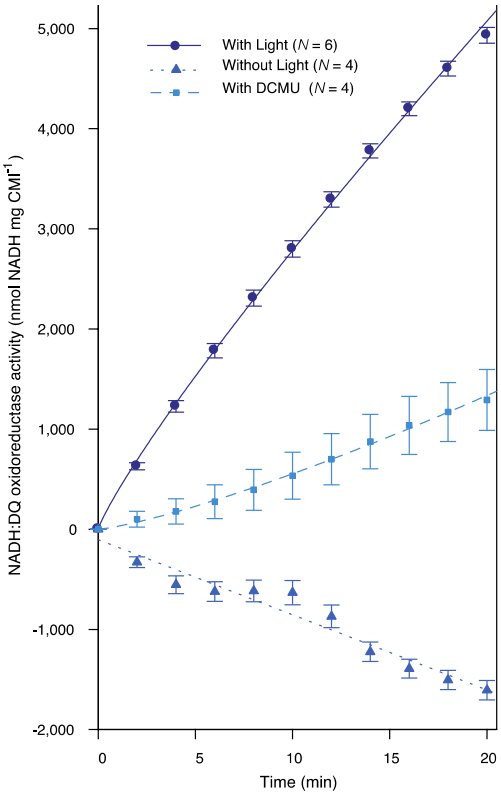

Figure 4.9 | Figure 2c shown with NADH:DQ Oxidoreductase activity of PCR-4 proteoliposomes incubated in the dark. The rate for samples incubated in the dark over the first 5 minutes is -139.5 ± 28.5 nmol min^{-1} mg CMI^{-1}. The error bars represent the standard error of the mean (SEM) of N biological replicates each with three technical replicates.

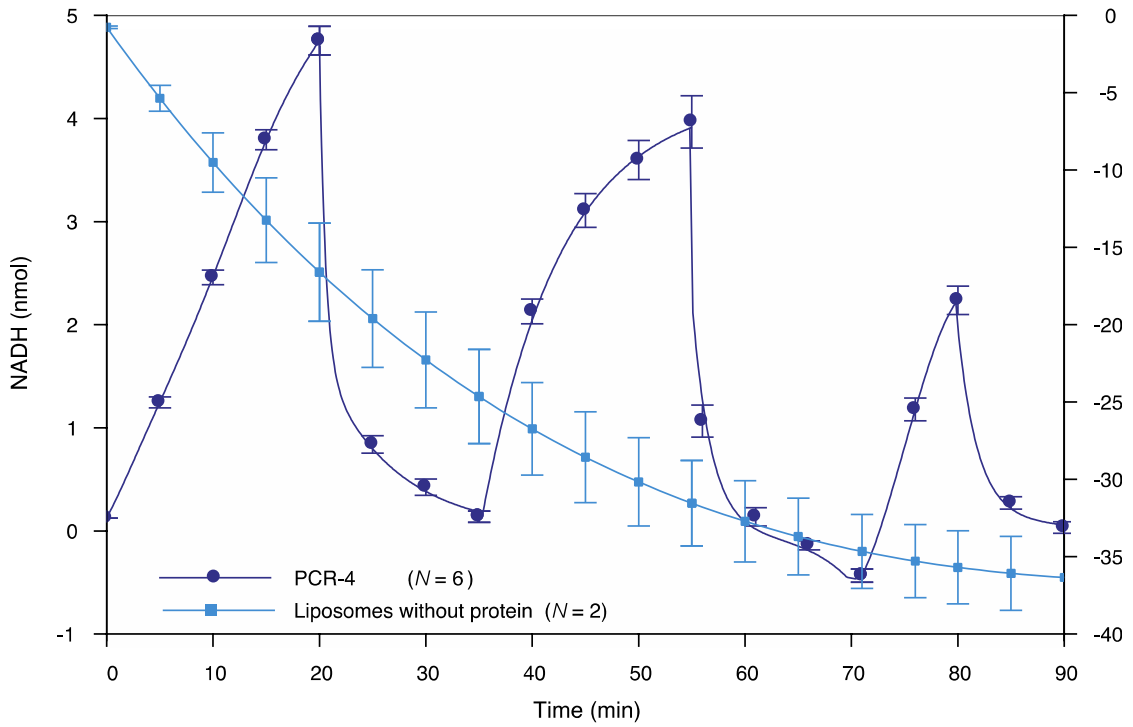

Figure 4.10 | Figure 4a shown in nmols of NADH with liposomes without protein as control included. Values for the liposomes without protein are on the right y-axis. The error bars represent the SEM of N biological replicates each with three technical replicates.

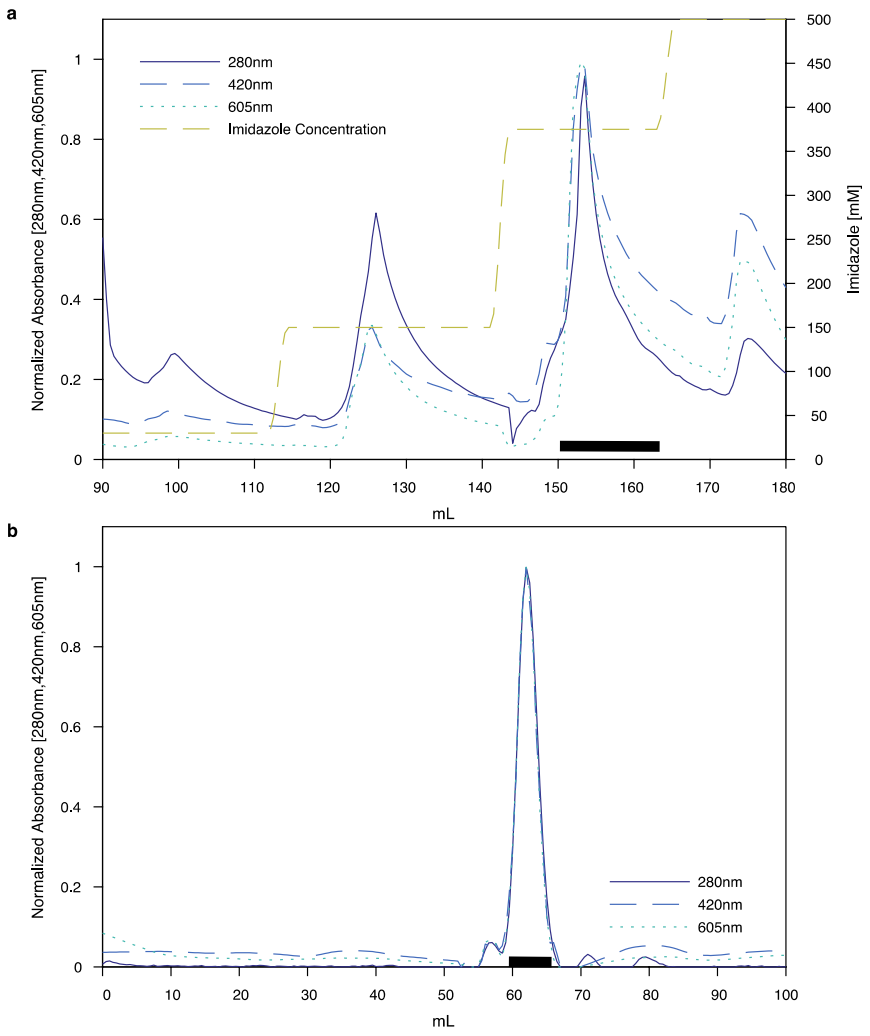

Figure 4.11 | Purification of Complex I. Absorbance at each wavelength are normalized. a, Chromatogram from nickel affinity purification of Complex I. b, Chromatogram of material from Fig. a applied to a HiLoad 16/600 Superdex 200 column. The black bars indicate the fractions which are pooled for subsequent steps.

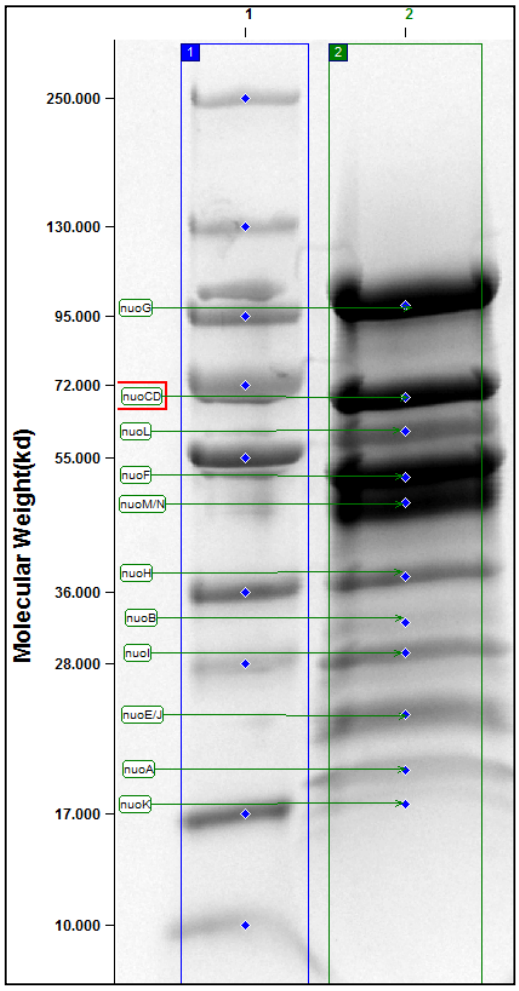

Figure 4.12 | SDS-PAGE of purified Complex I. Lane 1, molecular weight markers, Lane 2 100 μg of purified Complex I. All 13 (nuoCD fused) subunits of Complex I are present with no contaminating bands. Bands are labeled by the apparent molecular weight of the subunits

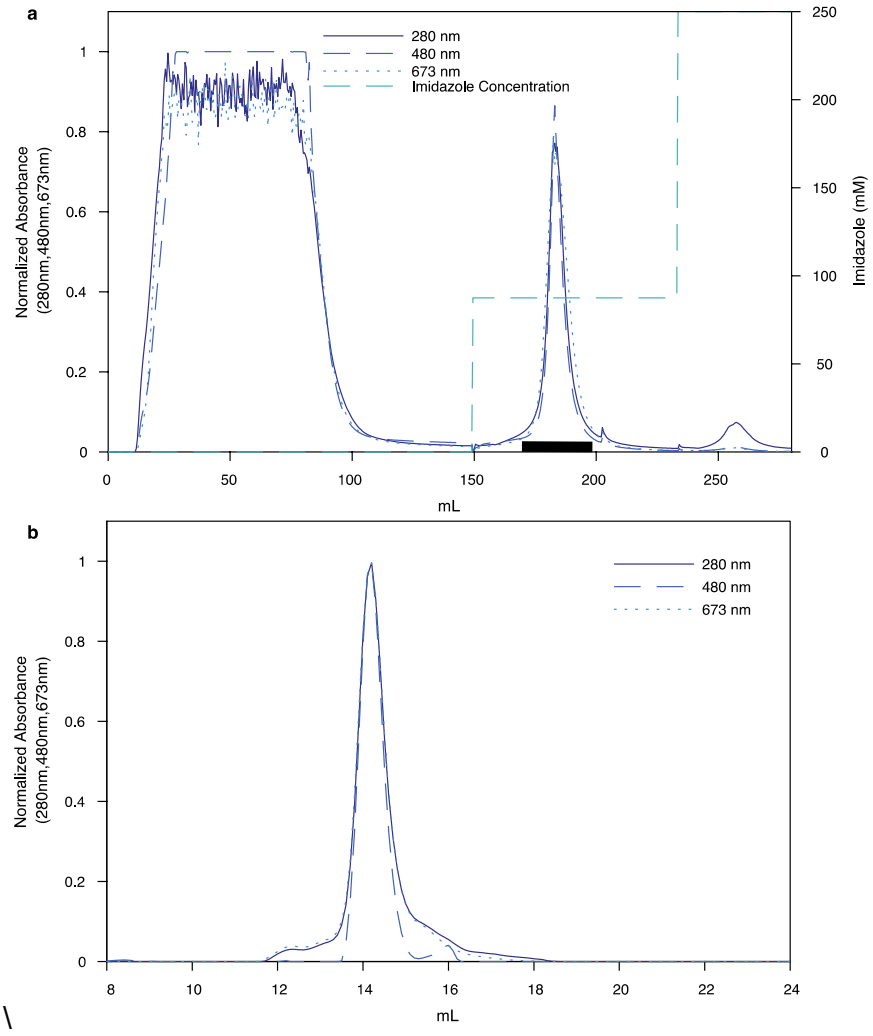

Figure 4.13 | Purification of Photosystem II. a, Chromatogram from nickel affinity. The black bar indicates the fractions which are pooled for subsequent steps. b, Chromatogram the final purified Photosystem II applied to a Superose 6 Increase 10/300 column to test the homogeneity of the purified protein. The protein eluted with 97.8% purity at 14.17 mL.

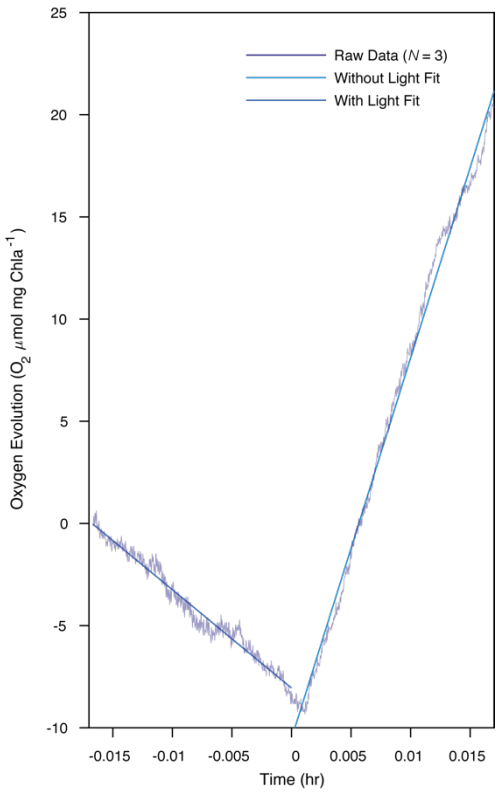

Figure 4.14 | Oxygen evolution activity of purified Photosystem II. Results of one technical measurement of N PSII preparations. At time = 0 Photosystem II was activated by the addition of saturated red light. The solid lines are 1st degree polynomial fits of the dark (y = -(481 ± 6.6)*x – (8.051 ± 0.064)) and light (y = -(1,863 ± 11)*x – (10.53± 0.11)) portions of the experiment. The dark correct oxygen evolution rate is 2,343.9 ± 24.8 μmol O2 hr^{-1} mg $Chla^{-1}$.

Table 4-1 | The amount of NADH produced after 20 min of illumination for different Photosystem II to Complex I mole ratios (PCR) including control sample, liposomes without protein. The results are the representation of two biological replicates each with three technical repeats.

Photosystem II to Complex I mole ratio (PCR)	NADH Produced after 20 min (nmol)
Without Protein	-6.51 ± 1.36
2	1.42 ± 0.95
3	2.87 ± 0.41
4	3.04 ± 0.12
5	1.73 ± 0.08

Table 4-2 | Results from NADH titration photoreduction experiment. The standard deviation of n technical repeats of single biological replicate are reported.

NADH (μM) Added	Max rate NAD^+ reduction (nmol min^{-1} mg CMI^{-1})	Max production of NADH (μM)	NADH (μM) remaining before photoreduction	Sum NADH remaining and produced (μM)
100	194.8 ± 7.3	8.71 ± 0.66	44.84 ± 1.10	57.56 ± 8.18
200	229.2 ± 20.5	9.40 ± 2.03	46.79 ± 1.62	59.88 ± 10.37
300	198.4 ± 14.1	6.65 ± 0.58	50.94 ± 2.07	60.63 ± 8.04
400	117 ± 11.1	1.57 ± 0.45	56.25 ± 0.96	58.38 ± 2.77

Table 4-3 | Results from reconstitution detergent screening for Complex I. Max ΔACMA is from three technical measurements of a single preparation.

Detergent	Detergent Concentration (mM)	Max ΔACMA	NADH:DQ oxidoreductase activity (μmol NADH min^{-1} mg CMI^{-1})
CHAPS	3.0	0.58 ± 0.39%	N/A[1]
CHAPS	7.0	74.54 ± 0.60 %	N/A[1]
Triton X-100	1.8	-2.75 ± 0.26%	-0.00
Triton X-100	7.0	-4.90 ± 0.57%	9.05
OG	18.0	0.71 ± %	5.24
OG	26.0	-0.16 ± %	8.95
DDM	3.8	1.46 ± 0.30%	13.43
DDM	7.0	0.32 ± 0.16 %	0.76

[1]Rates were too fast to measure, and confirmed by the inhibition with 50 μM Piericidin A. Rates for inhibited samples CHAPS 3.0, and 7.0 mM proteoliposomes were -1.05 and -0.48 μmol NADH min^{-1} mg CMI^{-1}, respectively.

Table 4-4 | Results from reconstitution detergent screening for Photosystem II. O_2 Results are three technical repeats of a single preparation

Detergent	Detergent Concentration (mM)	O2 Evolution (umol O2 hr-1 mg ChlA-1)	ΔACMA Percent
CHAPS	3.0	178.08 ± 9.91	49.86 ± 3.07%
CHAPS	7	509.24 ± 256.84	42.76 ± 6.78%
DDM	3.8	565.87 ± 25.19	N/A[1]
DDM	6.8	396.55 ± 69.76	N/A[1]
OG	18	306.95 ± 44.24	N/A[1]
OG	26	481.01 ± 192.16	N/A[1]
TRITON X-100	1.8	530.72 ± 2.53	N/A[1]
TRITON X-100	7	218.69 ± 67.01	N/A[1]

[1]ΔACMA experiments were not performed for samples because of the poor performance of Complex I in reconstitution experiments with the associated detergent.

Table 4-5 | Diode type and optical characteristics for Clark-type electrode system (Hansatech Instruments, Ltd.) and our LED array.

Device	Manufacturer	Part Number	Maximum wavelength	Spectral half-width
LED array	Philips Lumileds	LMX2-PD01	627 nm	20 nm
Clark-type Electrode	Philips Lumileds	LXML-PD01	627 nm	29 nm

References

1. Efrati, A.; Lu, C.-H.; Michaeli, D.; Nechushtai, R.; Alsaoub, S.; Schuhmann, W.; Willner, I., Assembly of photo-bioelectrochemical cells using photosystem I-functionalized electrodes. *Nature Energy* **2016,** *1*, 15021.

2. Carlson, E. D.; Gan, R.; Hodgman, C. E.; Jewett, M. C., Cell-free protein synthesis: Applications come of age. *Biotechnol Adv* **2012,** *30* (5), 1185-1194.

3. Wendell, D.; Todd, J.; Montemagno, C., Artificial Photosynthesis in Ranaspumin-2 Based Foam. *Nano Lett* **2010,** *10* (9), 3231-3236.

4. Keller, M. W.; Schut, G. J.; Lipscomb, G. L.; Menon, A. L.; Iwuchukwu, I. J.; Leuko, T. T.; Thorgersen, M. P.; Nixon, W. J.; Hawkins, A. S.; Kelly, R. M.; Adams, M. W. W., Exploiting microbial hyperthermophilicity to produce an industrial chemical, using hydrogen and carbon dioxide. *Proceedings of the National Academy of Sciences* **2013,** *110* (15), 5840-5845.

5. Schultheisz, H. L.; Szymczyna, B. R.; Scott, L. G.; Williamson, J. R., Pathway Engineered Enzymatic de Novo Purine Nucleotide Synthesis. *Acs Chem Biol* **2008,** *3* (8), 499-511.

6. Mutti, F. G.; Knaus, T.; Scrutton, N. S.; Breuer, M.; Turner, N. J., Conversion of alcohols to enantiopure amines through dual-enzyme hydrogen-borrowing cascades. *Science* **2015,** *349* (6255), 1525-1529.

7. Guterl, J. K.; Garbe, D.; Carsten, J.; Steffler, F.; Sommer, B.; Reisse, S.; Philipp, A.; Haack, M.; Ruhmann, B.; Koltermann, A.; Kettling, U.; Bruck, T.; Sieber, V., Cell-

Free Metabolic Engineering: Production of Chemicals by Minimized Reaction Cascades. *ChemSusChem* **2012,** *5* (11), 2165-2172.

8. Krutsakorn, B.; Honda, K.; Ye, X.; Imagawa, T.; Bei, X.; Okano, K.; Ohtake, H., In vitro production of n-butanol from glucose. *Metabolic engineering* **2013,** *20*, 84-91.

9. Opgenorth, P. H.; Korman, T. P.; Bowie, J. U., A synthetic biochemistry module for production of bio-based chemicals from glucose. *Nature chemical biology* **2016,** *12* (6), 393-U29.

10. Opgenorth, P. H.; Korman, T. P.; Bowie, J. U., A synthetic biochemistry molecular purge valve module that maintains redox balance. *Nature communications* **2014,** *5*, 4113.

11. Lee, H.; Ho, D.; Kuo, K.; Montemagno, C. D., Vectorial insertion of bacteriorhodopsin for directed orientation assays in various polymeric biomembranes. *Polymer* **2006,** *47* (9), 2935-2941.

12. Luo, T. J. M.; Soong, R.; Lan, E.; Dunn, B.; Montemagno, C., Photo-induced proton gradients and ATP biosynthesis produced by vesicles encapsulated in a silica matrix. *Nature materials* **2005,** *4* (3), 220-224.

13. Pitard, B.; Richard, P.; Dunach, M.; Rigaud, J. L., ATP synthesis by the F0F1 ATP synthase from thermophilic Bacillus PS3 reconstituted into liposomes with bacteriorhodopsin .2. Relationships between proton motive force and ATP synthesis. *European Journal of Biochemistry* **1996,** *235* (3), 779-788.

14. Zhang, Y.-H. P., Production of biofuels and biochemicals by in vitro synthetic biosystems: Opportunities and challenges. *Biotechnol Adv* **2015,** *33* (7), 1467-1483.

15. Uppada, V.; Satpute, K.; Noronha, S. B., 10 - Redesigning Cofactor Availability: An Essential Requirement for Metabolic Engineering. In *Current Developments in Biotechnology and Bioengineering*, Elsevier: 2017; pp 223-242.

16. Bezborodov, A. M.; Zagustina, N. A., Enzymatic biocatalysis in chemical synthesis of pharmaceuticals (Review). *Applied Biochemistry and Microbiology* **2016,** *52* (3), 237-249.

17. Muh, F.; Glockner, C.; Hellmich, J.; Zouni, A., Light-induced quinone reduction in photosystem II. *Bba-Bioenergetics* **2012,** *1817* (1), 44-65.

18. Barber, J., Photosystem II: a multisubunit membrane protein that oxidises water. *Current opinion in structural biology* **2002,** *12* (4), 523-530.

19. Brandt, U., Energy Converting NADH: Quinone Oxidoreductase (Complex I). *Annual review of biochemistry* **2006,** *75* (1), 69-92.

20. Armstrong, F. A.; Hirst, J., Reversibility and efficiency in electrocatalytic energy conversion and lessons from enzymes. *Proceedings of the National Academy of Sciences* **2011,** *108* (34), 14049-14054.

21. Baradaran, R.; Berrisford, J. M.; Minhas, G. S.; Sazanov, L. A., Crystal structure of the entire respiratory complex I. *Nature* **2013,** *494* (7438), 443-448.

22. Umena, Y.; Kawakami, K.; Shen, J.-R.; Kamiya, N., Crystal structure of oxygen-evolving photosystem II at a resolution of 1.9[thinsp]A. *Nature* **2011,** *473* (7345), 55-60.

23. Rigaud, J. L.; Levy, D., Reconstitution of membrane proteins into liposomes. *Liposomes, Pt B* **2003,** *372*, 65-86.

24. Pryde, K. R.; Hirst, J., Superoxide Is Produced by the Reduced Flavin in Mitochondrial Complex I A Single, Unifed Mechanism that Applies During Both Forward

and Reverse Electron Transfer. *Journal of Biological Chemistry* **2011,** *286* (20), 18056-18065.

25. Kotlyar, A. B.; Vinogradov, A. D., Slow Active Inactive Transition of the Mitochondrial Nadh-Ubiquinone Reductase. *Biochimica et biophysica acta* **1990,** *1019* (2), 151-158.

26. Hsu, B. D.; Lee, J. Y.; Pan, R. L., The two binding sites for DCMU in Photosystem II. *Biochemical and biophysical research communications* **1986,** *141* (2), 682-8.

27. Trebst, A., Inhibitors in the functional dissection of the photosynthetic electron transport system. *Photosynthesis research* **2007,** *92* (2), 217-224.

28. Convent, B.; Briquet, M., Properties of 3-(3,4-Dichlorophenyl)-1,1-dimethylurea and Other Inhibitors of the Cytochrome bc1 Segment of the Mitochondrial Respiratory Chain in Saccharomyces cerevisiae. *European Journal of Biochemistry* **1978,** *82* (2), 473-481.

29. Liu, L.-N.; Bryan, S. J.; Huang, F.; Yu, J.; Nixon, P. J.; Rich, P. R.; Mullineaux, C. W., Control of electron transport routes through redox-regulated redistribution of respiratory complexes. *Proceedings of the National Academy of Sciences* **2012,** *109* (28), 11431-11436.

30. Degli Esposti, M., Inhibitors of NADH-ubiquinone reductase: an overview. *Biochimica et biophysica acta* **1998,** *1364* (2), 222-35.

31. Casadio, R., Measurements of Transmembrane Ph Differences of Low Extents in Bacterial Chromatophores - a Study with the Fluorescent-Probe 9-Amino, 6-Chloro, 2-Methoxyacridine. *European Biophysics Journal* **1991,** *19* (4), 189-201.

32. D'Alessandro, M.; Turina, P.; Melandri, B. A., Quantitative evaluation of the intrinsic uncoupling modulated by ADP and Pi in the reconstituted ATP synthase of Escherichia coli. *Biochimica et Biophysica Acta (BBA) - Bioenergetics* **2011,** *1807* (1), 130-143.

33. Vinogradov, A. D.; Gavrikova, E. V.; Grivennikova, V. G.; Zharova, T. V.; Zakharova, N. V., Catalytic properties of mitochondrial NADH-ubiquinone reductase (Complex I). *Biochemistry. Biokhimiia* **1999,** *64* (2), 136-52.

34. vanBelzen, R.; Kotlyar, A. B.; Moon, N.; Dunham, W. R.; Albracht, S. P. J., The iron-sulfur clusters 2 and ubisemiquinone radicals of NADH:ubiquinone oxidoreductase are involved in energy coupling in submitochondrial particles. *Biochemistry-Us* **1997,** *36* (4), 886-893.

35. De Jong, A. M. P.; Albracht, S. P. J., Ubisemiquinones as obligatory intermediates in the electron transfer from NADH to ubiquinone. *European Journal of Biochemistry* **1994,** *222* (3), 975-982.

36. Hirst, J.; Roessler, M. M., Energy conversion, redox catalysis and generation of reactive oxygen species by respiratory complex I. *Bba-Bioenergetics* **2016,** *1857* (7), 872-883.

37. Oursel, D.; Loutelier-Bourhis, C.; Orange, N.; Chevalier, S.; Norris, V.; Lange, C. M., Lipid composition of membranes of Escherichia coli by liquid chromatography/tandem mass spectrometry using negative electrospray ionization. *Rapid Commun Mass Sp* **2007,** *21* (11), 1721-1728.

38. van Eerden, F. J.; de Jong, D. H.; de Vries, A. H.; Wassenaar, T. A.; Marrink, S. J., Characterization of thylakoid lipid membranes from cyanobacteria and higher plants

by molecular dynamics simulations. *Biochimica et Biophysica Acta (BBA) - Biomembranes* **2015,** *1848* (6), 1319-1330.

39. Sakurai, I.; Jian-Ren, S.; Jing, L.; Ohashi, S.; Kobayashi, M.; Wada, H., Lipids in Oxygen-Evolving Photosystem II Complexes of Cyanobacteria and Higher Plants. *Journal of biochemistry* **2006,** *140* (2), 201-209.

40. Spehr, V.; Schlitt, A.; Scheide, D.; Guenebaut, V.; Friedrich, T., Overexpression of the Escherichia coli nuo-operon and isolation of the overproduced NADH:ubiquinone oxidoreductase (complex I). *Biochemistry-Us* **1999,** *38* (49), 16261-7.

41. Pohl, T.; Uhlmann, M.; Kaufenstein, M.; Friedrich, T., Lambda Red-mediated mutagenesis and efficient large scale affinity purification of the Escherichia coli NADH:ubiquinone oxidoreductase (complex I). *Biochemistry-Us* **2007,** *46* (37), 10694-702.

42. Bricker, T. M.; Morvant, J.; Masri, N.; Sutton, H. M.; Frankel, L. K., Isolation of a highly active Photosystem II preparation from Synechocystis 6803 using a histidine-tagged mutant of CP 47. *Bba-Bioenergetics* **1998,** *1409* (1), 50-57.

43. Vavilin, D. V., Methods for the Isolation of Functional Photosystem II Core Particles from the Cyanobacterium Synechocystis sp PCC 6803. In *Photosynthesis Research Protocols, Second Edition*, Carpentier, R., Ed. Humana Press Inc: Totowa, 2011; Vol. 684, pp 29-40.

5. Summary and Conclusions

The objectives of this research were to engineer artificial organelle capable of converting light energy into the reduced NADH. This work demonstrates that PSII and CMI can be co-reconstituted into a lipid bilayer to combined their respective metabolisms.

Reported in chapter 2 is a procedure for the rapid and scalable purification of bR. This chapter illustrates the use of TFF to isolate the 2D-crystalline membrane protein at purities > 90% and the use of AIEX chromatography for the capture of solubilized bR and the removal of excess detergent.

The activities performed for the work presented in chapter 3 were completed to illustrate, explicitly, that CMI can utilize a ΔpH to transfer electrons from QH2 to NAD^+. Additionally, it is shown that the CMI inhibitor Piericidin A, does not inhibit the R.E.T. activity of CMI. This work also supports the decision for controls to be used in chapter 4.

Chapter 5 details the work and results conclusively demonstrating that the associated metabolisms of PSII and CMI can be combined to reduce NAD^+ consuming only photos and H_2O. Moreover, the results from this study show, the optimum molecular ratio of PSII and CMI is 4 to 1, the rate of NAD^+ photoreduction is controllable via the intensity of the quantum flux, the activities of PSII and CMI are coupled at >95% efficiently.

Pros and cons of cell-free metabolic systems

Cell-free metabolic systems (CFMS) are beginning to demonstrate their potential to disrupt current methods for producing chemicals, pharmaceuticals, and biologics. The

potential of becoming a disruptive technology is driven by the advantages that CFMS have over whole-cell biocatalysts (WBC) and traditional chemistry. After decoupling the cellular machinery not required for the biochemical pathway of interest, all biological constraints are removed. By removing these constraints, the result is a system which is highly energy efficient with high production yields and allows for more straightforward metabolic pathway engineering and control then WBC[1-3]. By capitalizing on the ability of biological molecules to catalyze reactions with unprecedented specificity at physiological temperatures and pH, many green alternative synthetic pathways become available to replace traditional chemistry.

However, some challenges need to be addressed for CFMS to be widely adopted. The challenges of CFMS include the isolation and stabilization of the enzymes and replenishing energy in the CFMS. The most significant disadvantages in isolated enzymes are costs associated with purification of the enzymes and the enzymatic cofactors and the stability of the isolated enzymes[1]. The issue of enzyme stability is circumvented by immobilizing or entrapment techniques[3-11]. Moreover, immobilizing and entrapment platforms must be developed for each enzyme which requires additional development and research efforts. For CFMS to be self-sustaining and have high productivity, replenishing energy in the system as enzymatic cofactors like ATP and NAD(P)H is imperative. Maintaining energy requirements is a considerable challenge for CFMS due to the absence of the complicated regulatory networks that produce and balance enzymatic cofactors and adding stoichiometric quantities of cofactors is not economically feasible[12-16].

Future challenges

There are two major developments that need to be addressed before enabling CFMS to become a disruptive technology across all industrial sectors. The first is a technology that will allow the procurement sufficient quantities of the required enzymes at a price point that would allow the CFMS of interest to be economically viable. This will require significant efforts for production and isolation of membrane proteins. The second development will be to assemble artificial organelles (e.g. bR-ATPase proteoliposomes and PSII-CMI proteoliposomes) rapidly at large scale while controlling orientation of the membrane protein within the membrane bilayer. Of these two challenges identified here, I believe the assembly of artificial organelles will prove to be the more challenging of the two. This will require a technology that will facilitate the controlled and instantaneous insertion of membrane proteins into a membrane, possibly with the use of an affinity tag-type[17] technology and polymeric membranes. However, the promise and advantages of CFMS will continue to drive researchers to overcome these challenges and any others that may be identified as the technology matures.

References

1. Dudley, Q. M.; Karim, A. S.; Jewett, M. C., Cell-free metabolic engineering: Biomanufacturing beyond the cell. *Biotechnol J* **2014**.

2. Nestl, B. M.; Nebel, B. A.; Hauer, B., Recent progress in industrial biocatalysis. *Current Opinion in Chemical Biology* **2011,** *15* (2), 187-193.

3. Illanes, A.; Cauerhff, A.; Wilson, L.; Castro, G. R., Recent trends in biocatalysis engineering. *Bioresource Technol* **2012,** *115* (0), 48-57.

4. Nestl, B. M.; Hammer, S. C.; Nebel, B. A.; Hauer, B., New Generation of Biocatalysts for Organic Synthesis. *Angew Chem Int Edit* **2014,** *53* (12), 3070-3095.

5. Wells, A., 9.11 Industrial Applications of Biocatalysis: An Overview. In *Comprehensive Chirality*, Carreira, E. M.; Yamamoto, H., Eds. Elsevier: Amsterdam, 2012; pp 253-287.

6. Tufvesson, P.; Fu, W.; Jensen, J. S.; Woodley, J. M., Process considerations for the scale-up and implementation of biocatalysis. *Food and Bioproducts Processing* **2010,** *88* (1), 3-11.

7. Sahare, P.; Ayala, M.; Vazquez-Duhalt, R.; Agrawal, V., Immobilization of peroxidase enzyme onto the porous silicon structure for enhancing its activity and stability. *Nanoscale research letters* **2014,** *9* (1), 409.

8. Jang, E.; Ryu, B. H.; Kim, T. D., Identification, characterization, and immobilization of an organic solvent-stable alkaline hydrolase (PA27) from Pseudomonas aeruginosa MH38. *Molecules* **2014,** *19* (9), 14396-405.

9. Talbert, J. N.; Wang, L. S.; Duncan, B.; Jeong, Y.; Andler, S. M.; Rotello, V. M.; Goddard, J. M., Immobilization and Stabilization of Lipase (CaLB) through Hierarchical Interfacial Assembly. *Biomacromolecules* **2014**.

10. Vashist, S. K.; Lam, E.; Hrapovic, S.; Male, K. B.; Luong, J. H., Immobilization of Antibodies and Enzymes on 3-Aminopropyltriethoxysilane-Functionalized Bioanalytical Platforms for Biosensors and Diagnostics. *Chem Rev* **2014**.

11. Lee, J. H.; Nam, D. H.; Lee, S. H.; Park, J. H.; Park, S. J.; Lee, S. H.; Park, C. B.; Jeong, K. J., New Platform for Cytochrome P450 Reaction Combining in Situ Immobilization on Biopolymer. *Bioconjugate chemistry* **2014**.

12. Hollmann, F.; Schmid, A., Electrochemical regeneration of oxidoreductases for cell-free biocatalytic redox reactions. *Biocatal Biotransfor* **2004,** *22* (2), 63-88.

13. Quinto, T.; Kohler, V.; Ward, T. R., Recent Trends in Biomimetic NADH Regeneration. *Top Catal* **2014,** *57* (5), 321-331.

14. Wu, H.; Tian, C.; Song, X.; Liu, C.; Yang, D.; Jiang, Z., Methods for the regeneration of nicotinamide coenzymes. *Green Chem* **2013,** *15* (7), 1773-1789.

15. Liu, W.; Wang, P., Cofactor regeneration for sustainable enzymatic biosynthesis. *Biotechnol Adv* **2007,** *25* (4), 369-84.

16. Uppada, V.; Bhaduri, S.; Noronha, S. B., Cofactor regeneration - an important aspect of biocatalysis. *Curr Sci India* **2014,** *106* (7), 946-957.

17. Gao, X.; Fang, J.; Xue, B.; Fu, L.; Li, H., Engineering Protein Hydrogels Using SpyCatcher-SpyTag Chemistry. *Biomacromolecules* **2016,** *17* (9), 2812-9

References

Chapter 1

1. Ardao, I.; Hwang, E. T.; Zeng, A. P., In vitro multienzymatic reaction systems for biosynthesis. *Advances in biochemical engineering/biotechnology* **2013,** *137*, 153-84.

2. van Oers, M. C. M.; Rutjes, F.; van Hest, J. C. M., Cascade reactions in nanoreactors. *Current Opinion in Biotechnology* **2014,** *28*, 10-16.

3. Ho, D.; Chu, B.; Lee, H.; Brooks, E. K.; Kuo, K.; Montemagno, C. D., Fabrication of biomolecule-copolymer hybrid nanovesicles as energy conversion systems. *Nanotechnology* **2005,** *16* (12), 3120-3132.

4. Choi, H. J.; Montemagno, C. D., Artificial organelle: ATP synthesis from cellular mimetic polymersomes. *Nano Lett* **2005,** *5* (12), 2538-2542.

5. Choi, H. J.; Lee, H.; Montemagno, C. D., Toward hybrid proteo-polymeric vesicles generating a photoinduced proton gradient for biofuel cells. *Nanotechnology* **2005,** *16* (9), 1589-1597.

6. Chu, B. M.; Ho, D.; Lee, H.; Kuo, K.; Montemagno, C., Coupled-protein functionality for energy conversion in biomimetic systems. *2005 IEEE International Conference on Robotics and Biomimetics* **2006**, 356-359.

7. Choi, H. J.; Montemagno, C. D., Light-driven hybrid bioreactor based on protein-incorporated polymer vesicles. *Ieee T Nanotechnol* **2007,** *6* (2), 171-176.

8. Heldt, H.-W.; Heldt, F., 6 - The Calvin cycle catalyzes photosynthetic CO2 assimilation. **2005**.

9. Dudley, Q. M.; Karim, A. S.; Jewett, M. C., Cell-free metabolic engineering: Biomanufacturing beyond the cell. *Biotechnol J* **2014**.

10. Uppada, V.; Bhaduri, S.; Noronha, S. B., Cofactor regeneration - an important aspect of biocatalysis. *Curr Sci India* **2014,** *106* (7), 946-957.

11. Liu, W.; Wang, P., Cofactor regeneration for sustainable enzymatic biosynthesis. *Biotechnol Adv* **2007,** *25* (4), 369-84.

12. Bornscheuer, U. T.; Buchholz, K., Highlights in Biocatalysis – Historical Landmarks and Current Trends. *Eng Life Sci* **2005,** *5* (4), 309-323.

13. Tufvesson, P.; Fu, W.; Jensen, J. S.; Woodley, J. M., Process considerations for the scale-up and implementation of biocatalysis. *Food and Bioproducts Processing* **2010,** *88* (1), 3-11.

14. Nestl, B. M.; Nebel, B. A.; Hauer, B., Recent progress in industrial biocatalysis. *Current Opinion in Chemical Biology* **2011,** *15* (2), 187-193.

15. Wells, A., 9.11 Industrial Applications of Biocatalysis: An Overview. In *Comprehensive Chirality*, Carreira, E. M.; Yamamoto, H., Eds. Elsevier: Amsterdam, 2012; pp 253-287.

16. Sanchez, S.; Demain, A. L., Enzymes and Bioconversions of Industrial, Pharmaceutical, and Biotechnological Significance. *Org Process Res Dev* **2011,** *15* (1), 224-230.

17. Solano, D. M.; Hoyos, P.; Hernaiz, M. J.; Alcantara, A. R.; Sanchez-Montero, J. M., Industrial biotransformations in the synthesis of building blocks leading to enantiopure drugs. *Bioresource Technol* **2012,** *115*, 196-207.

18. de Carvalho, C. C. C. R., Enzymatic and whole cell catalysis: Finding new strategies for old processes. *Biotechnol Adv* **2011,** *29* (1), 75-83.

19. Wandrey, C.; Liese, A.; Kihumbu, D., Industrial biocatalysis: Past, present, and future. *Org Process Res Dev* **2000,** *4* (4), 286-290.

20. Sheldon, R. A.; van Rantwijk, F., Biocatalysis for sustainable organic synthesis. *Australian journal of chemistry* **2004,** *57* (4), 281-289.

21. Nestl, B. M.; Hammer, S. C.; Nebel, B. A.; Hauer, B., New Generation of Biocatalysts for Organic Synthesis. *Angew Chem Int Edit* **2014,** *53* (12), 3070-3095.

22. Illanes, A.; Cauerhff, A.; Wilson, L.; Castro, G. R., Recent trends in biocatalysis engineering. *Bioresource Technol* **2012,** *115* (0), 48-57.

23. Sahare, P.; Ayala, M.; Vazquez-Duhalt, R.; Agrawal, V., Immobilization of peroxidase enzyme onto the porous silicon structure for enhancing its activity and stability. *Nanoscale research letters* **2014,** *9* (1), 409.

24. Jang, E.; Ryu, B. H.; Kim, T. D., Identification, characterization, and immobilization of an organic solvent-stable alkaline hydrolase (PA27) from Pseudomonas aeruginosa MH38. *Molecules* **2014,** *19* (9), 14396-405.

25. Talbert, J. N.; Wang, L. S.; Duncan, B.; Jeong, Y.; Andler, S. M.; Rotello, V. M.; Goddard, J. M., Immobilization and Stabilization of Lipase (CaLB) through Hierarchical Interfacial Assembly. *Biomacromolecules* **2014**.

26. Vashist, S. K.; Lam, E.; Hrapovic, S.; Male, K. B.; Luong, J. H., Immobilization of Antibodies and Enzymes on 3-Aminopropyltriethoxysilane-Functionalized Bioanalytical Platforms for Biosensors and Diagnostics. *Chem Rev* **2014**.

27. Lee, J. H.; Nam, D. H.; Lee, S. H.; Park, J. H.; Park, S. J.; Lee, S. H.; Park, C. B.; Jeong, K. J., New Platform for Cytochrome P450 Reaction Combining in Situ Immobilization on Biopolymer. *Bioconjugate chemistry* **2014**.

28. Straathof, A. J. J., Transformation of Biomass into Commodity Chemicals Using Enzymes or Cells. *Chem Rev* **2013,** *114* (3), 1871-1908.

29. Kaur, G.; Srivastava, A. K.; Chand, S., Advances in biotechnological production of 1,3-propanediol. *Biochemical Engineering Journal* **2012,** *64*, 106-118.

30. Hollmann, F.; Arends, I. W. C. E.; Buehler, K., Biocatalytic Redox Reactions for Organic Synthesis: Nonconventional Regeneration Methods. *Chemcatchem* **2010,** *2* (7), 762-782.

31. Meyer, H. P.; Eichhorn, E.; Hanlon, S.; Lutz, S.; Schurmann, M.; Wohlgemuth, R.; Coppolecchia, R., The use of enzymes in organic synthesis and the life sciences: perspectives from the Swiss Industrial Biocatalysis Consortium (SIBC). *Catal Sci Technol* **2013,** *3* (1), 29-40.

32. Kuchel, P. W., Biochemistry. In *Schaum's outline series* [Online] 3rd ed.; McGraw-Hill: New York, 2012; pp. 1 online resource (xiii, 492 p.). http://accessengineeringlibrary.com/browse/schaums-outline-of-biochemistry-third-edition.

33. Wu, H.; Tian, C.; Song, X.; Liu, C.; Yang, D.; Jiang, Z., Methods for the regeneration of nicotinamide coenzymes. *Green Chem* **2013,** *15* (7), 1773-1789.

34. Chenault, H. K.; Whitesides, G. M., Regeneration of Nicotinamide Cofactors for Use in Organic-Synthesis. *Applied biochemistry and biotechnology* **1987,** *14* (2), 147-197.

35. Hollmann, F.; Schmid, A., Electrochemical regeneration of oxidoreductases for cell-free biocatalytic redox reactions. *Biocatal Biotransfor* **2004,** *22* (2), 63-88.

36. Quinto, T.; Kohler, V.; Ward, T. R., Recent Trends in Biomimetic NADH Regeneration. *Top Catal* **2014,** *57* (5), 321-331.

37. Wandrey, C., Biochemical reaction engineering for redox reactions. *Chem Rec* **2004,** *4* (4), 254-265.

38. Ali, I.; Soomro, B.; Omanovic, S., Electrochemical regeneration of NADH on a glassy carbon electrode surface: The influence of electrolysis potential. *Electrochem Commun* **2011,** *13* (6), 562-565.

39. Ali, I.; Gill, A.; Omanovic, S., Direct electrochemical regeneration of the enzymatic cofactor 1,4-NADH employing nano-patterned glassy carbon/Pt and glassy carbon/Ni electrodes. *Chem Eng J* **2012,** *188*, 173-180.

40. Azem, A.; Man, F.; Omanovic, S., Direct regeneration of NADH on a ruthenium modified glassy carbon electrode. *J Mol Catal a-Chem* **2004,** *219* (2), 283-299.

41. Man, F.; Omanovic, S., A kinetic study of NAD(+) reduction on a ruthenium modified glassy carbon electrode. *J Electroanal Chem* **2004,** *568* (1-2), 301-313.

42. Vuorilehto, K.; Lutz, S.; Wandrey, C., Indirect electrochemical reduction of nicotinamide coenzymes. *Bioelectrochemistry* **2004,** *65* (1), 1-7.

43. Steckhan, E., Electroenzymatic Synthesis. *Electrochemistry V* **1994,** *170*, 83-111.

44. Lutz, J.; Hollmann, F.; Ho, T. V.; Schnyder, A.; Fish, R. H.; Schmid, A., Bioorganometallic chemistry: biocatalytic oxidation reactions with biomimetic NAD(+)/NADH co-factors and [Cp*Rh(bpy)H](+) for selective organic synthesis. *J Organomet Chem* **2004,** *689* (25), 4783-4790.

45. Truppo, M. D., 7.4 Cofactor Recycling for Enzyme Catalyzed Processes. In *Comprehensive Chirality*, Carreira, E. M.; Yamamoto, H., Eds. Elsevier: Amsterdam, 2012; pp 46-70.

46. Walsh, K. A. J.; Daniel, R. M.; Morgan, H. W., A Soluble Nadh Dehydrogenase (Nadh-Ferricyanide Oxidoreductase) from Thermus-Aquaticus Strain T351. *Biochemical Journal* **1983,** *209* (2), 427-433.

47. Shively, J. M.; Cannon, G. C.; Heinhorst, S.; Fuerst, J. A.; Bryant, D. A.; Gantt, E.; Maupin-Furlow, J. A.; Schüler, D.; Pfeifer, F.; Docampo, R.; Dahl, C.; Preiss, J.; Steinbüchel, A.; Federici, B. A., Intracellular Structures of Prokaryotes: Inclusions, Compartments and Assemblages. In *Encyclopedia of Microbiology (Third Edition)*, Schaechter, M., Ed. Academic Press: Oxford, 2009; pp 404-424.

48. Marguet, M.; Bonduelle, C.; Lecommandoux, S., Multicompartmentalized polymeric systems: towards biomimetic cellular structure and function. *Chemical Society reviews* **2013,** *42* (2), 512-529.

49. Ho, D.; Chu, B.; Schmidt, J. J.; Brooks, E. K.; Montemagno, C. D., Hybrid protein-polymer biomimetic membranes. *Ieee T Nanotechnol* **2004,** *3* (2), 256-263.

50. Ho, D.; Schmidt, J. J.; Montemagno, C. D., Protein/polymer hybrid biomimetic valves. *Bioinspired Nanoscale Hybrid Systems* **2003,** *735*, 45-48.

51. Ho, D.; Chu, B.; Schmidt, J. J.; Brooks, E. K.; Montemagno, C. D., Hybrid protein/polymer biomimetic membranes. *2003 Third Ieee Conference on Nanotechnology, Vols One and Two, Proceedings* **2003**, 379-382.

52. Tanner, P.; Egli, S.; Balasubramanian, V.; Onaca, O.; Palivan, C. G.; Meier, W., Can polymeric vesicles that confine enzymatic reactions act as simplified organelles? *FEBS letters* **2011,** *585* (11), 1699-1706.

53. Almen, M. S.; Nordstrom, K. J. V.; Fredriksson, R.; Schioth, H. B., Mapping the human membrane proteome: a majority of the human membrane proteins can be classified according to function and evolutionary origin. *Bmc Biol* **2009,** *7*.

54. Nelson, D. L.; Lehninger, A. L.; Cox, M. M., *Lehninger principles of biochemistry*. 5th ed.; W.H. Freeman: New York, 2008; p 1158, [105] p.

55. Choi, H. J.; Montemagno, C. D., Recent Progress in Advanced Nanobiological Materials for Energy and Environmental Applications. *Materials* **2013,** *6* (12), 5821-5856.

56. Steffen, W.; Steuber, J., Cation transport by the respiratory NADH: quinone oxidoreductase (complex I): facts and hypotheses. *Biochemical Society transactions* **2013,** *41*, 1280-1287.

57. Baradaran, R.; Berrisford, J. M.; Minhas, G. S.; Sazanov, L. A., Crystal structure of the entire respiratory complex I. *Nature* **2013,** *494* (7438), 443-448.

58. Brandt, U., Energy Converting NADH: Quinone Oxidoreductase (Complex I). *Annual review of biochemistry* **2006,** *75* (1), 69-92.

59. Efremov, R. G.; Baradaran, R.; Sazanov, L. A., The architecture of respiratory complex I. *Nature* **2010,** *465* (7297), 441-U61.

60. Ohnishi, T.; Nakamaru-Ogiso, E.; Ohnishi, S. T., A new hypothesis on the simultaneous direct and indirect proton pump mechanisms in NADH-quinone oxidoreductase (complex I). *FEBS letters* **2010,** *584* (19), 4131-4137.

61. Nore, B. F., ΔpH driven energy-linked NAD+ reduction in Rhodospirillum rubrum chromatophores. *Archives of biochemistry and biophysics* **1989,** *274* (1), 285-289.

62. Kriegel, S.; Uchida, T.; Osawa, M.; Friedrich, T.; Hellwig, P., Biomimetic Environment to Study E. coli Complex I through Surface-Enhanced IR Absorption Spectroscopy. *Biochemistry-Us* **2014**.

63. Ohnishi, T.; Ohnishi, S. T.; Shinzawa-Ito, K.; Yoshikawa, S., Functional role of Coenzyme Q in the energy coupling of NADH-CoQ oxidoreductase (Complex I): Stabilization of the semiquinone state with the application of inside-positive membrane potential to proteoliposomes. *BioFactors* **2008,** *32* (1-4), 13-22.

64. Selivanov, V. A.; Votyakova, T. V.; Pivtoraiko, V. N.; Zeak, J.; Sukhomlin, T.; Trucco, M.; Roca, J.; Cascante, M., Reactive Oxygen Species Production by Forward and Reverse Electron Fluxes in the Mitochondrial Respiratory Chain. *Plos Comput Biol* **2011,** *7* (3).

65. Kotlyar, A. B.; Borovok, N., NADH oxidation and NAD+ reduction catalysed by tightly coupled inside-out vesicles from Paracoccus denitrificans. *European journal of biochemistry / FEBS* **2002,** *269* (16), 4020-4.

66. Wang, Z. G.; Xu, T. H.; Liu, C.; Yang, C. H., Fast Isolation of Highly Active Photosystem II Core Complexes from Spinach. *J Integr Plant Biol* **2010,** *52* (9), 793-800.

67. Ramesh, V. M.; Fish, A.; Michaeli, D.; Keren, N.; Ohad, I.; Vorchovsky, L.; Nechushtai, R., Isolation and characterization of an oxygen evolving photosystem 2 core complex from the thermophilic cyanobacterium Mastigocladus laminosus. *Photosynthetica* **2002,** *40* (3), 355-361.

68. Kato, M.; Zhang, J. Z.; Paul, N.; Reisner, E., Protein film photoelectrochemistry of the water oxidation enzyme photosystem II. *Chemical Society reviews* **2014,** *43* (18), 6485-6497.

69. Barber, J., Photosystem II: a multisubunit membrane protein that oxidises water. *Current opinion in structural biology* **2002,** *12* (4), 523-530.

70. Saito, K.; Rutherford, A. W.; Ishikita, H., Mechanism of proton-coupled quinone reduction in Photosystem II. *P Natl Acad Sci USA* **2013,** *110* (3), 954-959.

71. Mavelli, F.; Trotta, M.; Ciriaco, F.; Agostiano, A.; Giotta, L.; Italiano, F.; Milano, F., The binding of quinone to the photosynthetic reaction centers: kinetics and thermodynamics of reactions occurring at the Q(B)-site in zwitterionic and anionic liposomes. *Eur Biophys J Biophy* **2014,** *43* (6-7), 301-315.

72. Glockner, C.; Kern, J.; Broser, M.; Zouni, A.; Yachandra, V.; Yano, J., Structural Changes of the Oxygen-evolving Complex in Photosystem II during the Catalytic Cycle. *Journal of Biological Chemistry* **2013,** *288* (31), 22607-22620.

73. Brudvig, G. W., Water oxidation chemistry of photosystem II. *Philosophical Transactions of the Royal Society B: Biological Sciences* **2008,** *363* (1494), 1211-1219.

Chapter 2

1. Neugebauer, D.-C.; Zingsheim, H.-P.; Oesterhelt, D., [21] Biogenesis of purple membrane in halobacteria. In *Methods in Enzymology*, Academic Press: 1983; Vol. Volume 97, pp 218-226.

2. Krebs, M. P.; Isenbarger, T. A., Structural determinants of purple membrane assembly. *Biochimica et biophysica acta* **2000,** *1460* (1), 15-26.

3. Stoeckenius, W.; Lozier, R. H.; Bogomolni, R. A., Bacteriorhodopsin and the purple membrane of halobacteria. *Biochimica et Biophysica Acta (BBA) - Reviews on Bioenergetics* **1979,** *505* (3), 215-278.

4. Mahyad, B.; Janfaza, S.; Hosseini, E. S., Bio-nano hybrid materials based on bacteriorhodopsin: Potential applications and future strategies. *Advances in colloid and interface science* **2015,** *225*, 194-202.

5. Wagner, N. L.; Greco, J. A.; Ranaghan, M. J.; Birge, R. R., Directed evolution of bacteriorhodopsin for applications in bioelectronics. *Journal of the Royal Society Interface* **2013,** *10* (84).

6. Huang, K. S.; Bayley, H.; Khorana, H. G., Delipidation of bacteriorhodopsin and reconstitution with exogenous phospholipid. *Proceedings of the National Academy of Sciences of the United States of America* **1980,** *77* (1), 323-7.

7. Yu, S. M.; McQuade, D. T.; Quinn, M. A.; Hackenberger, C. P.; Krebs, M. P.; Polans, A. S.; Gellman, S. H., An improved tripod amphiphile for membrane protein solubilization. *Protein science : a publication of the Protein Society* **2000,** *9* (12), 2518-27.

8. Shiu, P.-J.; Ju, Y.-H.; Chen, H.-M.; Lee, C.-K., Facile isolation of purple membrane from Halobacterium salinarum via aqueous-two-phase system. *Protein expression and purification* **2013,** *89* (2), 219-224.

9. Becher, B. M.; Cassim, S. Y., Improved Isolation Procedures for the Purple Membrane of Halobacterium Halobium. *Preparative biochemistry* **1975,** *5* (2), 161-178.

10. Shiu, P.-J.; Chen, H.-M.; Lee, C.-K., One-step purification of delipidated Bacteriorhodopsin by aqueous-three-phase system from purple membrane of Halobacterium. *Food and Bioproducts Processing* **2014,** *92* (2), 113-119.

11. Genji, T.; Nozawa, A.; Tozawa, Y., Efficient production and purification of functional bacteriorhodopsin with a wheat-germ cell-free system and a combination of Fos-choline and CHAPS detergents. *Biochemical and biophysical research communications* **2010,** *400* (4), 638-42.

12. Nekrasova, O. V.; Wulfson, A. N.; Tikhonov, R. V.; Yakimov, S. A.; Simonova, T. N.; Tagvey, A. I.; Dolgikh, D. A.; Ostrovsky, M. A.; Kirpichnikov, M. P., A new hybrid protein for production of recombinant bacteriorhodopsin in Escherichia coli. *Journal of biotechnology* **2010,** *147* (3), 145-150.

13. Link, A. J.; Georgiou, G., Advances and challenges in membrane protein expression. *AIChE Journal* **2007,** *53* (4), 752-756.

14. Ghasemi, M. F.; Shodjai-Arani, A.; Moazami, N., Optimization of bacteriorhodopsin production by Halobacterium salinarium PTCC 1685. *Process Biochemistry* **2008,** *43* (10), 1077-1082.

15. Seigneuret, M.; Neumann, J. M.; Rigaud, J. L., Detergent delipidation and solubilization strategies for high-resolution NMR of the membrane protein bacteriorhodopsin. *Journal of Biological Chemistry* **1991,** *266* (16), 10066-10069.

16. Linke, D., Chapter 34 Detergents: An Overview. In *Methods in Enzymology*, Burgess, R. R.; Deutscher, M. P., Eds. Academic Press: 2009; Vol. 463, pp 603-617.

17. Sehgal, S. N.; Kates, M.; Gibbons, N. E., LIPIDS OF HALOBACTERIUM CUTIRUBRUM. *Canadian Journal of Biochemistry and Physiology* **1962,** *40* (1), 69-81.

18. Paradies, H. H., Shape and size of a nonionic surfactant micelle. Triton X-100 in aqueous solution. *The Journal of Physical Chemistry* **1980,** *84* (6), 599-607.

19. Rigaud, J. L.; Levy, D., Reconstitution of membrane proteins into liposomes. *Liposomes, Pt B* **2003,** *372*, 65-86.

20. Miercke, L. J.; Ross, P. E.; Stroud, R. M.; Dratz, E. A., Purification of bacteriorhodopsin and characterization of mature and partially processed forms. *Journal of Biological Chemistry* **1989,** *264* (13), 7531-7535.

21. Tschapek, B.; Smits, S. H. J.; Schmitt, L., Analyzing the Physico-Chemical Parameters of Detergents and Detergent Mixtures. *Advances in Chemical Engineering and Science* **2015,** *Vol.05No.03*, 10.

22. Lee, H.; Ho, D.; Kuo, K.; Montemagno, C. D., Vectorial insertion of bacteriorhodopsin for directed orientation assays in various polymeric biomembranes. *Polymer* **2006,** *47* (9), 2935-2941.

Chapter 3

1. Efrati, A.; Lu, C.-H.; Michaeli, D.; Nechushtai, R.; Alsaoub, S.; Schuhmann, W.; Willner, I., Assembly of photo-bioelectrochemical cells using photosystem I-functionalized electrodes. *Nature Energy* **2016,** *1*, 15021.

2. Carlson, E. D.; Gan, R.; Hodgman, C. E.; Jewett, M. C., Cell-free protein synthesis: Applications come of age. *Biotechnol Adv* **2012,** *30* (5), 1185-1194.

3. Wendell, D.; Todd, J.; Montemagno, C., Artificial Photosynthesis in Ranaspumin-2 Based Foam. *Nano Lett* **2010,** *10* (9), 3231-3236.

4. Keller, M. W.; Schut, G. J.; Lipscomb, G. L.; Menon, A. L.; Iwuchukwu, I. J.; Leuko, T. T.; Thorgersen, M. P.; Nixon, W. J.; Hawkins, A. S.; Kelly, R. M.; Adams, M.

W. W., Exploiting microbial hyperthermophilicity to produce an industrial chemical, using hydrogen and carbon dioxide. *Proceedings of the National Academy of Sciences* **2013,** *110* (15), 5840-5845.

5. Schultheisz, H. L.; Szymczyna, B. R.; Scott, L. G.; Williamson, J. R., Pathway Engineered Enzymatic de Novo Purine Nucleotide Synthesis. *Acs Chem Biol* **2008,** *3* (8), 499-511.

6. Mutti, F. G.; Knaus, T.; Scrutton, N. S.; Breuer, M.; Turner, N. J., Conversion of alcohols to enantiopure amines through dual-enzyme hydrogen-borrowing cascades. *Science* **2015,** *349* (6255), 1525-1529.

7. Guterl, J. K.; Garbe, D.; Carsten, J.; Steffler, F.; Sommer, B.; Reisse, S.; Philipp, A.; Haack, M.; Ruhmann, B.; Koltermann, A.; Kettling, U.; Bruck, T.; Sieber, V., Cell-Free Metabolic Engineering: Production of Chemicals by Minimized Reaction Cascades. *ChemSusChem* **2012,** *5* (11), 2165-2172.

8. Krutsakorn, B.; Honda, K.; Ye, X.; Imagawa, T.; Bei, X.; Okano, K.; Ohtake, H., In vitro production of n-butanol from glucose. *Metabolic engineering* **2013,** *20*, 84-91.

9. Opgenorth, P. H.; Korman, T. P.; Bowie, J. U., A synthetic biochemistry module for production of bio-based chemicals from glucose. *Nature chemical biology* **2016,** *12* (6), 393-U29.

10. Opgenorth, P. H.; Korman, T. P.; Bowie, J. U., A synthetic biochemistry molecular purge valve module that maintains redox balance. *Nature communications* **2014,** *5*, 4113.

11. Lee, H.; Ho, D.; Kuo, K.; Montemagno, C. D., Vectorial insertion of bacteriorhodopsin for directed orientation assays in various polymeric biomembranes. *Polymer* **2006,** *47* (9), 2935-2941.

12. Luo, T. J. M.; Soong, R.; Lan, E.; Dunn, B.; Montemagno, C., Photo-induced proton gradients and ATP biosynthesis produced by vesicles encapsulated in a silica matrix. *Nature materials* **2005,** *4* (3), 220-224.

13. Pitard, B.; Richard, P.; Dunach, M.; Rigaud, J. L., ATP synthesis by the F0F1 ATP synthase from thermophilic Bacillus PS3 reconstituted into liposomes with bacteriorhodopsin .2. Relationships between proton motive force and ATP synthesis. *European Journal of Biochemistry* **1996,** *235* (3), 779-788.

14. Zhang, Y.-H. P., Production of biofuels and biochemicals by in vitro synthetic biosystems: Opportunities and challenges. *Biotechnol Adv* **2015,** *33* (7), 1467-1483.

15. Uppada, V.; Satpute, K.; Noronha, S. B., 10 - Redesigning Cofactor Availability: An Essential Requirement for Metabolic Engineering. In *Current Developments in Biotechnology and Bioengineering*, Elsevier: 2017; pp 223-242.

16. Bezborodov, A. M.; Zagustina, N. A., Enzymatic biocatalysis in chemical synthesis of pharmaceuticals (Review). *Applied Biochemistry and Microbiology* **2016,** *52* (3), 237-249.

17. Brandt, U., Energy Converting NADH: Quinone Oxidoreductase (Complex I). *Annual review of biochemistry* **2006,** *75* (1), 69-92.

18. Armstrong, F. A.; Hirst, J., Reversibility and efficiency in electrocatalytic energy conversion and lessons from enzymes. *Proceedings of the National Academy of Sciences* **2011,** *108* (34), 14049-14054.

19. Baradaran, R.; Berrisford, J. M.; Minhas, G. S.; Sazanov, L. A., Crystal structure of the entire respiratory complex I. *Nature* **2013,** *494* (7438), 443-448.

20. Faham, S.; Yang, D.; Bare, E.; Yohannan, S.; Whitelegge, J. P.; Bowie, J. U., Side-chain Contributions to Membrane Protein Structure and Stability. *Journal of molecular biology* **2004,** *335* (1), 297-305.

21. Pryde, K. R.; Hirst, J., Superoxide Is Produced by the Reduced Flavin in Mitochondrial Complex I A Single, Unifed Mechanism that Applies During Both Forward and Reverse Electron Transfer. *Journal of Biological Chemistry* **2011,** *286* (20), 18056-18065.

22. Seigneuret, M.; Rigaud, J. L., Analysis of Passive and Light-Driven Ion Movements in Large Bacteriorhodopsin Liposomes Reconstituted by Reverse-Phase Evaporation .2. Influence of Passive Permeability and Back-Pressure Effects Upon Light-Induced Proton Uptake. *Biochemistry-Us* **1986,** *25* (21), 6723-6730.

23. Hazard, A.; Montemagno, C., Improved purification for thermophilic F1F0 ATP synthase using n-dodecyl beta-D-maltoside. *Archives of biochemistry and biophysics* **2002,** *407* (1), 117-124.

24. Vinogradov, A. D.; Grivennikova, V. G., Oxidation of NADH and ROS production by respiratory complex I. *Biochimica et Biophysica Acta (BBA) - Bioenergetics* **2016,** *1857* (7), 863-871.

25. Zu, Y.; Shannon, R. J.; Hirst, J., Reversible, Electrochemical Interconversion of NADH and NAD+ by the Catalytic (Iλ) Subcomplex of Mitochondrial NADH:Ubiquinone Oxidoreductase (Complex I). *J Am Chem Soc* **2003,** *125* (20), 6020-6021.

26. Friedrich, T.; Ohnishi, T.; Forche, E.; Kunze, B.; Jansen, R.; Trowitzsch, W.; Hofle, G.; Reichenbach, H.; Weiss, H., 2 Binding-Sites for Naturally-Occurring Inhibitors in Mitochondrial and Bacterial Nadh-Ubiquinone Oxidoreductase (Complex-I). *Biochemical Society transactions* **1994,** *22* (1), 226-230.

27. Kotlyar, A. B.; Borovok, N., NADH oxidation and NAD+ reduction catalysed by tightly coupled inside-out vesicles from Paracoccus denitrificans. *European journal of biochemistry / FEBS* **2002,** *269* (16), 4020-4.

28. Ohnishi, S. T.; Salerno, J. C.; Ohnishi, T., Possible roles of two quinone molecules in direct and indirect proton pumps of bovine heart NADH-quinone oxidoreductase (complex I). *Biochimica et Biophysica Acta (BBA) - Bioenergetics* **2010,** *1797* (12), 1891-1893.

29. Belevich, N.; Belevich, G.; Chen, Z.; Sinha, S. C.; Verkhovskaya, M., Activation of respiratory Complex I from Escherichia coli studied by fluorescent probes. *Heliyon* **2017,** *3* (1), e00224.

30. Casadio, R., Measurements of Transmembrane Ph Differences of Low Extents in Bacterial Chromatophores - a Study with the Fluorescent-Probe 9-Amino, 6-Chloro, 2-Methoxyacridine. *European Biophysics Journal* **1991,** *19* (4), 189-201.

31. D'Alessandro, M.; Turina, P.; Melandri, B. A., Quantitative evaluation of the intrinsic uncoupling modulated by ADP and Pi in the reconstituted ATP synthase of Escherichia coli. *Biochimica et Biophysica Acta (BBA) - Bioenergetics* **2011,** *1807* (1), 130-143.

32. Spehr, V.; Schlitt, A.; Scheide, D.; Guenebaut, V.; Friedrich, T., Overexpression of the Escherichia coli nuo-operon and isolation of the overproduced NADH:ubiquinone oxidoreductase (complex I). *Biochemistry-Us* **1999,** *38* (49), 16261-7.

33. Pohl, T.; Uhlmann, M.; Kaufenstein, M.; Friedrich, T., Lambda Red-mediated mutagenesis and efficient large scale affinity purification of the Escherichia coli NADH:ubiquinone oxidoreductase (complex I). *Biochemistry-Us* **2007,** *46* (37), 10694-702.

Chapter 4

1. Efrati, A.; Lu, C.-H.; Michaeli, D.; Nechushtai, R.; Alsaoub, S.; Schuhmann, W.; Willner, I., Assembly of photo-bioelectrochemical cells using photosystem I-functionalized electrodes. *Nature Energy* **2016,** *1*, 15021.

2. Carlson, E. D.; Gan, R.; Hodgman, C. E.; Jewett, M. C., Cell-free protein synthesis: Applications come of age. *Biotechnol Adv* **2012,** *30* (5), 1185-1194.

3. Wendell, D.; Todd, J.; Montemagno, C., Artificial Photosynthesis in Ranaspumin-2 Based Foam. *Nano Lett* **2010,** *10* (9), 3231-3236.

4. Keller, M. W.; Schut, G. J.; Lipscomb, G. L.; Menon, A. L.; Iwuchukwu, I. J.; Leuko, T. T.; Thorgersen, M. P.; Nixon, W. J.; Hawkins, A. S.; Kelly, R. M.; Adams, M. W. W., Exploiting microbial hyperthermophilicity to produce an industrial chemical, using hydrogen and carbon dioxide. *Proceedings of the National Academy of Sciences* **2013,** *110* (15), 5840-5845.

5. Schultheisz, H. L.; Szymczyna, B. R.; Scott, L. G.; Williamson, J. R., Pathway Engineered Enzymatic de Novo Purine Nucleotide Synthesis. *Acs Chem Biol* **2008,** *3* (8), 499-511.

6. Mutti, F. G.; Knaus, T.; Scrutton, N. S.; Breuer, M.; Turner, N. J., Conversion of alcohols to enantiopure amines through dual-enzyme hydrogen-borrowing cascades. *Science* **2015,** *349* (6255), 1525-1529.

7. Guterl, J. K.; Garbe, D.; Carsten, J.; Steffler, F.; Sommer, B.; Reisse, S.; Philipp, A.; Haack, M.; Ruhmann, B.; Koltermann, A.; Kettling, U.; Bruck, T.; Sieber, V., Cell-Free Metabolic Engineering: Production of Chemicals by Minimized Reaction Cascades. *ChemSusChem* **2012,** *5* (11), 2165-2172.

8. Krutsakorn, B.; Honda, K.; Ye, X.; Imagawa, T.; Bei, X.; Okano, K.; Ohtake, H., In vitro production of n-butanol from glucose. *Metabolic engineering* **2013,** *20*, 84-91.

9. Opgenorth, P. H.; Korman, T. P.; Bowie, J. U., A synthetic biochemistry module for production of bio-based chemicals from glucose. *Nature chemical biology* **2016,** *12* (6), 393-U29.

10. Opgenorth, P. H.; Korman, T. P.; Bowie, J. U., A synthetic biochemistry molecular purge valve module that maintains redox balance. *Nature communications* **2014,** *5*, 4113.

11. Lee, H.; Ho, D.; Kuo, K.; Montemagno, C. D., Vectorial insertion of bacteriorhodopsin for directed orientation assays in various polymeric biomembranes. *Polymer* **2006,** *47* (9), 2935-2941.

12. Luo, T. J. M.; Soong, R.; Lan, E.; Dunn, B.; Montemagno, C., Photo-induced proton gradients and ATP biosynthesis produced by vesicles encapsulated in a silica matrix. *Nature materials* **2005,** *4* (3), 220-224.

13. Pitard, B.; Richard, P.; Dunach, M.; Rigaud, J. L., ATP synthesis by the F0F1 ATP synthase from thermophilic Bacillus PS3 reconstituted into liposomes with

bacteriorhodopsin .2. Relationships between proton motive force and ATP synthesis. *European Journal of Biochemistry* **1996,** *235* (3), 779-788.

14. Zhang, Y.-H. P., Production of biofuels and biochemicals by in vitro synthetic biosystems: Opportunities and challenges. *Biotechnol Adv* **2015,** *33* (7), 1467-1483.

15. Uppada, V.; Satpute, K.; Noronha, S. B., 10 - Redesigning Cofactor Availability: An Essential Requirement for Metabolic Engineering. In *Current Developments in Biotechnology and Bioengineering*, Elsevier: 2017; pp 223-242.

16. Bezborodov, A. M.; Zagustina, N. A., Enzymatic biocatalysis in chemical synthesis of pharmaceuticals (Review). *Applied Biochemistry and Microbiology* **2016,** *52* (3), 237-249.

17. Muh, F.; Glockner, C.; Hellmich, J.; Zouni, A., Light-induced quinone reduction in photosystem II. *Bba-Bioenergetics* **2012,** *1817* (1), 44-65.

18. Barber, J., Photosystem II: a multisubunit membrane protein that oxidises water. *Current opinion in structural biology* **2002,** *12* (4), 523-530.

19. Brandt, U., Energy Converting NADH: Quinone Oxidoreductase (Complex I). *Annual review of biochemistry* **2006,** *75* (1), 69-92.

20. Armstrong, F. A.; Hirst, J., Reversibility and efficiency in electrocatalytic energy conversion and lessons from enzymes. *Proceedings of the National Academy of Sciences* **2011,** *108* (34), 14049-14054.

21. Baradaran, R.; Berrisford, J. M.; Minhas, G. S.; Sazanov, L. A., Crystal structure of the entire respiratory complex I. *Nature* **2013,** *494* (7438), 443-448.

22. Umena, Y.; Kawakami, K.; Shen, J.-R.; Kamiya, N., Crystal structure of oxygen-evolving photosystem II at a resolution of 1.9[thinsp]A. *Nature* **2011,** *473* (7345), 55-60.

23. Rigaud, J. L.; Levy, D., Reconstitution of membrane proteins into liposomes. *Liposomes, Pt B* **2003,** *372*, 65-86.

24. Pryde, K. R.; Hirst, J., Superoxide Is Produced by the Reduced Flavin in Mitochondrial Complex I A Single, Unifed Mechanism that Applies During Both Forward and Reverse Electron Transfer. *Journal of Biological Chemistry* **2011,** *286* (20), 18056-18065.

25. Kotlyar, A. B.; Vinogradov, A. D., Slow Active Inactive Transition of the Mitochondrial Nadh-Ubiquinone Reductase. *Biochimica et biophysica acta* **1990,** *1019* (2), 151-158.

26. Hsu, B. D.; Lee, J. Y.; Pan, R. L., The two binding sites for DCMU in Photosystem II. *Biochemical and biophysical research communications* **1986,** *141* (2), 682-8.

27. Trebst, A., Inhibitors in the functional dissection of the photosynthetic electron transport system. *Photosynthesis research* **2007,** *92* (2), 217-224.

28. Convent, B.; Briquet, M., Properties of 3-(3,4-Dichlorophenyl)-1,1-dimethylurea and Other Inhibitors of the Cytochrome bc1 Segment of the Mitochondrial Respiratory Chain in Saccharomyces cerevisiae. *European Journal of Biochemistry* **1978,** *82* (2), 473-481.

29. Liu, L.-N.; Bryan, S. J.; Huang, F.; Yu, J.; Nixon, P. J.; Rich, P. R.; Mullineaux, C. W., Control of electron transport routes through redox-regulated redistribution of respiratory complexes. *Proceedings of the National Academy of Sciences* **2012,** *109* (28), 11431-11436.

30. Degli Esposti, M., Inhibitors of NADH-ubiquinone reductase: an overview. *Biochimica et biophysica acta* **1998,** *1364* (2), 222-35.

31. Casadio, R., Measurements of Transmembrane Ph Differences of Low Extents in Bacterial Chromatophores - a Study with the Fluorescent-Probe 9-Amino, 6-Chloro, 2-Methoxyacridine. *European Biophysics Journal* **1991,** *19* (4), 189-201.

32. D'Alessandro, M.; Turina, P.; Melandri, B. A., Quantitative evaluation of the intrinsic uncoupling modulated by ADP and Pi in the reconstituted ATP synthase of Escherichia coli. *Biochimica et Biophysica Acta (BBA) - Bioenergetics* **2011,** *1807* (1), 130-143.

33. Vinogradov, A. D.; Gavrikova, E. V.; Grivennikova, V. G.; Zharova, T. V.; Zakharova, N. V., Catalytic properties of mitochondrial NADH-ubiquinone reductase (Complex I). *Biochemistry. Biokhimiia* **1999,** *64* (2), 136-52.

34. vanBelzen, R.; Kotlyar, A. B.; Moon, N.; Dunham, W. R.; Albracht, S. P. J., The iron-sulfur clusters 2 and ubisemiquinone radicals of NADH:ubiquinone oxidoreductase are involved in energy coupling in submitochondrial particles. *Biochemistry-Us* **1997,** *36* (4), 886-893.

35. De Jong, A. M. P.; Albracht, S. P. J., Ubisemiquinones as obligatory intermediates in the electron transfer from NADH to ubiquinone. *European Journal of Biochemistry* **1994,** *222* (3), 975-982.

36. Hirst, J.; Roessler, M. M., Energy conversion, redox catalysis and generation of reactive oxygen species by respiratory complex I. *Bba-Bioenergetics* **2016,** *1857* (7), 872-883.

37. Oursel, D.; Loutelier-Bourhis, C.; Orange, N.; Chevalier, S.; Norris, V.; Lange, C. M., Lipid composition of membranes of Escherichia coli by liquid chromatography/tandem mass spectrometry using negative electrospray ionization. *Rapid Commun Mass Sp* **2007,** *21* (11), 1721-1728.

38. van Eerden, F. J.; de Jong, D. H.; de Vries, A. H.; Wassenaar, T. A.; Marrink, S. J., Characterization of thylakoid lipid membranes from cyanobacteria and higher plants by molecular dynamics simulations. *Biochimica et Biophysica Acta (BBA) - Biomembranes* **2015,** *1848* (6), 1319-1330.

39. Sakurai, I.; Jian-Ren, S.; Jing, L.; Ohashi, S.; Kobayashi, M.; Wada, H., Lipids in Oxygen-Evolving Photosystem II Complexes of Cyanobacteria and Higher Plants. *Journal of biochemistry* **2006,** *140* (2), 201-209.

40. Spehr, V.; Schlitt, A.; Scheide, D.; Guenebaut, V.; Friedrich, T., Overexpression of the Escherichia coli nuo-operon and isolation of the overproduced NADH:ubiquinone oxidoreductase (complex I). *Biochemistry-Us* **1999,** *38* (49), 16261-7.

41. Pohl, T.; Uhlmann, M.; Kaufenstein, M.; Friedrich, T., Lambda Red-mediated mutagenesis and efficient large scale affinity purification of the Escherichia coli NADH:ubiquinone oxidoreductase (complex I). *Biochemistry-Us* **2007,** *46* (37), 10694-702.

42. Bricker, T. M.; Morvant, J.; Masri, N.; Sutton, H. M.; Frankel, L. K., Isolation of a highly active Photosystem II preparation from Synechocystis 6803 using a histidine-tagged mutant of CP 47. *Bba-Bioenergetics* **1998,** *1409* (1), 50-57.

43. Vavilin, D. V., Methods for the Isolation of Functional Photosystem II Core Particles from the Cyanobacterium Synechocystis sp PCC 6803. In *Photosynthesis*

Research Protocols, Second Edition, Carpentier, R., Ed. Humana Press Inc: Totowa, 2011; Vol. 684, pp 29-40.

Chapter 5

1. Dudley, Q. M.; Karim, A. S.; Jewett, M. C., Cell-free metabolic engineering: Biomanufacturing beyond the cell. *Biotechnol J* **2014**.

2. Nestl, B. M.; Nebel, B. A.; Hauer, B., Recent progress in industrial biocatalysis. *Current Opinion in Chemical Biology* **2011,** *15* (2), 187-193.

3. Illanes, A.; Cauerhff, A.; Wilson, L.; Castro, G. R., Recent trends in biocatalysis engineering. *Bioresource Technol* **2012,** *115* (0), 48-57.

4. Nestl, B. M.; Hammer, S. C.; Nebel, B. A.; Hauer, B., New Generation of Biocatalysts for Organic Synthesis. *Angew Chem Int Edit* **2014,** *53* (12), 3070-3095.

5. Wells, A., 9.11 Industrial Applications of Biocatalysis: An Overview. In *Comprehensive Chirality*, Carreira, E. M.; Yamamoto, H., Eds. Elsevier: Amsterdam, 2012; pp 253-287.

6. Tufvesson, P.; Fu, W.; Jensen, J. S.; Woodley, J. M., Process considerations for the scale-up and implementation of biocatalysis. *Food and Bioproducts Processing* **2010,** *88* (1), 3-11.

7. Sahare, P.; Ayala, M.; Vazquez-Duhalt, R.; Agrawal, V., Immobilization of peroxidase enzyme onto the porous silicon structure for enhancing its activity and stability. *Nanoscale research letters* **2014,** *9* (1), 409.

8. Jang, E.; Ryu, B. H.; Kim, T. D., Identification, characterization, and immobilization of an organic solvent-stable alkaline hydrolase (PA27) from Pseudomonas aeruginosa MH38. *Molecules* **2014,** *19* (9), 14396-405.

9. Talbert, J. N.; Wang, L. S.; Duncan, B.; Jeong, Y.; Andler, S. M.; Rotello, V. M.; Goddard, J. M., Immobilization and Stabilization of Lipase (CaLB) through Hierarchical Interfacial Assembly. *Biomacromolecules* **2014**.

10. Vashist, S. K.; Lam, E.; Hrapovic, S.; Male, K. B.; Luong, J. H., Immobilization of Antibodies and Enzymes on 3-Aminopropyltriethoxysilane-Functionalized Bioanalytical Platforms for Biosensors and Diagnostics. *Chem Rev* **2014**.

11. Lee, J. H.; Nam, D. H.; Lee, S. H.; Park, J. H.; Park, S. J.; Lee, S. H.; Park, C. B.; Jeong, K. J., New Platform for Cytochrome P450 Reaction Combining in Situ Immobilization on Biopolymer. *Bioconjugate chemistry* **2014**.

12. Hollmann, F.; Schmid, A., Electrochemical regeneration of oxidoreductases for cell-free biocatalytic redox reactions. *Biocatal Biotransfor* **2004,** *22* (2), 63-88.

13. Quinto, T.; Kohler, V.; Ward, T. R., Recent Trends in Biomimetic NADH Regeneration. *Top Catal* **2014,** *57* (5), 321-331.

14. Wu, H.; Tian, C.; Song, X.; Liu, C.; Yang, D.; Jiang, Z., Methods for the regeneration of nicotinamide coenzymes. *Green Chem* **2013,** *15* (7), 1773-1789.

15. Liu, W.; Wang, P., Cofactor regeneration for sustainable enzymatic biosynthesis. *Biotechnol Adv* **2007,** *25* (4), 369-84.

16. Uppada, V.; Bhaduri, S.; Noronha, S. B., Cofactor regeneration - an important aspect of biocatalysis. *Curr Sci India* **2014,** *106* (7), 946-957.

17. Gao, X.; Fang, J.; Xue, B.; Fu, L.; Li, H., Engineering Protein Hydrogels Using SpyCatcher-SpyTag Chemistry. *Biomacromolecules* **2016,** *17* (9), 2812-9.

Appendix A: Procedure for the production and isolation of PSII

All chromatographic steps were performed using a GE ÄKTA pure 25 or ÄKTA Avant 125 (GE Healthcare Life Sciences, Inc.) at 4°C. All ultracentrifugation steps use a Beckman Coulter Type 45-Ti Rotor unless indicated otherwise. Protein concentration was determined using Millipore Direct Detect® infrared spectrometer (EMD Millipore, Inc.).

Cyanobacteria BG-11 Culture Medium Preparation

Trace Mineral Solution Recipe

1. To prepare 1 L of trace mineral solution add the amount indicated of the compounds listed in Table 1 in the order specified with constant stirring to 800mL of deionized H_2O (dH_2O).
2. After the materials are dissolved completely Q.S. the solution to 1 L with dH_2O.
3. Store the solution at 4-8°C.

Table 1 | BG-11 trace mineral stock solutions

Order	Component	Mass (g L^{-1})	Concentration (mM)
1	H_3BO_3	2.86	46
2	$MnCl_2 \bullet 4H_2O$	1.81	9
3	$ZnSO_4 \bullet 7H_2O$	0.22	0.77
4	$Na_2MoO_4 \bullet 2H_2O$	0.39	1.6
5	$CuSO_4 \bullet 5H_2O$	0.079	0.3
6	$Co(NO_3)_2 \bullet 6H_2O$	0.00494	0.17

BG-11 Medium Recipe

1. Using dH_2O prepare stock solutions of the compounds listed in Table 2.

2. To prepare 1 L of BG-11 medium, add the volume indicated of the concentration stock solutions of the components listed in Table 2 in the order specified with constant stirring in 800 mL of dH_2O.
3. After the materials are dissolved completely use 1 M NaOH or 1 M HCl to pH the medium to 6.8.
4. Q.S. the solution to 1 L with dH_2O.
5. Filter the medium using a 0.2 μm filter using aseptic techniques.

Table 2 | BG-11 medium component and concentration list

Order	Component	Stock Concentration ($mg\ mL^{-1}$)	Volume ($mL\ L^{-1}$)	Final Concentration (mM)
1	$NaNO_3$	150	10	17.6
2	K_2HPO_4	4	10	0.23
3	$MgSO_4 \bullet 7H_2O$	7.5	10	0.3
4	$CaCl_2 \bullet 2H_2O$	3.6	10	0.24
5	Citric Acid$\bullet H_2O$	0.6	10	0.031
6	Ferric Ammonium Citrate	0.6	10	0.021
7	$Na_2EDTA \bullet 2H_2O$	0.6	10	0.0027
8	Na_2CO_3	0.1	10	0.19
9	BG-11 Trace Mineral solution	N/A	1	N/A
10	Glucose	36	10	2
11	Kanamycin	10	1	0.05

Recovery and expansion of cyanobacterium *Synechocystis* 6803 HT-3 cells

1. Remove an aliquot of cells from the cyrofreezer. The HT-3 cell stocks are stored in BG-11 medium + 8 %(v/v) DMSO.
2. Place the cell stock in a water bath set to 30°C for 10 min.
3. Following the thaw, centrifuge the cells for 3 min at 7,000 rpm using a tabletop micro-centrifuge.

4. Discard the supernatant and resuspend the cells in 1 mL of freshly prepared BG-11 media.
5. In a 250 mL Erlenmeyer flask, inoculate 49 mL of freshly prepared BG-11 media with the resuspended cells.
6. Wrap the flask with tin foil to protect the culture from light.
7. Place the culture in a shaker set to 30°C and 100 rpm for 24 hrs.
8. After 24 hr, remove the tin foil and introduce 50 μmol photons m^{-2} s^{-1} of white light to culture and increase the agitation speed of the shaker to 250 rpm.
9. Using 1mL of the culture and 1 cm path length cuvette measure the optical absorbance (OD) of the culture at 730 nm daily.
10. Once the cells have reached an OD ≥0.8, expand the culture by adding the 50 mL culture to 450 mL of warmed BG-11 medium in a 1 L Erlenmeyer flask.
11. Incubate the 500 mL culture at 30°C at 250 rpm placed under 50 μmol photons m^{-2} s^{-1} of white light until the culture has reached an OD ≥0.8.

Production of Cyanobacterium *Synechocystis* 6803 HT-3 cells

1. After the 500 mL culture has reached an OD ≥0.8, 250 mL is used to inoculate 9.75 L of warmed BG-11 medium in a clear 10L carboy with a three-port cap.
    a. **Note**: A piece of peristaltic tubing long enough to reach the bottom of the carboy must be placed on one of three ports.

2. Place the 10L culture in an incubator set at 30°C, surrounded with white lights capable of distributing 50 μmol photons m^{-2} s^{-1} to the entire culture.
3. Connect the house gas to the port on the carboy that has the peristaltic tubing connected to it.
    a. **Note**: Place a 0.2 μm filter in-line to the house gas.
4. Increase the flow of the house gas until the culture is vigorously bubbling to ensure adequate mixing and CO_2 delivery to the culture.
5. Measure the OD of the culture daily, once the OD ≥1.0 (typically 3 days) the cells are ready for harvest.

Cyanobacterium *Synechocystis* 6803 HT-3 Culture harvest

1. Using a Beckman JLA-9.1000 centrifuge rotor or equivalent, pellet the cells by centrifugation at 5,000 rcf x 10 min.
2. Combined the cell pellets and wash once by resuspending the cells in PSII Buffer A using a motorized pipet and centrifuge the resuspended cells at 10,000 rcf x 10 min.
3. Resuspend the cells in a small amount of PSII Buffer A, approximately 0.5% of the culture volume.
    a. **Note**: To ensure the cells are resuspended entirely, a glass Teflon homogenizer can be used.
4. Measure the chlorophyll-A (chlA) concentration of resuspended cells.
    a. Mix 10 μL of resuspended cells from step 3 into 990 μL of 80 %(v/v) acetone.

b. Sonicate the cell/acetone mixture for 2-3 min and pellet the cell material using a bench-top micro-centrifuge for 3 min at 18,000 rcf.
c. Decant the supernatant and place into a cuvette with 1 cm path length and measure and record the OD at 663 nm and 643 nm.
d. Resuspend the pelleted cells from 4.b using 1 mL of 80%(v/v) acetone, and repeat step 4.c.
    i. **Note:** Steps 4.b-d may need to repeated 2-3 times, until the chlA is completely extracted.
e. Calculate the chlA concentration in the extracts using Equation 1.
    i. **Note:** When the chlA extraction procedure is repeated multiple times the summation of the concentrations of each extract is the chlA concentration of the resuspended cells.
    ii. A_{663} – OD at 663 nm; A_{645} – OD at 645 nm; DF – Dilution Factor

Equation 1 | chlA Concentration calculation

$$chlA\left[\frac{\mu g}{mL}\right] = \left[12.7\left(A_{663}\right) - 2.59\left(A_{645}\right)\right] x \left(DF\right)$$

5. The target concentration of chlA of resuspended cells is 1 mg mL^{-1}, add the appropriate volume of PSII Buffer A to the resuspended cells from step 3 and repeat step 4 to confirm the chlA concentration.

Purification of PSII

Solutions

The solutions that are required for the isolation of PSII are listed in Table 3. After preparing the solutions, they should be 0.2 μM filtered and stored at 4-8˚C. The user should degas all buffers used for affinity chromatography purification (e.g. PSII Binding Buffer and PSII Elution Buffer).

Table 3: Solutions Required for the Purification of PSII

Solution Name	Composition
PSII Buffer A	50 mM MES-NaOH, pH 6.0, 10 mM $MgCl_2$, 5 mM $CaCl_2$, 25%(v/v) glycerol
PSII Binding Buffer	PSII Buffer A + 0.04% (w/v) DDM
PSII Elution Buffer	PSII Binding Buffer + 200 mM L-Histidine (or Imidazole)
PSII Precipitation Buffer	30 mM MES-NaOH, pH 6.0, 25% (v/v) PEG-8000
20% (w/v) DDM	20% (w/v) DDM in dH_2O
20% (v/v) EtOH	20% (v/v) EtOH, 80% (v/v) dH_2O
80% (v/v) Acetone	80% (v/v) Acetone, 20% (v/v) dH_2O
100x PMSF	100 mM PMSF in EtOH
100x ε-amino caproic acid	100 mM ε-amino caproic acid in dH_2O
100x DNAse	5 mg mL^{-1} DNAse in dH_2O

Cell lysis and clarification

Note: From this point on of the purification procedure keep all samples on ice and protected from light.

1. Using 100x concentration stocks bring the 1 mg chlA mL^{-1} suspension of cells to 1.0 mM PMSF, 1.0 mM ε-amino caproic acid and, 50 μg mL^{-1} DNAase.
2. Prepare the cell disruptor (Constant Systems Ltd. CF or equivalent), by pre-chilling to 4°C.

a. Wash the cell disrupter with 50 mL dH_2O followed by 50 mL of PSII Buffer A at with the disrupter set to 10,000 psig.

3. Disrupt the cells by passing the cells through the disrupter 2 times at 35,000 psig.
    a. After the second pass wash the disrupter with 15 mL of PSII Buffer A and collect the material. Add the wash to the disrupted cells.
4. Centrifuge the disrupted cells at 1,500 rcf x 10 min using a Beckman Coulter type 45-Ti rotor or equivalent to remove unbroken cells and cellular debris.
5. Carefully decant the clarified cell lysate from the pelted material.

<u>Thylakoid membrane isolation and solubilization</u>

6. Centrifuge the clarified cell lysate (supernatant from step 5) at 80,000 rcf x 30 min using a Beckman Coulter Type 45-Ti rotor or equivalent.
7. Decant the supernatant and resuspended the pelleted material, which is the thylakoid membranes, in PSII Buffer A using 80% of the volume of clarified cell lysate.
8. Bring the resuspended thylakoid membranes to 0.8% (w/v) dodecyl maltoside (DDM) by drop-wise addition of 20% (w/v) DDM in dH_2O with continuous stirring.
9. Place the thylakoid membrane + 0.8 % (w/v) DDM in a pre-chilled centrifuge tube and gently mix using a rotator at 4°C for 20 min.

10. Centrifuge in a Beckman Coulter Type 45-Ti rotor or equivalent at 100 rcf x 1 min, 2,900 rcf x 1 min, 4,900 rcf x 1 min, 8,000 rcf x 1 min, 15,100 rcf x 1 min and, final 22,100 rcf x 10 min.
11. Decant the solubilized thylakoid membrane extract and measure the chlA concentration as done in step 6.1.5.4.

Affinity chromatography purification

Note: All chromatography steps are performed at a linear flow rate of 38 cm h^{-1}.

1. Prepare the FPLC by placing PSII Binding Buffer on inlet A1, PSII Elution Buffer on inlet B1, 2 M NaCl on inlet B2.
2. Wash inlet A2 with PSII Binding Buffer
3. Be sure all pump heads are purged after placing the inlets into the appropriate buffer bottles.
4. Connect a (GE Healthcare Life Sciences, Inc.) XK 2.6 cm diameter column with a 10 cm bed height with Ni^{2+} Sepharose High Performance resin (GE Healthcare Life Sciences, Inc.).
5. Place the thylakoid membrane extract onto inlet A2
6. Pre-equilibrate the column with 4 CVs of PSII binding Buffer.
7. The load the thylakoid membrane extract on to the column.
8. Wash column with PSII Binding Buffer until the Abs_{280} falls below 90 mAU.
9. Following the wash, elute the bound PSII from the column using a 40% (v/v) step gradient of PSII Elution Buffer, collecting 2 mL fractions

a. **Note:** To elute at higher concentrations (e.g. tighter peak) perform the elution step in up-flow operation.

10. Pool the fractions contained in the center 90% if the elution peak.
11. Add 80% (v/v) of PSII Precipitation Buffer to the pooled fractions.
12. Centrifuge the solution from step 11 at 18,000 rcf x 20 min.
13. Carefully pour off the supernatant and gently wash the inner wall of the centrifuge tube with PSII Binding Buffer without disturbing the pellet.
14. Resuspend the pellet in PSII Binding Buffer by gently pipetting and allow to incubate on ice for 10 min.
    a. **Note:** Use extra care not to introduce bubbles. This step is time consuming when done with care.
    b. **Note:** The scientist may want to do the resuspension step first with a small volume, measure the chlA concentration and add addition PSII Binding Buffer. This will depend on the concentration of PSII needed for the users experiments.
15. Centrifuge the solution from step 14 at 6,000 rcf x 5 min at RT.
16. Remove the green PSII containing, supernatant to a labeled tube. Depending on the users experiment plans for the material, the material should be aliquoted into smaller volumes among several tubes to minimize freeze-thaw cycles.
    a. **Note:** The isolated PSII may lose > 20% of its original oxygen evolution activity with every freeze-thaw cycle.

17. Snap freeze the material using liquid nitrogen and store in -80˚C until further use.

Appendix B: Procedure for the production and isolation of CMI

E. coli strain ANN0221/pBAD*nuo*/His-*nuoF* cell and expansion

All chromatographic steps were performed using a GE ÄKTA pure 25 or ÄKTA Avant 125 (GE Healthcare Life Sciences, Inc.) at 4°C. All ultracentrifugation steps use a Beckman Coulter Type 45-Ti Rotor unless indicated otherwise. Protein concentration was determined using Millipore Direct Detect® infrared spectrometer (EMD Millipore, Inc.).

Stock solutions

Stock solutions that are useful to have aliquoted and stored frozen (-20ºC) for the purification of CMI are listed in Table 1.

Table 1 | Useful stocks of reagents needed for the production and isolation of CMI.

Stock	Composition
1000x chloramphenicol	25 mg mL^{-1} chloramphenicol in EtOH
100x PMSF	1 mM PMSF in EtOH
100x DNAse	10 mg mL^{-1} DNAse in dH_2O
100x lysozyme	50 mg mL^{-1} lysozyme in dH_2O
100x L-arabinose	20% (w/v) L-arabinose in dH_2O
100x L-cysteine	50 mM L-cysteine in dH_2O

Table 2 | Composition of supplemented TB medium

Component	Amount/Concentration
Terrific Broth (TB)	50.8 g L^{-1}
1000x chloramphenicol	1 mL L^{-1}
riboflavin	50 mg L^{-1}
100x L-cysteine	10 mL L^{-1}
ferric ammonium citrate	30 mg L^{-1-}

Supplemented media preparation

4. To prepare 1 L of supplemented media add the amount indicated of the compounds listed in Table 2 in the order specified with constant stirring to 800mL of deionized H_2O (dH_2O).
5. After the materials are dissolved completely use 1 M NaOH or 1 M HCl to pH the medium to 7.0.
6. Q.S. the solution to 1 L with dH_2O.
7. Filter the medium using a 0.2 μm filter the medium using aseptic techniques.

Recovery and expansion of *E. coli* strain ANN0221/pBAD*nuo*/His-*nuoF* cells

1. Remove an aliquot of cells from the cyrofreezer. The cell stocks are stored in supplemented TB medium + 10%(v/v) glycerol.
2. Place the cell stock in a water bath set to 30°C for 10 min.
3. In a 250 mL Erlenmeyer flask, inoculate 29 mL of freshly prepared supplemented TB medium media with the thawed cells.
4. Place the culture in a shaker set to 27°C and 100 rpm for overnight.
5. Inoculated 1:100 pre-warmed (37°C) supplemented TB medium (500 mL in 2 L Erlenmeyer flask) with the overnight culture.
6. Place in the inoculated 500 mL culture in an incubator set to 37°C and 350 rpm.
7. After 1 hr induce the *nuo*-operon by introducing 10 mL L^{-1} of the 20%(w/v) L-arabinose.

8. Continue to monitor the culture using 1mL of the culture and 1 cm path length cuvette. Measure the optical absorbance (OD) of the culture at 600 nm.
9. Once the cells have reached the stationary growth phase, typically 6 hrs, harvest the cells by centrifugation at 16,000 rcf x 20 min and 4°C using a Beckman Coulter JLA-9.1000 centrifuge rotor.
10. If cells are going to be used immediately proceed to the next section, otherwise they can be frozen and stored at -80°C.

Isolation and solubilization of the cytoplasmic membranes

The solutions that are required for the isolation and solubilization of the cytoplasmic membranes are listed in Table 3. After preparing the solutions, they should be 0.2 µM filtered and stored at 4-8°C. The user should degas all buffers used for affinity chromatography purification (e.g. CMI Binding Buffer, CMI Elution Buffer, and CMI Polishing Buffer).

Table 3 | Solutions of the isolation and solubilization of the cytoplasmic membranes

Solution Name	Composition
CMI Resuspension Buffer	50 mM MES-NaOH, pH 6.0, 200 mM NaCl, 0.1 mM PMSF, 10 µg mL^{-1} DNAse, 10 µg mL^{-1} lysozyme
20% (w/v) DDM	20% (w/v) DDM in dH_2O

Isolation of the cytoplasmic membranes

1. If the cells were frozen, allow them to thaw on ice.
2. Resuspend the cell pellet in 5-fold CMI Resuspension Buffer (5 mL CMI Resuspension Buffer per g of wet cell mass).

a. **Note**: To ensure the cells are resuspended entirely, a glass Teflon homogenizer can be used.

6. Prepare the cell disruptor (Constant Systems Ltd. CF or equivalent), by pre-chilling to 4°C.
    a. Wash the cell disrupter with 50 mL dH_2O followed by 50 mL of CMI Resuspension Buffer at with the disrupter set to 10,000 psig.
7. Disrupt the cells by using a single pass the through the disrupter at 25,000 psig.
    b. After the disrupted cell material has exited the disrupter, wash the disrupter with 15 mL of CMI Resuspension Buffer and collect the material. Add the wash to the disrupted cells.
8. Centrifuge the disrupted cells at 36,000 rcf x 20 min using a Beckman Coulter type 45-Ti rotor or equivalent to remove unbroken cells and cellular debris.
9. Carefully decant the clarified cell lysate from the pelted material.
10. Obtain cytoplasmic membranes by centrifugation of clarified cell lysate from step 4 by centrifugation at 235,000 rcf x 2 hr at 4°C. Flash freeze membrane pellets and store at -80°C, if not going to be used immediately.
    c. **Note:** If the cytoplasmic membranes were frozen, thaw the membranes on ice before proceeding to step 6.
    d. **Note:** All steps from this point forward should be performed on ice or in a cold room.

Solubilization of the cytoplasmic membranes

1. Using a glass Teflon homogenizer, resuspend the membranes in CMI Resuspension Buffer to a protein concentration of 50 mg mL^{-1}.
    a. **Note:** Continuing forward the resuspended membrane solution from step 6 is referred to as the Membrane solution.
2. Using the 20% (w/v) DDM stock, bring the Membrane solution to a concentration of 3% (w/v) DDM using drop-wise addition with constant stirring.
    a. **Note:** It is suggested to perform this step in the centrifuge tube that that step 9 will be perform with.
3. Incubate the solution using a tube rotator for 15 min.
4. Remove the unsolubilized material by centrifugation at 250,000 rcf x 20 min.
5. Carefully decant the supernatant and filter using a 0.45 µm syringe filter.
6. Using the appropriate amounts of CMI Binding Buffer and CMI Elution Buffer, adjust the filtered solubilized membrane solution to a protein concentration of 5 mg mL^{-1} and an imidazole concentration of 50 mM.

Isolation of CMI

The solutions that are required for the isolation of the CMI are listed in Table 4. After preparing the solutions, they should be 0.2 µM filtered and stored at 4-8˚C. The user should degas all buffers used for affinity chromatography purification (e.g CMI Binding Buffer, CMI Elution Buffer and CMI Polishing Buffer).

Table 4 | Solutions for the isolation of CMI

Solution Name	Composition
CMI Binding Buffer	50 mM MES-NaOH, pH 6.0, 200 mM NaCl, 0.1% (w/v) DDM
CMI Elution Buffer	50 mM MES-NaOH, pH 6.0, 200 mM NaCl, 0.1% (w/v) DDM, 500 mM imidazole
CMI Polishing Buffer	50 mM MES-NaOH, pH 6.0, 50 mM NaCl, 0.1% (w/v) DDM

Affinity chromatography purification

1. Prepare the FPLC by placing CMI Binding Buffer on inlet A1, CMI Elution Buffer on inlet B1.
2. Wash inlet A2 with CMI Binding Buffer
3. Be sure all pump heads are purged after placing the inlets into the appropriate buffer bottles.
4. Connect a (GE Healthcare Life Sciences, Inc.) Tricorn 1.0 cm diameter column with a 10 cm bed height with Ni^{2+} Sepharose High Performance resin (GE Healthcare Life Sciences, Inc.).
5. Place the adjusted filtered solubilized membrane solution inlet A2
6. Pre-equilibrate the column with 4 CVs of 90% CMI binding Buffer and 10% CMI Elution Buffer using a linear flow velocity of 153 cm h^{-1}.
7. Load the adjusted filtered solubilized membrane solution on to the column using a linear flow rate of 153 cm h^{-1}.
8. Chase the adjusted filtered solubilized membrane solution with 90% CMI Binding Buffer, 10% CMI Elution buffer using a linear flow rate of 153 cm h^{-1} until the Abs_{280} falls below 200 mAU.

9. Remove contaminating proteins using a wash step with 150 mM imidazole and until the wash until the Abs_{280} falls below 200 mAU.
10. The CMI protein is eluted using a step gradient of 375 mM imidazole using a linear flow velocity of 76.5 cm h^{-1} in up-flow operation while collecting 1 mL fractions.
11. Pool the fractions contained in the center 90% if the elution peak.
12. Concentrate the pooled fractions using a 100 kDa MWCO Amicon® Ultra centrifugal filter (EDM Millipore, Inc.) to 2-3 mL.
    a. **Note:** It is normal for precipitation to occur at this point resulting in up to 30% lose of protein. To accelerate the process the scientist may want to transfer the material to new centrifugal filter when significant precipitation has occurred.

Polish and desalting of CMI

1. Pre-equilibrate a HiLoad 16/600 Superdex 200 (GE Healthcare Life Sciences, Inc) with 3 CVs of CMI Polishing Buffer.
2. Inject the concentrate CMI from the affinity chromatography step into a 5 mL loop , which has been wash with 15 mL of CMI Polishing Buffer.
3. Inject the material from the loop onto the column with 7 mL of CMI Polishing Buffer using a linear flow velocity of 22 cm h^{-1}.
4. Elute the material using the CMI Polishing buffer using a linear flow velocity of 22 cm h^{-1}.

a. **Note:** Begin collecting 1 mL fractions after the void volume of the chromatography column being that the size of CMI is at edge of the fractionation range of the chromatography column.

5. Pool the fractions containing CMI.
6. Concentrate the pooled fractions using a 100 kDa MWCO Amicon® Ultra centrifugal filter (EDM Millipore, Inc.) to 4-5 mg mL^{-1}.
7. Depending on the users experiment plans for the material, the material should be aliquoted into smaller volumes among several tubes to minimize freeze-thaw cycles.
8. Snap freeze the material using liquid nitrogen and store in -80˚C until further use.

Appendix C: Procedure for the production and isolation of PM and bR

All chromatographic steps were performed using a ÄKTA Avant 125 (GE Healthcare Life Sciences, Inc.) at room temperature. All ultracentrifugation steps use a Beckman Coulter Type 45-Ti Rotor unless indicated otherwise. Protein concentration was determined using Millipore Direct Detect® infrared spectrometer (EMD Millipore, Inc.).

H. salinarium S9 culture medium preparation

1. To prepare 1 L of *H. salinarium* culture medium add the amount indicated of the compounds listed in Table 1 in the order specified with constant stirring to 800 mL of deionized H_2O (dH_2O).
    a. **Note:** The order of addition of the components for the medium is critical in preventing precipitation.
2. After the materials are dissolved completely using NaOH pellets to adjust the pH to 7.0 .
3. Q.S. the solution to 1 L with dH_2O.
4. Filter the medium using a 0.2 μm filter using aseptic techniques.

Table 1| Composition of *H. salinarium* S9 medium

Order	Component	Amount/Concentration
1	NaCl	250 g L^{-1}
2	$MgSO_4$	9.77 g L^{-1}
3	KCl	2.0 g L^{-1}
4	NH_4Cl	5.0 g L^{-1}
5	$C_6H_5O_7Na_3 \cdot 2H_2O$	3.0 g L^{-1}
6	glycerol	1 mL L^{-1}

7	KH_2PO_4	100 mg L^{-1}
8	$CaCl_2$	200 mg L^{-1}
9	Oxoid Bacteriological Peptone L-37®	10 g L^{-1}

Recovery and expansion of *H. salinarium* S9 cells

1. Remove an aliquot of cells from the cyrofreezer. The cell stocks are stored in *H. salinarum* S9 medium + 10%(v/v) glycerol.
2. Place the cell stock in a water bath set to 30°C for 10 min.
3. In a 250 mL Erlenmeyer flask, inoculate 29 mL of freshly prepared supplemented *H. salinarum* S9 medium with the thawed cells.
4. Wrap the flask with tin foil to protect the culture from light.
5. Place the culture in a shaker set to 40°C and 100 rpm for 24 hr.
6. After 24 hr remove the tin foil from the flask and introduce 80 μmol photons m^{-2} s^{-1} of green light to the culture.
    a. **Note:** The introduction of green light to culture is critical for induction of bR production.
7. Inoculated 1:100 pre-warmed (40°C) *H. salinarum* S9 medium (500 mL in 2 L Erlenmeyer flask) with the overnight culture.
8. Place in the inoculated 500 mL culture in an incubator set to 40°C and 350 rpm and introduce 80 μmol photons m^{-2} s^{-1} of green light to the culture.
9. Continue to monitor the culture using 1mL of the culture and 1 cm path length cuvette. Measure the optical absorbance (OD) of the culture at 600 nm.

10. Once the cells have reached the stationary growth phase (OD_{600} ≥ 0.8), typically 48-56 hr, harvest the cells by centrifugation at 10,000 rcf x 20 min and 4°C using a Beckman Coulter JLA-9.1000 centrifuge rotor.
11. Remove the supernatant and transfer the cells to an appropriately sized container.
    a. **Note:** Typically, 1 L of culture will generate 4-6 g of wet cell mass.
12. If cells are going to be used immediately proceed to the next section, otherwise they can be frozen and stored at -80°C.

Isolation and solubilization of the purple membrane

The solutions that are required for the isolation PM and bR are listed in Table 2. After preparing the solutions; they should be 0.2 µM filtered and stored at 4-8°C. The user should degas all buffers used for affinity chromatography purification (e.g. bR Binding Buffer and bR Elution Buffer).

Table 2 | Solutions required for the isolation or PM and bR

Solution	Composition
Cell Lysis	4.2 mM $MgSO_4$, 100 µg mL^{-1} DNAse, 10 µg mL^{-1} lysozyme
PM Delipidation Buffer	10 mM Tris, pH 7.0, 2 mM CHAPS, 50 mM NaCl
PM Buffer	10 mM Tris, pH 8.0, 50mM NaCl
PM Solubilization Buffer	50 mM Tris, pH 7.5, 5.0% (w/w) Triton X-100
bR Running Buffer	50 mM Tris, pH 7.5, 0.01% (w/w) Triton X-100 or 0.03% (w/w) DDM
bR Elution Buffer	bR Running Buffer + 1 M NaCl

Purification and delipidation of PM

1. If the cells were frozen, allow them to thaw on ice.

2. Resuspend the cell pellet in 10 mL of Cell Lysis solution per gram of wet cell with continuous stirring and protected from light for 12 hours at room temperature.
3. Centrifuge the disrupted cells at 2,000 rcf x 10 min using a Beckman Coulter type 70-Ti rotor or equivalent to remove unbroken cells and cellular debris.
4. Carefully decant the clarified cell lysate from the pelted material.
5. Connect an appropriately size hollow fiber member (5 mg wet cell mass cm^{-2}) with an MWCO of 750 kDa to a KR2 TFF system (Spectrum, Inc.) with size 16 peristaltic tubing.
    a. **Note:** It is critical to select a reservoir sized to allow for $1/5^{th}$ of the volume of the clarified cell lysate. Additionally, the reservoir should have a flat bottom, place on a stir plate with a magnetic stir bar placed within the vessel.
6. Place the tubing from the filtrate size of the membrane and place it into the automatic back pressure pitch valve.
7. Set the back pressure pitch valve to permeate mode and 1 psig.
8. Equilibrate the system using 4.2 mM $MgSO_4$, allowing 2 mL cm^{-2} to permeate through the filter.
9. Empty the reservoir and place the clarified cell lysis into the reservoir.
10. Using a manual pitch value close the permeate side of the membrane.
11. Place a container onto a bench top scale and place the permeate tubing into the bottom, followed by zeroing the scale.

12. Start the system at a flow rate of 100 mL min^{-1}.
13. After 5 minutes begin to open the permeate by slowly losing the manual pitch valve.
14. Allow the system to permeate until the clarified cell lysis has been concentrated 5 fold.
15. Place the diafiltration buffer from the reservoir into the PM Delipidation Buffer.
16. Allow the system to permeate until 10 diavolumes (DVs) have permeated through the membrane. After each DV has permeated through the filter, gradually increase the flow rate until the maximum flow rate is reached while maintaining an inlet pressure below 30 psig.
    b. **Note:** At this point the permeate will begin to turn pink.
    c. **Note:** The CHAPS reduces the size of the PM fragments causing a reduction in the inlet and transmembrane pressure.
17. After 10 DVs have permeated the second DF step begins by placing the DF line of the reservoir into PM Buffer.
    e. **Note:** As the CHAPS is removed from the system, the PM fragments will begin to aggregated causing an increase in the system pressure. To avoid over pressurization of the system, gradually decrease the inlet flow rate.
    f. **Note:** Vigorous mixing is crucial at this step, if mixing is not adequate phase separation will begin to occur.

18. After 3 DVs of PM buffer has permeated through the filter, collect the delipidated PM from the system by placing the retentate line into a centrifuge tube until all the material has been removed from the system.
    a. **Note:** Wash the system allowing 10 mL cm^{-2} of 2% (v/v) Triton X-100, followed by 10 mL cm^{-2} of 30% (v/v) isopropyl alcohol and finally 10 mL cm^{-2} of 0.1N NaOH permeate through the filter.
    b. **Note:** Store the system in 0.1N NaOH.
19. Remove any remaining cellular debris and cellular organelles from the delipidated PM by centrifugation at 2,000 rcf x 10 min using a Beckman Coulter type 45-Ti rotor.
20. Carefully decant the isolated delipidated PM from the pelleted material.
    d. Depending on the users experiment plans for the material, the material can be aliquoted into smaller volumes among several tubes to store as purified PM at -80ºC.

Purification of bacteriorhodopsin

1. To solubilize the PM, dilute the PM at 1 mg mL^{-1} in PM Solubilization Buffer and incubate overnight protected from light.
2. Remove the nonsolubilized material by centrifugation at 40,000 rcf x 20 min using a Beckman Coulter type 70-Ti rotor.
3. Carefully decant the isolated supernatant from the pelleted material.
4. Prepare the FPLC by placing bR Binding Buffer on inlet A1, bR Elution Buffer on inlet B1.
5. Wash inlet A2 with bR Binding Buffer.

6. Be sure all pump heads are purged after placing the inlets into the appropriate buffer bottles.
7. Connect a column with 10 cm bed height with packed Capto Q resin (GE Healthcare Life Sciences, Inc.).
8. Place the solubilized PM solution on inlet A2
9. Pre-equilibrate the column with 4 CVs of bR Binding Buffer a linear flow velocity of 700 cm h^{-1}.
10. Load the solubilized PM on to the column using a linear flow rate of 700 cm h^{-1}.
11. Chase the solubilized PM with bR Binding Buffer, using a linear flow rate of 700 cm h^{-1} until the Abs_{280} stabilizes indicating excess Triton X-100 has been removed from the column.
12. The bR is eluted using an either a step gradient of 20% bR Elution buffer or a 10 CV linear gradient to 60% using a linear flow velocity of 250 cm h^{-1} in up-flow operation while collecting 1mL fractions.
    a. **Note:** Depending on the scientists need the step gradient will result in a mixture of trimeric, dimeric and monomeric bR. If the scientist requires homogeneous population of any of the three bR configurations the linear gradient is required.
13. Pool the fractions where the ratio OD_{500}:OD_{280} ≥ 0.5.
14. Desalt the pooled fractions by 3x DF into bR Binding Buffer using a 3 kDa MWCO Amicon® Ultra centrifugal filter (EDM Millipore, Inc.) to 2-3 mL by centrifugation at 4,000 rcf x 30 min.

15. Concentration the purified bR to 4-5 mg mL^{-1} using a 3 kDa MWCO Amicon® Ultra centrifugal filter (EDM Millipore, Inc.) by centrifugation at 4,000 rcf until the target concentration is reached.
16. Depending on the users experiment plans for the material, the material should be aliquoted into smaller volumes among several tubes to minimize freeze-thaw cycles.
17. Snap freeze the material using liquid nitrogen and store in -80˚C until further use.